DESIGN AND APPLICATION OF ANTI-BIOFOULING COATINGS ON

STAINLESS STEEL BY PLASMA ENHANCED CHEMICAL

VAPOR DEPOSITION

by

Carol A. Ellis-Terrell, B.S., M.S.

A dissertation submitted to the Graduate Council of
Texas State University in partial fulfillment
of the requirements for the degree of
Doctor of Philosophy
with a Major in Materials Science, Engineering, and Commercialization
May 2020

Committee Members:

Tania Betancourt, Chair

Gary Beall

Kent Coulter

Edwin Piner

Shannon Weigum

FAIR USE AND AUTHOR'S PERMISSION STATEMENT

Fair Use

Duplication Permission

DEDICATION

This book is dedicated to my husband (Wilson), daughter (Nia), mother (Marsha), and father (Billy) for believing in me no matter the circumstance.

ACKNOWLEDGEMENTS

First and foremost, I would like to thank God for keeping me lifted throughout this process. My family for their constant words of encouragement, support and willingness to follow me on this journey. Thank you, Wilson and Nia. To my parents (Marsha and Billy Ellis) for always knowing and telling me to dream big and work hard to achieve those dreams. To my aunts, uncles, cousins and grandma for your calls, prayers, and letting me know that you are proud of me. To my friends who heard me complain about some of my ongoing difficulties through the process thank you for your words of wisdom and your direction to Gods Word.

My advisor Dr. Betancourt, I appreciate you taking on a project that was outside of your scope of interest and working with me to learn and articulate all that I know with a level of confidence to my peers. Thank you for opening your lab up to me and training me on all the various equipment and allowing me to work with the undergraduate and graduate students in the lab. I am so grateful for the opportunities that you suggested to me to get my research out to others.

To my lab mates Niloofar, Emilio, Shadad, Tugba, Maddie, and Karoline thank you for your help with maintaining my cells and listening to me discuss my research.
To Jerry thank you so much for working with me during the summer and learning about cells and taking on the tedious task of maintaining the cells and imaging them.

To Southwest Research Institute® SwRI® thank you for the financial support and thank you to my many my colleagues for their praises, encouraging words and helping me understand our PECVD process and power source system and their aid in formatting this document.

To my committee I thank you for assisting me in the process. Talking to me about my dissertation proposal, providing classes related to my research and opening your doors to discuss various topics.

TABLE OF CONTENTS

Page

LIST OF TABLES

LIST OF FIGURES

LIST OF ABBREVIATIONS

Abbreviation	Description
AC	Alternating Current
ANOVA	Analysis of Variance
Ar	Argon
BMS	Bare Metal Stents
CAD	Coronary Artery Disease
CCP	Capacitively Coupled Plasma
CW	Continuous Wave
DAPI	4,6-diamidino-2-phenylindole
DAPT	Dual Anti-Platelet Therapy
DC	Direct Current
DES	Drug Eluting Stent
DLC	Diamond-Like-Carbon
DPBS	Dulbecco Phosphate Buffered Saline
GCM	Gas Chamber Mixer
HCASMC	Human Coronary Artery Smooth Muscle Cell
HMDSO	Hexamethyldisiloxane
HUVEC	Human Umbilical Vein Endothelial Cell
ISR	In-Stent Restenosis

NIH	National Institute of Health
PBS	Phosphate Buffered Saline
PC	Passive Coatings
PCI	Percutaneous Coronary Intervention
PECVD	Plasma Enhanced Chemical Vapor Deposition
PLC	Polymer Like Coatings
RF	Radio Frequency
SCCM	Standard Cubic Centimeters per Minute
SLC	Silica Like Coatings
SS	Stainless Steel
SwRI	Southwest Research Institute
TMS	Trimethylsilane
TNS	Trypsin Neutralizing Solution

ABSTRACT

Presently, stents are the primary practice to treat coronary artery blockage. However, in-stent restenosis remains a problem that affects approximately 10-30% of patients with bare metal stents (BMS).[1,2] To mitigate this problem, BMS are coated with either drug-eluting (active) or a biologically inert (passive) coatings to provide anti-biofouling properties. Plasma based surface modification is a method used to impart specific surface properties on medical devices. Coatings produced by plasma-enhanced chemical vapor deposition (PECVD) techniques are known to be effective at reducing cell adhesion, similar to conventional solution-based coating methods. Despite radio frequency (RF) power supplies being the most commonly used power generator for PECVD, there are a couple of drawbacks to this power source: 1. difficult adaptability to large scale industrial processes; 2. limited control of deposition process. Instead, pulsed-direct current (DC) PECVD is more translatable to industrial processes and has been shown to allow for more selective fragmentation of chemical precursors due to the use of short duty cycles. In this work, plasma-polymerized hexamethyldisiloxane (HMDSO) coatings were deposited on flat stent-like material with pulsed-DC PECVD and evaluated as anti-biofouling coatings to inhibit or promote accumulation of specific cells to the surface. The anti-biofouling coatings were prepared at three different flow rates of HMDSO (2, 2-3, and 3 g/hr) and two different voltages (1000 V and 1500 V). The interaction of human umbilical vein endothelial cells (HUVECs) and human coronary artery smooth muscle cells

(HCASMCs) was investigated on the coated surfaces after 2 and 7 days of incubation. Two fluorescent stains, 4,6-diamidino-2-phenylindole dihydrochloride (DAPI) and CytoPainter Phalloidin iFluor 594 were used for imaging the nucleus and cytoskeleton of the cells adhered to the surface.

Our results show that the coating chemistry, thickness and wetting properties are adaptable with respect to the applied voltage and monomer flow rate. An organosilicon polymer-like (1000 V) and silicon oxycarbide (1500 V) coating were deposited on 321 and 316 L stainless steel foil. An average water contact angle at 3 g/hr at 1000 V and 1500 V was 97 ° and 75 °, respectively on 316 L stainless steel foil, indicating a statistical difference. The cellular response of HUVECs and HCASMCs to the two different coated stent-like materials on deposited at 3 g/hr flow rate at 1000 V and 1500 V 316 L SS revealed a reduction in HCASMC cells adhering and proliferating across the organosilicon polymer-like coating (3 cells/mm^2 after 2 days and 7 cells/mm^2 after 7 days in comparison to uncoated 316 L SS foil (10 cells/mm^2 after 2 days and 18 cells/mm^2 after 7 days).

1. INTRODUCTION

1.1 Motivation

Coronary artery disease (CAD) is the leading cause of death in the US, accounting for nearly 43.8% of deaths.[3] CAD is triggered by the build-up of plaque on the walls of the arteries in the heart and other parts of the body, a process known as atherosclerosis. The accumulation of plaque on the artery walls causes the artery to narrow, thereby partially or completely blocking blood flow and potentially leading to a heart attack (myocardial infarction). Bare metal stents (BMS) are used to remedy CAD; however, in-stent restenosis (the obstruction of the blood vessel within the stent) and thrombosis (formation of blood clots) may arise, leading to the need for a second intervention to reopen the obstructed artery in the best-case scenario, or to a myocardial infarction or even death in the worst-case scenario.

Restenosis is triggered by biofouling, i.e. an accumulation of proteins and cells on the blood vessel or stent. Generally, the surface functionality of the stent material, established by its surface chemistry, controls the extent of biofouling occurrence. A coating may alter the surface chemistry. For example, anti-biofouling coatings can be used to mitigate protein and cell accumulation on BMS. Two of the main problems associated with anti-biofouling coatings on BMS are 1) non-specific inhibition of proteins and cells; 2) coating uniformity on 3-D samples. In this project, we addressed the problem of non-specificity of anti-biofouling coating using pulsed-direct current (DC) plasma-enhanced chemical vapor deposition (PECVD).

1.2 Overall Research Project

Anti-biofouling coating's work to prevent the accumulations of macromolecules, micro-organisms and patient's cells on biomedical devices. This research focuses on the preparation of anti-biofouling coatings that will regulate the adsorption of specific proteins and adhesion of specific cells onto samples relevant to cardiovascular stents. In particular, an array of anti-biofouling coatings that vary in chemical composition and, consequently, physical properties are fabricated from biocompatible organo-silicon by modulating key PECVD process parameters.

This study hypothesizes that pulsed-DC PECVD could be used to tailor the surface chemistry on a sample by altering the process parameters such as voltage and gas flow rate to generate coatings with hydrophobic and hydrophilic properties. When the voltage and gas flow rate increases the coating is hydrophilic, as opposed to hydrophobic when the voltage and gas flow rate decreases.

In this work, anti-biofouling coatings with a carbon-silicon-oxygen backbone (shown in **Figure 1**) are prepared by plasma enhanced chemical vapor deposition employing hexamethyldisiloxane (HMDSO) as the coating's chemical precursor.
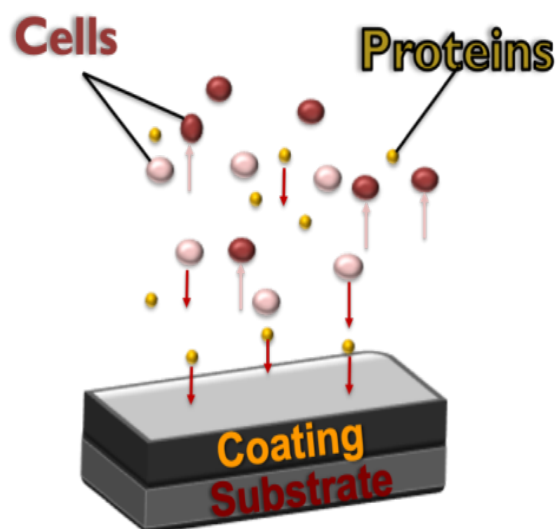
Figure 1. Schematic of the HMDSO-coated sample in an aqueous media of cells and proteins.

1.3 Specific Aims

The following specific aims were addressed in this project:

1. **Design and fabricate coatings to prevent biofouling using pulsed-DC plasma enhanced chemical vapor deposition (PECVD).** The coatings were prepared by pulsed direct current PECVD using the chemical precursor HMDSO. The coating's wetting properties ranged from hydrophobic to hydrophilic to enable correlation between the coating's chemistry and prevention of biofouling in the next aim. The precursor flow rate and applied voltage were studied to demonstrate the governance of the plasma chemistry in the presence of pulsed-DC power source to achieve an array of coating chemistries on flat samples. The coating thickness, wetting properties, and chemical composition were determined.

2. **Perform *in vitro* studies to establish the correlation between coating properties and the coatings' ability to inhibit or promote accumulation of**

specific cells. The interaction of human vascular endothelial and human coronary artery smooth muscle cells with the samples was evaluated using fluorescence microscopy to assess the number of cells adhered on the surface of coated and uncoated samples. The correlation between coating properties and cell adhesion was determined.

1.4 Dissertation Outline

Chapter 2 describes the background relevant to coronary artery blockage with respect to the coatings utilized on stents for the prevention of biofouling. A brief introduction of antibiofouling coatings used in medical applications is presented along with an overview of plasma-based surface modification techniques used for biomedical applications. Chapter 3 describes the plasma chamber and deposition process used in this study along with the power supply. After that, the physical (goniometer and profilometer), and chemical (Raman) techniques that were employed for characterization of the coatings are summarized. This is followed by the results associated with plasma deposition of HMDSO through the use of pulsed-DC PECVD. Our results show that the coating chemistry, thickness and wetting properties are adaptable with respect to the applied voltage and monomer flow rate. Chapter 4 describes the investigation of the interaction of vascular endothelial and smooth muscle cells with the coated samples described in the previous chapter. Additionally, characterization of the adhesion to and proliferation rate of the cells on the samples was performed. Chapter 5 summarizes the results of the work presented in the previous chapters and provides a prospective on future research.

2. BACKGROUND & IMPACT

2.1   Use Of Stents In The Treatment Of Coronary Artery Disease

Affecting around 16.7 million people in the U.S., coronary artery disease (CAD) is

regarded as the number one cause of death in the U.S..[4] Furthermore, the common cause

of CAD in about 50% of patients is atherosclerotic plaque buildup in the arteries.[5]

Atherosclerotic plaque consists of lipids, cells (smooth muscle cells), fibrous tissue

(collagen fibers), and debris that accumulates on the interior walls of the coronary artery,

reducing blood flow to the heart. To remedy coronary artery blockage, percutaneous

coronary interventions (PCI), specifically balloon angioplasty and stents are the primary

practice;[6] yet, in-stent restenosis (ISR) remains a problem in (PCI), afflicting

approximately 10 – 30 % of patients with bare metal stent (BMS) implants and ~ 5% of

patients with drug-eluting stent (DES) implants.[1,2,7]

The first successful PCI took place in the late 1970's, when Andrea Gruentzig expanded

a small section of a patient's artery with a polymeric balloon, revolutionizing the

treatment for CAD.[8,9] A catheter tube is inserted into the patient's blood vessel via there

wrist or groin. The catheter tube is then guided toward the heart. Once in place a

contrasting dye is injected to view the blocked artery. After the occluded section of the

artery is found, another catheter tube is passed over the guidewire and is inflated in the

area of blockage and then removed. The inflated catheter, polymeric balloon angioplasty,

will only temporarily expand the arterial wall to improve the blood flow. Typically,

within 6 months plaque builds up along the wall occluding the vessel again. To improve

on the accomplishments of the initial PCI, tubular mesh's known as stents may be placed

over the balloon angioplasty and permanently or temporarily positioned to widen the blocked artery.

Stents are implanted into the blood vessel to alleviate narrowing (stenosis) resulting from plaque buildup on the blood vessel walls. However, it became evident that an alternative healing response arose due to the stent. Following stent implantation, a physiological response is triggered, followed by an inflammatory response. This incident can be attributed to vascular damage by the stent to the arterial wall, thereby removing the protective endothelium lining and revealing the smooth muscle cells (SMC) to constituents in the blood. [10–14] The trauma to the arterial wall tissue quickly initiates an inflammatory response, known as neointimal hyperplasia. Neointimal causes protein adsorption and coagulation and SMC's proliferation and migration toward the lesion, resulting in the formation of a film of coagulated fibrinogen and SMC's around the surface of the stent.

Figure 2 depicts initial atherosclerotic lesion, implantation of the stent, and neointimal hyperplasia leading to in-stent restenosis, all within a blood vessel. These events lead to scar tissue development within the stent and the potential for blood clot formation. Thereby compromising the performance of the stent and leading to the need for a second procedure which includes stent removal and reopening of the occluded vessel.
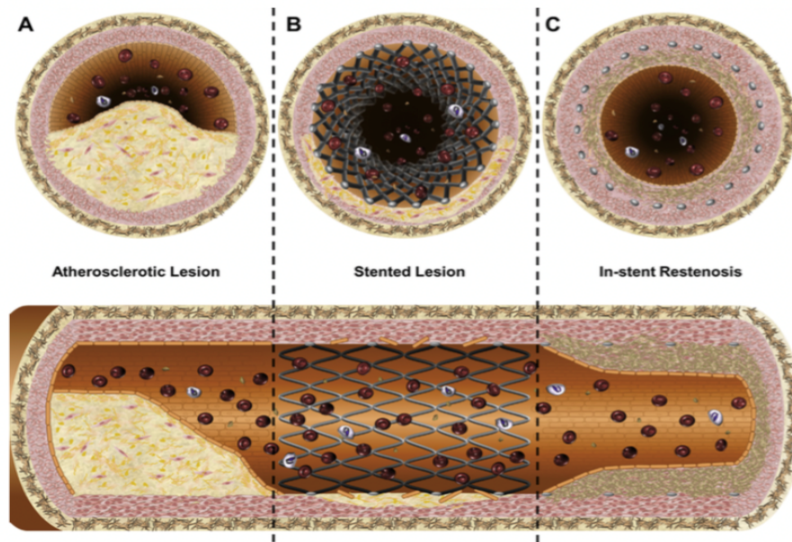
Figure 2. The progression of restenosis within a blood vessel prior to and after stenting.[12]

 Three types of stents that are used to alleviate plaque-build in the artery will be described in the next few paragraphs: 1) bare metal stents (BMS); 2) actively coated stents; and 3) passively coated stents.

In 1986 the first BMS was implanted into a human coronary artery using a self-expanding stainless steel stent.[15] Although the implantation was considered a success, the use of the stent was limited due to issues with deployment (elastic recoil). The stainless-steel stent technology was further developed by Palmer and coworkers through the use of a balloon expandable stainless steel stent system.[9,15] The recoil issue was reduced with this system. Also, the onset of plaque buildup (restenosis) in the arteries was lengthened. However there were still a significant number of drawbacks as result of these stents being used such as restenosis, stent thrombosis, failed deployment, and embolism.[16]

BMSs (depicted in **Figure 3**) are generally offered in assorted metal composition,[17] different strut thickness, varying designs and geometries, and may be treated with a coating[16,18,19] to improve their biocompatibility. BMS's are porous mesh structures that were initial made of corrosion resistant 316 L stainless steel. However flexible, shape memory, and degradable materials such as cobalt chromium, nitinol and magnesium alloy emerged. While 316 L has excellent resistance to corrosion and is considered biocompatible, it's ISR rates are high, between 15-20%. To prevent biofouling, or the chronic aggregation of protein and blood cells on BMS, surface properties such as material composition and structural design need to be carefully considered. The overarching goal is to have a fully functional layer of endothelial cells encompassing the luminal surface of the stent. This endothelial cell layer has been shown to prevent the onset of thrombosis [12,20–22]and reduce the occurrence of ISR.[12,23–26]
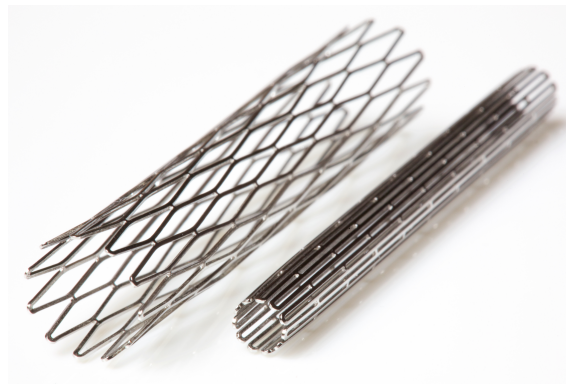
Figure 3. Assortment of bare metal stents.

2.2   Antibiofouling Coatings

To overcome the high rate of ISR, anti-biofouling surface modification techniques by way of active or passive coatings are applied to stents, such that active coatings interfere

with intimal hyperplasia while passive coatings block interaction between the blood vessel and stent material.[27]

Stents with active coatings also known as drug eluting stents (DES), elute immunosuppressive or anti-proliferative drugs (paclitaxel,[12] zotarolimus,[12] sirolimus,[28] and heparin[29]) to regulate cell adhesion, thereby preventing excess tissue growth inside and outside the stent that would lead to the re-narrowing of the artery and clotting within the stent. Typically the drug is loaded into the pores of the base metal or chemically attached to a permanent and/or biodegradable polymer such as poly(styrene-*b*-isobutylene-*b*-styrene) or poly(L-lactic acid), respectively.

In order for the drug to be effective in a DES, it needs to be released for at least 30 days. The inorganic coating or metal pore size and density are used to control the release rate of the drug, whereas the drug release rates from polymer-coated stents depends typically on physical mechanisms including drug diffusion through the polymer, degradation of polymer, polymer relaxation and osmotic pressure.[30,31] Typically drug release from DES lasts between 3 and 9 months[32] and, after that, the polymeric coating serves more as a passive coating. After DES implantation, it is recommended that oral dual anti-platelet therapy (DAPT) (aspirin plus a P_2Y_{12} inhibitor such as clopidogrel, prasugrel, ticagrelor, or cangrelor) be taken for at least 12 months. The length of time for DAPT is still being debated with some studies indicating that 3 months of DAPT is enough for patients with stable coronary disease.[33,34]

The first generation of DES, i.e. those coated with a permanent polymer, have been

reported to exhibit a higher decrease of ISR than bare metal stents, albeit with a slight

increase risk of late stent thrombosis and very late stent thrombosis after discontinuing

DAPT.[6] The occurrence of stent thrombosis can cause major complications that may lead

to myocardial infarction, resulting from accumulated platelets and coagulated proteins

reducing or blocking the flow of blood. Research to improve the efficacy and safety of

DES has experienced exponential growth since their first generation of DES with second,

third and fourth generation DES now being developed and evaluated. The four

generations of DES are shown in **Figure 4**.
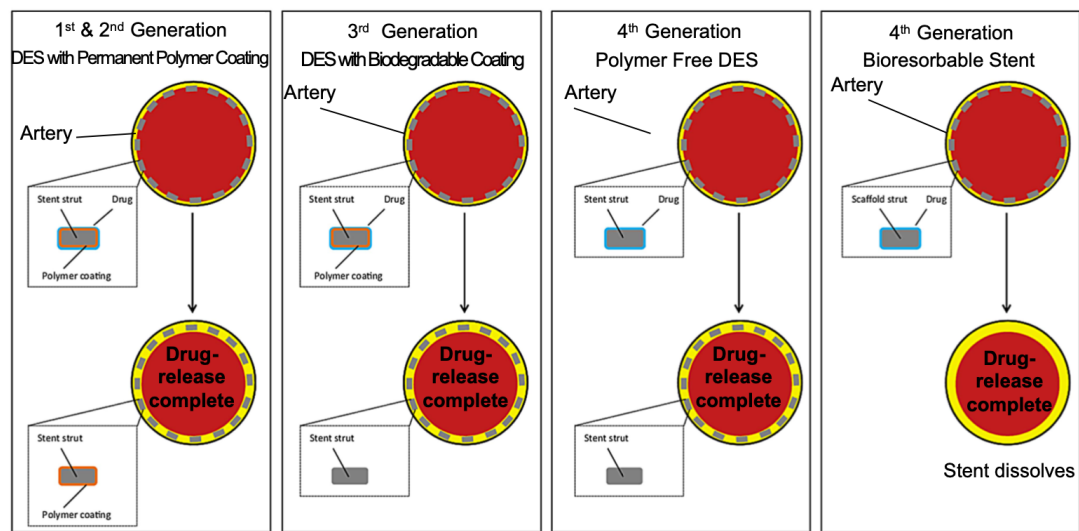
Figure 4. Drug eluting stents [14]

Recent studies on second generation DES demonstrate a reduced risk of late stent

thrombosis through the use of new drugs and stent platforms (i.e. material composition

and design). Second generation DES also demonstrate a superiority to BMS in reducing

ISR.[13,35] To improve the biocompatibility of stents, third generation DES replace the

permanent polymers employed with a bioresorbable polymers such as poly (L-lactic acid). However, a key issue experienced with third generation stents is stent thrombosis, which may result from polymer-related inflammation and hypersensitivity.[36] While, fourth generation DES is a mix of polymer-free stents using stainless steel platform, and biodegradable stent platforms centered on poly(L-lactic acid) or magnesium alloy. A list of bare metal stents and a few 1st, 2nd, 3rd, and 4th generation drug eluting stents are provided in Table 1.

In the era of DES, why look at passive coatings for BMS?

Even though drug eluting coatings are on the rise, there are still issues such as poor or delayed endothelization, and long-term use of DAPT for patients with high bleeding risk. **Figure 5** highlights the concerns of DES and BMS in the blood vessel. In addition, a hotly debated issue in healthcare industry today is "cost", which is much higher for DES than BMS.
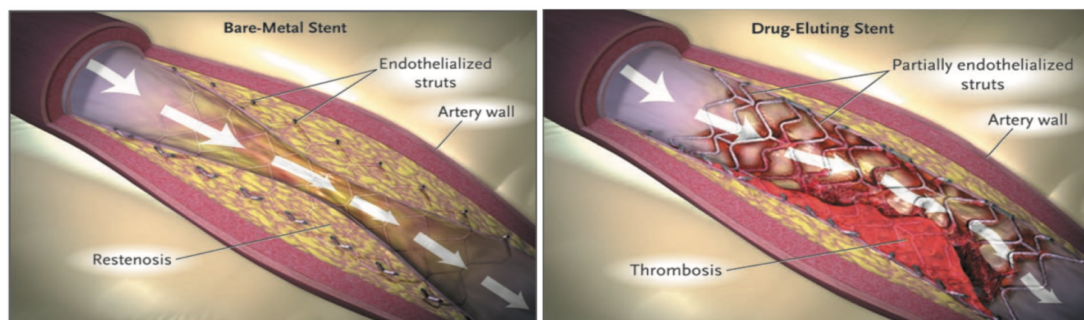
Figure 5. Comparison of bare-metal stent and drug-eluting stent in the blood vessel. Reproduced with permissions from Drug-eluting Coronary Stents Promise and Uncertainty, Copyrights Massachusetts Medical Society.[37]

Passive coatings (PCs) are considered to have a less complex design at a lower cost[17] and less long-term safety issues[1] than DES. PC's are typically designed to be biologically inert and prevent protein adsorption and vascular smooth muscle cell adhesion. Coating chemistries that have shown promise at reducing restenosis and accelerating endothelialization are titanium nitride oxide, silicon oxide, silicon carbide and carbide.[38–41] Biotronik's Pro-Kinetic stent, which uses an amorphous silicon carbide coating was designed to reduce thrombosis by applying a protective coating to preventing ion release and reducing select protein adsorption and smooth muscle cells adhesion while at the same time increasing endothelial cell adhesion. This coating was applied using silane, methane, and phosphine chemistry using a plasma deposition method. Furthermore, passive coatings such as silicon oxide or silicon carbide can serve as a protective coating, act as carriers to release drugs or can be coated together with a drug incorporated polymer. For example, Orsiro stents by Biotronik uses a passive amorphous silicon carbide coating (Pro-Kinetic), along with an immunosuppressive drug sirolimus incorporated within a biodegradable polymer poly(L-lactic acid) topping.[42,43]

In this work, we investigated the anti-biofouling properties of different organo-silicon coatings applied to relevant stent samples (316 L SS) using PECVD. Furthermore, we assessed the effect of the coating chemistries generated by pulsed-DC on the coatings' surface properties and biological performance.

Table 1. Bare metal, passively coated and drug eluting stents.

Stent Name	Type of Stent	Composition	Type of Coating	Drug/release rate	Restenosis
N/A	BMS	316 L Stainless Steel	N/A	N/A	15-20 %
N/A	BMS	Cobalt-Chromium	N/A	N/A	16.8%[44]
PRO-Kinetic Energy	Passively coated BMS	Cobalt-Chromium	Silicon Carbide	N/A	28.1%[45]
Axetis	Passively coated BMS	Stainless Steel	Silicon Oxide	N/A	33.3% at 6 months[46]
Cypher	DES (1st generation)	Stainless Steel	Poly-ethylene-co-vinyl acetate/poly n-butyl methacrylate	Sirolimus (30 days)	4-7% after 4 months[47]
Taxus	DES (1st generation)	Stainless Steel	Poly(styrene-b-isobutylene-b-styrene	Paclitaxel (30 days)	3.7 % after 1 year[48]
ResoluteTM	DES (2nd generation)	Cobalt-Chromium	BioLinx tri-Polymer coating	Zotarolimus	4.0 % at 8 months[49]
Xience	DES (2nd generation)	Cobalt-Chromium	Vinylidene fluoride and hexafluoropropylene	Everolimus	18.2 % after 10 years[50]
Yukon PC	DES (3rd generation)	Stainless Steel	Poly-DL-lactic acid	Sirolimus (30 days)	20.3% after 10 years[50]
Orsio	DES (3rd generation)	Cobalt-Chromium	Silicon Carbide/poly-l-lactic acid polymer	Sirolimus (30 days)	3.2 % after 3 years[51]
Absorb	DES (4th generation)	N/A	Poly-l-lactic acid polymer	Everolimus	6% at 3 years[52,53]
BioFreedomTM	DES (4th generation)	Stainless Steel	N/A	Biolimus (2 days)	6.7% between 1 year and 5 years[54]

www.stentys.com; www.bostonscientific.com; www.medtronic.com; www.Biotroniks.com

2.3   Plasma Surface Modification

Plasma is known as one of the four states of matter, occurring naturally in the universe. It is an ionized gas that contains an equal number of positively and negatively charged particles, ions and electrons respectively, that move freely and randomly in an unbound gaseous state. In particular, the energy from an electrical source is built up from electron collisions and then imparted onto neutral gas particles, causing the formation of charged particles. The accumulation of charged particles consequently generates a non-thermal plasma where the electron temperature is at least 1 eV (11,604 K). Laboratory plasma is used to remove material or deposit material onto the surface of a sample such as stainless steel.

Plasma-based surface modification techniques are widely used on biomaterials to alter surface properties and ultimately enhance device performance.[55] Specifically, many low vacuum and atmospheric plasma processes have been used to deposit biofouling and anti-biofouling films on the surface of biomaterials to modulate cell adhesion and proliferation, control protein adsorption and improve blood compatibility.[55–57] Plasma processes, such as plasma sputtering, plasma implantation, plasma deposition, plasma spray, and atmospheric pressure plasma present advantages and disadvantages, making them uniquely suited for biomaterials applications.[58] A description of the plasma processes in addition to their advantages and disadvantages are outlined in **Table 2**.

Table 2. Comparison of low vacuum and atmospheric plasma processes.

Environment (Pressure)	Plasma Technique	Types	Description	Pros	Cons	References
Low vacuum	Plasma sputtering deposition	Magnetron sputtering	Low pressure sputtering method uses energetic ions from plasma to sputter the cathode target in the electric field and a magnetic field to trap the electrons to increase the collision rate between electrons and sputtering gas molecules, consequently depositing the target material on the sample surface.	Predictable and stable film deposition	Low deposition rate, takes a long time to coat sample; line-of-sight process, limited number of samples and poor coating coverage on complex shapes	10,11,59
	Plasma implantation	Plasma immersion ion implantation	Surface modification via implantation of high-energy ions	Good for 2-D samples	Poor uniformity; line of sight; alters the crystal structure of the sample below the surface	10,55,59–61
		Plasma immersion ion implantation & deposition	Formation of films by combining ion implantation and plasma deposition forming inorganic and organic coatings that can be doped or embedding nanoparticles on the near-surface of a sample.	Non-line-of-sight process; combines plasma deposition and ion implantation, modifies sample surfaces with irregular shape	Alters the crystal structure of the sample below the surface.	10,60,61

Table 2. Continued. Comparison of low vacuum and atmospheric plasma processes.

Environment (Pressure)	Plasma Technique	Types	Description	Pros	Cons	References
Low vacuum	Plasma deposition	Plasma enhanced chemical vapor deposition	A plasma source is used to initiate the formation of ions and radicals at the solid surface/gaseous interface leading to a new layer formed (organic or inorganic) on the sample's surface.	Low temperature, non-line-of-sight, high controllable deposition rate; organic and inorganic compounds can be deposited.	High cost of equipment; compressive and residual stress in films.	10,62
		Plasma polymerization based on PECVD	A plasma source is used to generate a gas discharge that induces the formation of radicals at the solid surface/gaseous monomer interface, then randomly recombines to form a polymer (organic).	High retention of polymeric functional groups.	High cost of equipment.	10,11,55,59,61
		Plasma grafting	Radicals are created on a polymer surface after exposure to plasma, followed by exposure to a monomer gas or a solution of monomer, thereby producing a graft copolymer.	Short modification time, only affects polymer surface.	Polymer must exist on sample surface prior to plasma treatment, poor repeatability.	55,59,61,63
		Dual plasma deposition	Simultaneous gas and metal plasma deposition is used to produce a film composed of multiple elements with varying compositions.	Films with multiple compositions, large area, uniform plasma deposition.	Low growth rate.	55
		Laser ablation	A laser beam is used to generate a plasma plume near the surface of a target. Particles are ejected from the target and transported to the sample producing a film.	Stoichiometric composition of target composition transferred to sample.	Surface topography varies from smooth to micro-roughened, Slow deposition rate, high local area temperature.	11,55

Table 2. Continued. Comparison of low vacuum and atmospheric plasma processes.

Environment (Pressure)	Plasma Technique	Types	Description	Pros	Cons	References
Atmospheric	Plasma spraying	Thermal plasma spray	A high temperature (>10,000°C) plasma jet, along with injected particles are subjected to an extremely high heating rate for a few seconds, creating molten particle droplets that are propelled toward the sample surface forming a coating.	Greater treatment depth	High temperature, thick coatings, sample's structural profile may be altered.	55,59
	Atmospheric pressure plasma	Corona plasma discharge	Plasma treatment consist of two parallel electrodes with a narrow gap between, one cylindrical shape electrode and a knife shaped electrode.	Treat large parts, and the interior of 3-D parts	Inhomogeneous plasma treatment of surface; Plasma is narrow, small treatment area.	61
		Dielectric barrier discharge (DBD)	Plasma treatment consist of two parallel electrodes with a narrow gap between, where either one or both electrodes are coated with dielectric material.	Operated at high pressure, capacitively coupled requiring AC voltage, plasma is uniformly distributed.	Plasma is narrow, small treatment area.	61
		Atmospheric pressure glow discharge/ plasma jet	Low voltage applied across balanced electrodes at high frequency.	Uniform and stable in comparison to DBD, low gas temperature and high electron temperature.	Transformation of glow to arc, plasma is narrow, small treatment area.	61

Plasma enhanced chemical vapor deposition (PECVD) process is performed in a low vacuum environment. The coating may be deposited onto a sample when plasma is generated using a gas precursor and an electrical source. An organic or inorganic coating may be formed depending on the precursor and experimental conditions. When an organic coating is deposited, the PECVD process is referred to as a plasma polymerization and the precursor is identified as a monomer. The plasma polymerization process alters low molecular weight monomers into high molecular weight polymers by plasma activation of the monomer into radicals and then recombination of the molecules to form an active polymer chain. Since the monomer is fragmented in the plasma the deposited coating may have a different chemical structure and elemental composition make up from conventional polymerization of monomers. Monomers such as methane, acetylene, silanes, and siloxanes are typical carbon and carbon-silicon based precursors employed in plasma polymerization. Plasma polymerization is a promising technique for depositing anti-biofouling coatings onto medical devices since it produces very thin coatings that retain the monomer's functional groups.

Capacitively coupled plasma (CCP) systems are the most commonly used plasma processes in the industry. In these processes, two electrodes are separated by a small distance, with one of the electrodes being connected to a power supply and the other to ground. The monomer used to generate the plasma may be excited by different types of electrical sources such as radio frequency (RF), direct current (DC), or pulsed-DC. When the gas monomer flows through the two electrodes (anode/cathode), as depicted in **Figure 6**, different species are generated, including electrons, ions and free radicals (unpaired electrons).

18
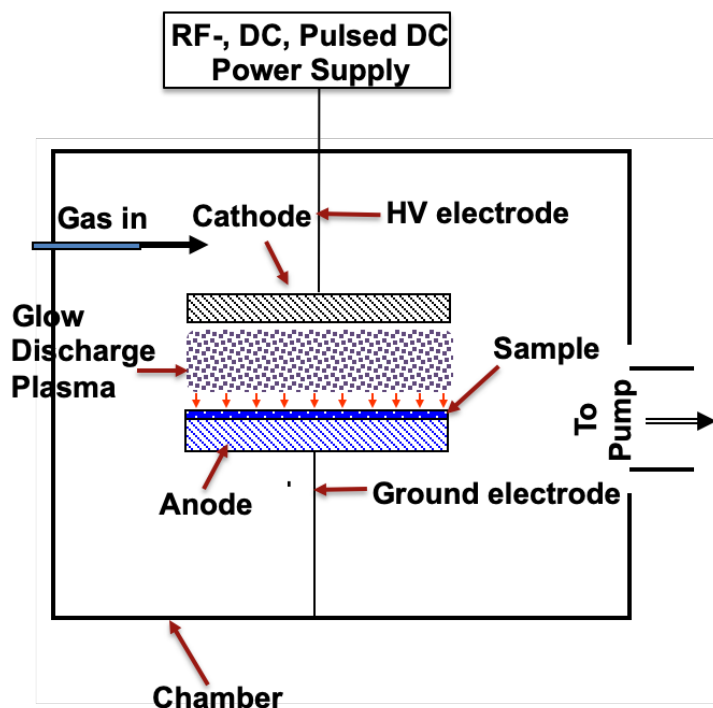
Figure 6. General schematic of plasma enhanced chemical vapor deposition (PECVD) chamber.

To sustain the plasma, molecules of the gas may be converted into ions as a result of collisions with the electrons.

$$MA \ (gas \ molecule) + e^- (electron) \rightarrow MA^+ (ion) + 2e^-$$
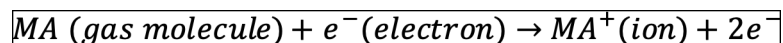
Similarly, gas molecules in the ground state may be promoted to various excited states

after colliding with a single or multiple electron as the kinetic energy is transferred.

$$MA \ (ground \ state) + e^- \rightarrow MA^* (excited) + e^-$$
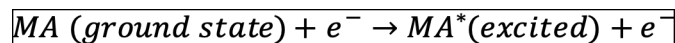
Now within the plasma there are multiple types of collisions that may occur:

Electron—electron
Electron—neutral gas molecule

Or electrons may transfer only a charge to gas molecules
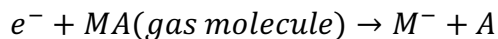
$$e^- + MA(gas\ molecule) \rightarrow M^- + A$$

Or gas molecules may undergo dissociative attachment or ionization

$$MA(gas\ molecule) + e^- \rightarrow M + A^-$$

$$e^- + MA \rightarrow M^+ + A + 2e^-$$
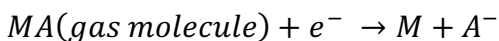
As well as
Positive ion—neutral gas molecule collisions
Negative ion—neutral gas molecule collisions

An example of electron -neutral gas collision such as methane will be discussed in the next few paragraphs.

The most commonly used power source for plasma generation is radio frequency (RF), generating a continuous waveform. The sample bias voltage is a key parameter in controlling the plasma polymerization process conditions. Typically, the voltage applied by a RF power supply is low in comparison to that applied in DC processes. Pulsed-DC power supplies serve as alternative technique to traditional RF systems, in that higher voltages can be achieved and more process control is attainable by pulsing the voltage on and off. Pulsing greatly decreases the potential required for arcing at the higher voltage and controls the gaseous collisions of the precursor molecules.

Most of the literature reports the use of RF-generated plasma to deposit anti-biofouling coatings.[40,41,64–69] Silicon oxide, titanium oxide and carbon-based coatings that have been

deposited onto biomedical samples using varying RF power result in slightly different coating compositions and physical properties depending on the fragmentation and rearrangement of species generated in the plasma.[64,68,70] New ions are generated through collisions of the carrier gas molecules (such as Ar) with ions of the precursor gas in the plasma. Precursor gases such as methane are present in abundance in comparison to the carrier gas. Precursor gas molecules like methane are ionized, fragmented and rearranged. The ionization and dissociation scheme for methane is shown in **Figure 7**.[71] The most prominent species that may be generated in pure methane plasma is shown in **Figure 8**.[72] The reactive species consist of free radicals, and positive and negative fragmented ions. The free radicals recombine forming covalent bonds increasing the size of the molecule.[73] The coating deposited on the surface consist of free radicals, which produces a new surface chemistry on the sample. The operating parameters such as RF power, voltage, gas pressure, and temperature can influence the different species generated in the plasma. Consequently, these parameters may be tuned to optimize the chemical and physical properties the deposited coating.

$$CH_4 + e^- \rightarrow \begin{cases} CH_4 + 2e^- & (1) \\ \cdot CH_3 + H + e^- & (2) \\ \cdot CH_2 + H_2 + e^- & (3) \\ \cdot CH + H_2 + H + e^- & (4) \\ CH_4^- & (5) \end{cases}$$
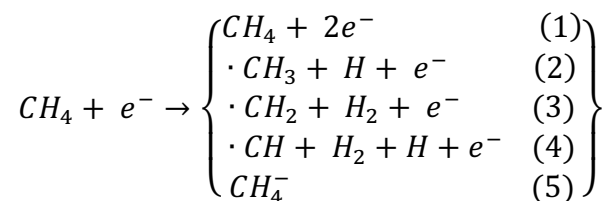
Figure 7. Species generated in the ionization, dissociation and electron impact process of methane.

$$H_2, C_2H_6, C_2H_4, C_2H_2, CH_3, CH_2, CH, C_2H_5, C_2H_3$$

Figure 8. Most prominent species that may be generated in pure methane plasma.

There are a few articles that discuss the effects of low and high RF power on a precursor, concluding that an inverse relationship exists between power and precursor functional group retention[11,39,74] For example, when methylacrylate is polymerized by RF plasma at lower power, the ester functional group is retained; however, at higher power, the ester functional group is lost.[74] Other operating conditions such as power, gas flow rate, non-reactive gas identity and concentration, and deposition time enable one to tailor the properties of the coatings.[68]

2.4 Radio Frequency And Pulsed-Direct Current Power Sources

Radio frequency (RF) power supplies with a frequency of 13.56 MHz, which is generally reserved internationally for industrial power supplies, are typically used on CCP systems. RF, DC, alternating current and pulsed-DC are a few of the power supplies that drive CCP systems. RF power supplies can be used with most materials; however, they are typically used to deposit dielectric material. Dielectric materials are insulators such as silicon oxide or aluminum oxide, which are used to coat small parts. DC power supplies are used mostly for depositing metals; however, in some cases they may be used to deposit dielectric material.

In contrast to RF, DC uses higher voltages (1.0 kV – 800 kV) than an RF source (10 V – 2.5 kV). At higher voltages the deposition rate is increased leading to faster breakdown of the chemical precursor. When a dielectric material such as silicon oxide or aluminum oxide is placed in an electrical field, current does not flow through the material as it would through electrically conductive materials like metals due to its behavior as an insulator. Breakdown of the dielectric material may occur as a result of concentrated

applied voltage exceeding the conductivity of the dielectric material, thereby introducing an electrical arc through the material to the sample. Furthermore, the dielectric material is removed leaving behind a small pit within the exposed sample.

To maintain the plasma and reduce arcing, pulsed-DC with pulses of a few to a few tens of microseconds is commonly used. The short on and off pulses can sustain the plasma and reduce arcing, thereby reducing potential damage to the sample's surface. Lewis et al. illustrated the difference between continuous wave (CW) excitation such as RF and pulsed-DC PECVD with an organo-silane.[75] As a result of continuous ion bombardment with CW excitation, the as-deposited coating exhibited more cross-linking as a result of increased fragmentation of the precursor gas, while pulsed-DC maintained more of the precursor's structure.[75] Another study by Prasad et al. demonstrated changes in the fragmentation of a precursor gas at different RF powers, resulting in different chemical and physical properties of the as-deposited coating.[64] There is only one parameter, power (P in Watts) i.e. the product of voltage (V) and current (A), that can be varied directly on an RF- power supply. Other parameters that may be altered in the process are the time of exposure, gas flow rate, and precursor gas concentration. On the other hand, many additional parameters can be varied in a pulsed-DC supply to tailor precursor fragmentation including applied voltage, pulse width and pulse frequency resulting in, various degrees of fragmentation of the precursor gas being easily achieved.

In principle, pulsed-DC is able to create a favorable number of reactive neutral species in the plasma, thereby reducing the amount of ion bombardment observed with RF-PECVD and leading to more controlled fragmentation of the precursor gas. In pulsed-DC, when

the excitation source is switched off for a few microseconds, excited ions are allowed to

drop to lower energy levels. This contrasts with RF-PECVD processes in which

continuous bombardment of species occurs. This type of control can allow for more

selective design of the chemical and physical properties of surfaces coated via pulsed-DC

processes than with traditional RF techniques. Studies have reported approximately

three-fold improved adhesion of polymer-like coatings (PLC) to stainless steel by using

pulsed-DC in comparison to RF with a PECVD setup.[38] PLC and silica like coatings

(SLC) are traditionally observed in plasma polymerization processes using organo-silanes

where low vacuum pressure and low bias potential generates amorphous structures.

PLC are high in hydrocarbons showing high content of CH, CH_2 and CH_3 bonds.[76] Non-

PLC are generally composed of amorphous carbon with a mix of sp^3 (C-C) and sp^2 (C=C)

carbon bonds. SLC bonds consist of bonds similar to those in non-PLC, along with Si-C

bonds and Si-O bonds.

A logical study on the effect of pulsed-DC plasma source in relation to the plasma

chemistry, surface chemistry, surface wetting and coating bio-fouling properties was

performed in this work to gain a better understanding of the relationship between

plasma current source characteristics and coating performance.

2.5 Organo-Silicon Coating Chemistry

Research on organo-silicon coatings continues to be of interest in the biomaterials

industry because of their potential application as anti-biofouling coatings for stents and

other bioimplants. Recent studies, have shown a reduction in fibroblast adhesion to

organosilicon-coated 316 stainless steel and titanium samples.[77,78] While preventing

biofouling of select cells is important, modulation of cell adhesion, detachment and proliferation on bioimplants is a very desirable property. Wei et al. demonstrated that by changing the wetting properties of an organosilicon coating from hydrophobic (106 °) to superhydrophilic (0 °), cell attachment and proliferation of fibroblast cells change. The cell study showed that the more hydrophilic the surface is, the higher the attachment and growth rate of fibroblasts.[79] In general, organosilicon coatings have been shown to inhibit or promote cell attachment to samples used for bioimplants depending on their properties.

Organosilicon chemistry consists of compounds with carbon-silicon bonds. At the same time, silicon is an element that is consistently found in many functional groups such as silanol (Si-OH), siloxides (Si-O-Metal) and siloxane (Si-O-Si). Siloxanes are manufactured compounds with varying chemical formulas ranging from $(R_3SiO)_2$ to $(RSiO_{1.5})_x$. The general chemical formula for silicones is $(RSiO)_x$, where R is an organic group such as methyl or ethyl. Most of the development of organosilicon compounds focuses on silicones. Silicones are naturally made or manufactured polymers that are comprised of repeating siloxane linkage.

Organo-silicon (polymer-like silica) coatings reveal hydrophobic wetting and retention of methyl groups, consequentially exhibiting similar chemical composition as polydimethylsiloxane. SLC, produced by plasma polymerization based on PECVD techniques have been shown to be effective at reducing protein and cell adsorption, similar to conventional solution-based coating methods.[80,81]

A common approach to prepare organo-silicon coatings is silanization, wherein hydrolysis and condensation of a silica surface has been used for coupling metallic/polymeric surfaces with polymers.[24,25] For example, Alcantar et al. applied this concept by using a silane precursor (SiH_4) along with water plasma to create a silanol (Si-OH) coating; the hydroxyl group was then chemically reacted with the hydroxyl end groups of poly(ethylene glycol) (PEG) to form a covalent Si-O-C ether bond.[26] The approach was considered an easier, more commercially viable method of depositing PEG. However, pure silane is a toxic precursor. To date, more environmentally friendly and less toxic silane-like precursors have been developed such as hexamethyldisiloxane (HMDSO) or trimethylsilane (TMS).

HMDSO is a monomer that can be reacted with other monomers to form a polymer chain via traditional polymerization and plasma polymerization processes. A coating made from monomers such as HMDSO may be termed polymer-like coatings (PLC) when deposited by PECVD. These coatings typically exhibit hydrophobic properties because of the presence of the methyl groups on the surface. The hydrocarbon composition of these coatings influences their wetting properties. Coatings or samples without hydrocarbon contribution such as ceramics are known to act as hydrophilic surfaces, typically repelling proteins and cells.[40,41,64]

A few different studies have shown that by using RF-PECVD with HMDSO, an anti-fouling coating can be deposited onto a stainless-steel sample.[40,82,83] Specifically, these studies have investigated the effect of power-to-flow rate ratio on coating characteristics, indicating that an increase in the ratio of power to flow rate increases the fragmentation

of HMDSO when deposited onto the sample surface.[84,85] RF plasma polymerized

HMDSO coatings that have low fragmentation and retain most of their organo-silicon

structure bind tightly with biological species such as the protein albumin and smooth

muscle cells because of their hydrophobic wetting properties.[40,82,83] However,

HMDSO/O_2 coatings that have a high degree of fragmentation exhibit more silicon-oxide

characteristics and tend to be less likely to interact with cells, because of their hydrophilic

behavior.[40]

Ceramics such as silicon oxide have been deposited on metal and glass surfaces using

HMDSO/O_2 PECVD techniques.[20–22,41,64] Silicon oxide offers unique coating properties

such as lower non-specific adhesion of aortic smooth muscle cells, improved coating

adhesion to sample because of the Si-O bond, and an interactive layer for increased

binding with hard-to-adhere coatings, such as polytetrafluoroethane (PTFE) or other

polymers.[23] Silicon oxide coatings have been successfully deposited by RF-PECVD and

exhibited low adsorption of fibrinogen in comparison to bare stainless steel.[39]

Amorphous silicon carbide coatings have been shown to reduce fibrinogen adhesion[86],

platelet adhesion and smooth muscle cell adhesion,[87,88] which may prevent the formation

of blood clots and restenosis. Moreover, when these coatings are exposed to endothelial

cells rapid adhesion of endothelial cells and the rapid formation of a continuous layer on

the coated surface is demonstrated. A key question to ask is what physical property of a

coating may prevent select molecular components from adhering to the surface and allow

others to adhere? The event is caused by the exchange of electronic properties between

the protein to the coating. Both the coating (amorphous silicon carbide) and fibrinogen

have similar electronic properties ~1.8-2 eV,[88] preventing the transfer of electrons and

hindering protein, platelet and smooth muscle cell activation. On the other hand, albumin

conduction band is smaller (1.48 eV)[89] enabling electron exchange with amorphous

silicon carbide leading to albumin and endothelial cell adhesion.

.

In this work, we have fabricated an organo-silicon and silicon oxycarbide coatings

using pulsed-DC PECVD that range from hydrophobic to hydrophilic moreover to

study the effect of varying both the chemical and wetting properties of the coatings

and their biofouling properties.

2.6   Projected Impact Of Research On Biomedical Market

In 2015, the biomedical coatings market was estimated at over $9 billion dollars per year

and is expected to continue to rise.[90] Specifically, anti-biofouling coatings are about

10 % of the biomedical coatings market.[91] Moreover, coating development in the anti-

biofouling area is still evolving with novel applications in smart systems and sensors for

heart monitoring, as well as advancing technologies related to antimicrobial surface

coatings for infection prevention. The work detailed in this dissertation will aid in

discovering the parameters for which plasma chemistry and as-deposited coating

composition can be tailored using pulsed-DC PECVD to result in coatings that selectively

inhibit protein adsorption and cell adhesion. The mechanism by which fragmentation of

the chemical precursors relates to voltage and pulse cycle will offer insight into the

design of new coating compositions for both barrier coatings and drug-eluting stent

coatings. This study could influence stent coating technology, possibly resulting in a

reduction in the number of cases of coronary obstructive disease related to in-stent

28

restenosis, increased patient survival rate, and reduced probability of myocardial

infarctions after several years of implantation.

3. PLASMA ENHANCED CHEMICAL VAPOR DEPOSITION OF HEXAMETHYLDISILOXANE COATING

3.1 Introduction

This chapter focuses on surface modification of stainless steel (SS) through the use of plasma enhanced chemical vapor deposition of hexamethyldisiloxane (HMDSO). The effect of key process parameters (voltage and precursor flow rate) on the modulation of coating chemistry and hydrophilicity for the preparation of anti-biofouling coatings is discussed. The coatings discussed in this chapter were deposited by using a pulsed-DC plasma enhanced chemical vapor deposition (PECVD) process. Southwest Research Institute® (SwRI®) has conducted prior work generating diamond-like-carbon (DLC) coatings with pulsed DC PECVD using glow discharge and hollow cathode methods on metallic samples.[92–94] With regards to the PECVD process, gas molecules are dissociated, ionized and activated using a power supply. PECVD is an advantageous alternative to traditional chemical depositions in that a number of new chemistries can be created from a single chemical precursor. RF power supplies are typically used in industrial and research applications. However, pulsed-DC power supplies offer significant advantages to RF in regards to control over precursor breakdown and reduction in arc discharge.[95] Pulsed-DC PECVD glow discharge offers flexibility in part size, shape, and quantity. In this work, pulsed-DC PECVD glow discharge process was used to break down HMDSO in a controlled manner. The deposited coatings are viable options for use on cardiovascular stents and other biomedical materials/devices.

3.2 Background

Plasma is a state of matter in which an equivalent number of positive and negatively charged particles move arbitrarily and freely within an unbound gaseous state. Plasma is known as one of the fourth states of matter, occurring naturally in the universe. It is currently thought that 99% of the visible material in the universe consist of plasma. This includes the sun, stars and other interstellar mediums. However, in earth's atmosphere the low temperature and high pressure does not prove favorable for the formation of plasma except for certain conditions. Therefore, plasma is generally artificially generated on earth. The reader should refer back to Section 2.3 and 2.4 for a more detailed discussion on plasma modification and the power sources. The reason for artificially generated plasma on earth is understood by the Saha equation, which determines the amount of ionization expected in a gas at thermal equilibrium:

$$\boxed{\frac{n_i}{n_n} \approx 2.4X10^{21} \frac{T^{\frac{3}{2}}}{n_i} e^{-U_i}/_{KT,}} \text{ (eq. 1)}$$

n_i and n_n represents the density of ionized and neutral atoms

It is understood that the fractional ionization $\boxed{n_i/n_n}$ will remain low until the ionization energy $\boxed{U_i}$ is only a few times the Boltzmann constant (K) and temperature (T), pushing the gas to a plasma state.[96] As the temperature rises, the kinetic energy in the neutral gas atoms increases. At high enough temperatures (>11,604K or 1eV), when atoms collide, a valence electron is released and the gas atoms are ionized, thereby decreasing the density of neutral atoms in the gas compared to the density of ionized atoms. Once the density of ionized atoms exceeds the density of neutral gas atoms, the plasma becomes fully ionized.

There are many ways in which plasma may be artificially generated on earth. One way is by applying an electrical current across a gas to produce an electric discharge in the gas known as plasma discharge.[97] The amount of discharge plasma generated depends on the geometry of the apparatus, gas type, pressure, and electric field strength.

Plasma discharge can be divided into two categories. The first type is "thermal" plasma similar to naturally-occurring plasma, being produced at high pressures (>10kPa) and high temperatures. The second type is "cold" discharge plasma that is characterized by low temperature gas particles (T_g) and high temperature electrons (T_e) in a relatively low-pressure environment. Both classes of discharge plasma use an electric source to generate plasma. A few examples of electrical sources are direct current or alternating current (DC or AC), radio frequency (RF), or microwave (MW) sources.

PECVD creates a glow discharge plasma that maybe generated using any of the electrical sources discussed in Section 2.4. Although RF power source are typically used in this process, other sources such as pulsed-DC are simpler to operate and offer more control when maintaining and manipulating the plasma via application of high voltages between electrodes for short microsecond intervals, thereby exciting the gas molecules to higher energy states and then allowing the excited molecules to fall to lower energy states between intervals. This provides better control of the fragmentation of precursor molecules and therefore of the composition of the deposited coating. The general fragmentation mechanism of HMDSO has been studied, as shown in **Figure 9**.[98]

$$((CH_3)_3Si)_2O + e^- \rightarrow (CH_3)_3SiO + (CH_3)_3Si + e^- \quad \text{Breaking of Si-O bond}$$

$$SiCH_3 + e^- \rightarrow Si + CH_3 + e^- \qquad\qquad\qquad \text{Breaking of Si-C bonds}$$

$$CH_3 + e^- \rightarrow CH_2 + H + e^- \qquad\qquad\qquad \text{Breaking of C-H bonds}$$
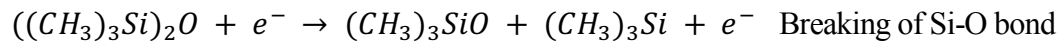
Figure 9. Ionization and dissociation of HMDSO

3.3 Deposition Of Organo-Silicon Polymer-Like And Silicon Oxycarbide Coating

This section includes a description of the experimental set-up and protocols used for plasma deposition of organo-silicon and silicon oxycarbide coatings.

3.3.1 Materials

3.3.1.1 Reagents

HMDSO was purchased from Millipore Sigma (St. Louis, MO, USA) and used as received. An argon gas cylinder was purchased from Airgas® (Radnor Township, Pennsylvania, USA) and used as received. 316 L (size-150 mm x 150 mm, thickness-0.125 mm) and 321 (100 mm x 100 mm) SS foil samples were purchased from Goodfellow (Coraopolis, Pennsylvania, USA). The foils were cut down into four 50 mm x 50 mm pieces for coating.

3.3.1.2 Plasma Reactor

A custom-built plasma reactor designed by SwRI was employed in all experiments conducted within the scope of this dissertation (**Figure 10**). This system is currently designed for two different processes in a single vacuum cycle: plasma treatment and plasma polymerization. The main components of the reactor system are a plasma chamber, vacuum system (turbo and mechanical pump), gas manifold, liquid flow controller system (not shown), power supply system, and process monitoring system (not

shown-oscilloscope which monitors the peak-to-peak voltage and current in plasma

treatment and plasma polymerization process), illustrated in **Figure 10**. **Figure 11**,

shows the inside of the plasma chamber.
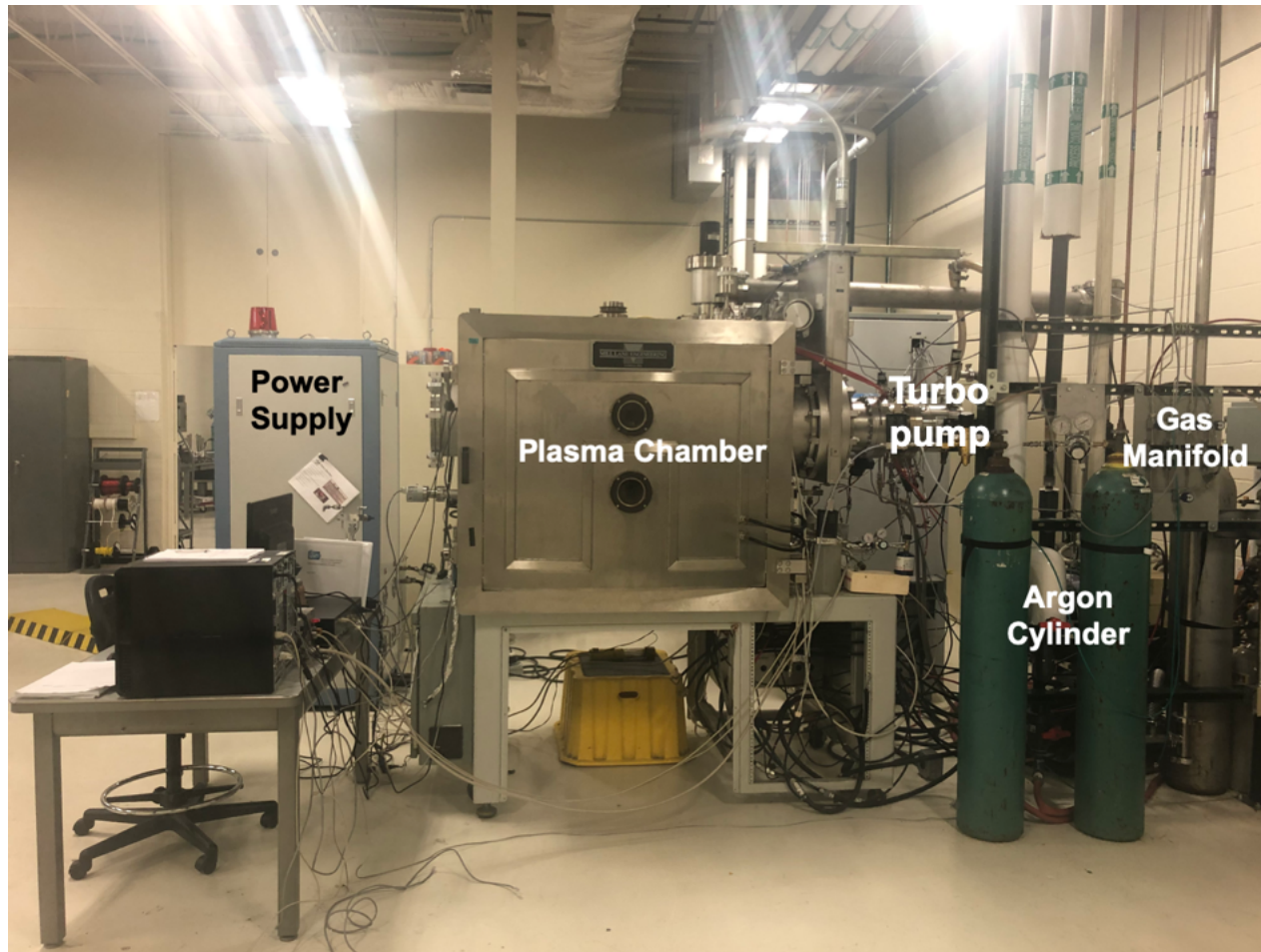
Figure 10. Research-grade plasma chamber system designed and assembled by SwRI.
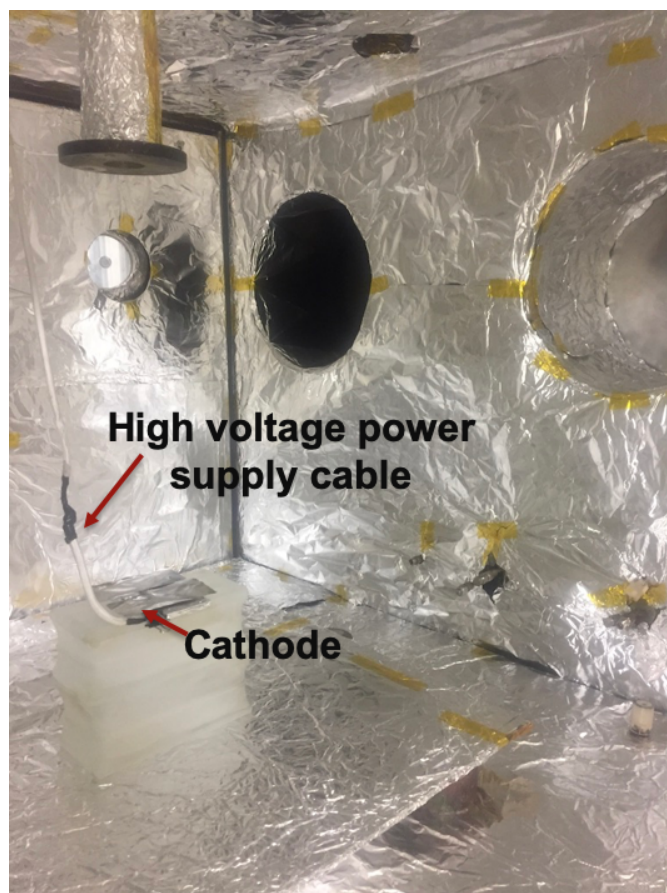
Figure 11. Research-grade reactor for pulsed DC plasma polymerization designed and assembled by SwRI.

The main electrode configuration assessed in this study was the horizontal parallel plate configuration. In this configuration, the sample to be coated is placed between two parallel plates that serve as a cathode and anode, respectively. **Figure 12** illustrates the parallel plate setup employed in the reactor. The precursor gas and carrier gas were introduced into the reactor through a single port on the side of the reactor.
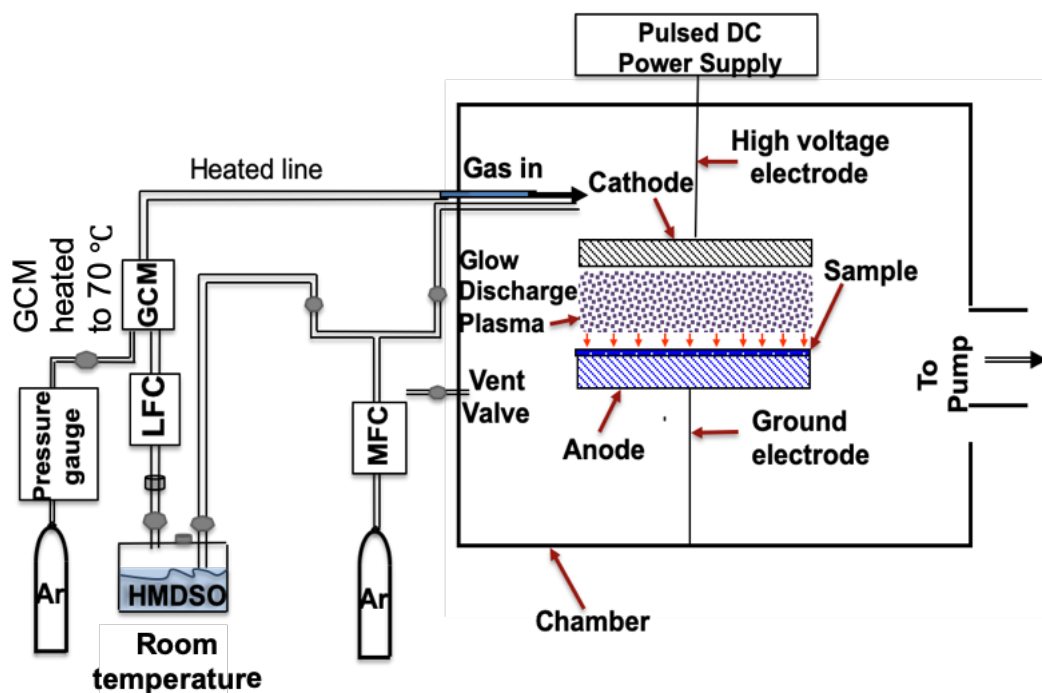
Figure 12. Schematic of the of the plasma reactor system. GCM-heated gas chamber mixer, MFC-mass flow controller, LFC-liquid flow controller, HMDSO-hexamethyldisiloxane, Ar-argon.

The main body of the reactor consist of a SS rectangular vacuum chamber of approximately 4 ft x 4 ft in size. There are two viewports on the chamber door and three more viewports on the other sides of the chamber. Each viewport is equipped with a Pyrex glass window to allow for observation of the plasma process. An orifice on top of the chamber allows for introduction of powered wiring or sensor wiring (i.e. high voltage probe and current sensor). The metal sample holder and electrode were configured inside the chamber and isolated from ground using ceramic spacers. The chamber walls serve as ground in this setup.

Gases can be introduced into the reactor through a mass flow controller (MFC) and liquid flow controller (LFC). The LFC is preferred for monomer introduction since MFCs' are traditional calibrated for less complex gases such as nitrogen and argon (Ar). The carrier

37

gas, Ar, is controlled by the MFC. Ar is pumped in using an Ar gas cylinder.

The liquid monomer, HMDSO, is held in a SS bubbler from STREM Chemicals, Inc.

(Newburyport, MA) equipped with an inlet and outlet, along with an internal dip tube.

HMDSO is transferred into the reactor chamber by bubbling a carrier gas (Argon)

through the container. The bubbler is maintained at room temperature during this

process. The liquid-gas flow system was setup to heat the monomer (70 °C) in the

Bronkhorst® (Ruurlo, Netherlands) gas chamber mixer (GCM). The monomer and Ar

gas are premixed in the GCM prior to flowing through the gas lines and entering the

chamber. The gas lines after the GCM were wrapped and heated to 70 °C with heat tape.

A differential pressure is required to introduce the monomer vapor into the chamber; this

differential was created by vapor pressure generated at the HMDSO liquid-gas interface.

The monomer evaporates and flows into the chamber once the partial pressure is equal to

the monomer's vapor pressure at the corresponding temperature.

3.3.1.3 Electrical Power Source

A pulsed, high-voltage DC source, PM- 200 A Pulse Modulator, capable of generating up

to 3000 V and 200 A was employed for this study. The pulse width, voltage and

frequency are adjustable on this system. For this study, the voltage was set to 1000 V

and 1500 V; the frequency and pulse width were held at 0.500 kHz and 20 μs,

respectively. These parameters were selected based on past experience of SwRI staff

with similar chemical precursors and this power supply.

3.3.2   Methods

3.3.2.1 Protocol for Plasma Polymerization Processes

This section describes the entire protocol for generation of coatings, detailing the steps employed to prepare the plasma-deposited film on the sample. The process consists of several preparative steps, followed by the plasma deposition process:

Step 1. Sample preparation and cleaning

Prior to coating, all SS samples were cut down to size (50 mm x 50 mm). The samples were then introduced into a beaker with isopropanol, placed into an ultrasonic bath for 20 minutes and then dried with a lint-free Kim-wipe. Each sample was then taped down with Kapton tape to the sample holder (cathode) and loaded into the chamber. The chamber was evacuated to a base pressure of at least 10-6 Torr. The chamber pressure was set to 40 mTorr for the plasma cleaning process. Prior to eliciting a plasma 90 sccm's of Ar was introduced into the system to bring the chamber pressure up to 40 mTorr. The pulsed-DC power supply operated at 1000 V with a pulse width of 20 microseconds. The samples were then plasma-cleaned in the chamber for 10 or 30 minutes. The process parameters used for plasma cleaning are described in Table 3. The same cleaning process was utilized for the silicon samples.

Table 3. Plasma cleaning process parameters.

Parameters	Chamber Pressure (mTorr)	Gas Types	Gas Flow Rate (sccm)	Pulse Width (µs)	Applied Voltage (V)	Applied Current (A)	Frequency (Hz)	Time (min)
1	40	Ar	90	20	1000	0.23	500	10
2	40	Ar	90	20	1000	0.23	500	30

SCCM = standard cubic centimeters per minute

Step 2. Organo-silicon and silicon oxycarbide deposition

After plasma cleaning, with the samples still in the chamber, the precursor flow line for

HMDSO was purged for 30 minutes or until the flow rate stabilized to either 2 or 3 g/hr,

depending on the deposition process to be carried out. The plasma was generated by

applying a high voltage (1000 – 1500 V) to the cathode. During plasma polymerization,

the peak-to-peak voltage and current were monitored using an oscilloscope. Visual

inspection and adjustment of the plasma was carried out frequently to ensure that arcing

or local glowing did not arise, which could cause negative effects to the film properties

such as pitting and inconsistency in the coating. The chamber pressure, percent opening

of throttle valve, gas type, gas flow rate, voltage, current, frequency, and pulse time were

recorded for the coating of all samples and are shown in **Table 4**. The deposition of each

coating was carried out using the following procedures: both Ar and HMDSO were

introduced into the chamber for approximately 10 minutes before the power source was

initialized. Ar was introduced at a flow rate of 90 standard cubic centimeters per minute

(SCCM), while HMDSO was introduced at either 2, 2-3, or 3 g/hr depending on the

sample. In regards to the 2-3 g/hr flow rate, the flow is initial set 2.0 g/hr for 4 minutes

and then increased to 2.5 g/hr for 4 minutes and finally 3.0 g/hr for 9 minutes.

The deposition time is increased from 10 mins to 17 mins to allow the flow rate to

stabilize between each set point. The 2-3 g/hr range was carried out as a result of

previous experiments at SwRI which revealed the highest water contact angle (WCA) on

samples coated with this setting. A high WCA is understood to reduce cell adhesion.

Table 4. Plasma polymerization process parameters.

Sample ID	Chamber pressure (mTorr)	Gas Types	HMDSO Flow Rate (g/hr)	Argon Flow Rate (sccm)	Applied Voltage (V)	Applied Current (A)	Frequency (Hz)	Time (min)
2g-1000V-SS 321	40	Ar/HMDSO	2	90	1000	0.23	500	10
2g-1500V-SS 321	40	Ar/HMDSO	2	90	1500	0.24	500	10
2-3g-1000V-SS 321	40	Ar/HMDSO	2-3	90	1000	0.23	500	17
2-3g-1500V-SS 321	40	Ar/HMDSO	2-3	90	1500	0.24	500	17
3g-1000V-SS 321	40	Ar/HMDSO	3	90	1000	0.23	500	10
3g-1500V-SS 321	40	Ar/HMDSO	3	90	1500	0.24	500	10
3g-1000V-SS 316	40	Ar/HMDSO	3	90	1000	0.23	500	10
3g-1500V-SS-316	40	Ar/HMDSO	3	90	1500	0.24	500	10

SCCM = Standard Cubic Centimeters per Minute

3.3.3   *Physical and Chemical Characterization Techniques*

The coating thickness was measured using a Dektak contact profilometer. Silicon

substrates were used for these measurements. A Ramé Hart goniometer was used to

assess the changes in the wetting properties before and after coating. The chemical

composition was identified using Raman spectroscopy using the Horiba Lab Ram 532 nm

laser. Prior to measuring the thickness, the coated silicon and stainless steel foil samples

were ultrasonically cleaned in isopropanol for 30 minutes and then dried with a lint free

Kim-wipe.

3.3.3.1 Contact Profilometry

A Dektak profilometer was used to measure the average coating thickness on all samples

coated in each deposition. A silicon sample was used to measure the coating thickness.

A line scan was taken in three locations across the sample. The step height of the three

locations were averaged for each sample and distinguished as the average coating

thickness. The scan range was set to 2000 μm. The measuring range, stylus tip force and

radius were set to 65 μm, 2 mg, and 12.5 μm, respectively.

3.3.3.2 Goniometry

A Ramé Hart (Model 190) goniometer system was used to measure the static water

contact angle along the surface of the uncoated and coated samples. A 10 μl droplet of

deionized water was released using a micro-pipette on to the surface.

The Ramé Hart DROPImage CA software was employed to measure the water contact

angle on the samples automatically.

3.3.3.3 Raman Spectroscopy

The chemical composition of the coating and uncoated sample was characterized using Raman analysis at SwRI. Raman is a non-destructive technique that interacts light with the chemical bonds within a material to observe vibrational, rotational and low frequency mode changes.[99] The coating composition was evaluated in three different locations within the middle of the sample. The Raman system is equipped with a confocal microscope. A 100 X objective lens was used to integrate the surface. A 532-nm laser along with a 25% or 10% neutral density filter was employed. The spectral range that was assessed was 100-3500 cm^{-1}.

3.4 Statistical Analysis

At least 3 – 7 data points were collected on each sample for voltage, current, WCA and thickness measurements. Data is expressed as average +/- standard deviation in between the means of replicate measurements of independent samples. The effect of the voltage and precursor flow rate on the average peak-to-peak voltage and current generated during the coating deposition process was analyzed using a two-sample t-test. The influence of the voltage and precursor flow rate on the thickness of the HMDSO-coated samples was evaluated using the two-sample t-test. Lastly, the effect of the voltage and flow rate on the water contact angle of all the HMDSO-coated samples was examined. All the studies considered a p-value of <0.05 as statistically significant.

3.5 Results And Discussion

3.5.1 Plasma Cleaning Process on 321 SS Foil Samples

Ar plasma cleaning is typically used to improve the coating's bond to the sample surface by removing contaminants such as oxides and organic molecules that are commonly found on the surface of the samples that are exposed to air. Ar plasma cleaning does not roughen the surface or oxidize the surface as oxygen plasma cleaning does. Ar plasma cleaning is used to break the bonds of the contaminants on the surface and generate lighter more reactive molecules (CO, OH, H_2O) that can be pumped out of the system or aid in the adhesion of new material on the sample surface. Polar hydroxyl molecules generated during plasma cleaning may be deposited on the surface of the sample, increasing the surface energy, increasing the wettability and improving the adhesion of a coating. The first set of samples were plasma cleaned for 10 minutes before polymerization of HMDSO. The coatings on these samples exhibited poor adhesion and were easily wiped off with gentle rubbing. This is probably due in part to a significant number of organic impurities remaining on the surface. The rest of the samples were plasma cleaned for 30 minutes prior to polymerization. The adhesion was significantly improved, establishing durable coatings that could not be wiped away. The extended plasma cleaning process removes most of the organic contaminants from the sample surface, allowing for better interaction between hydroxyl groups on the surface and HMDSO precursor.

3.5.2 Plasma Polymerization of HMDSO on 321 SS Foil Samples

When the trough-to-crest of the current or voltage is measured it is known as peak-to-peak current or voltage. These measurements are carried out during the deposition

process using an oscilloscope. An example of the peak-to-peak voltage and current observed on the oscilloscope is shown in **Figure 13**. When applying 1000 V to the cathode, the measured peak-to-peak voltage is nearly constant (~3000 V) at all three different HMDSO flow rates, as shown in **Figure 14**. The peak-to-peak voltage t-test showed that the only statistically significant difference is between the 3g/hr samples at 1000 V vs at 1500 V. The samples that are identified as undergoing only chemical or plasma cleaning did not undergo plasma polymerization and had a peak-to-peak voltage and current of zero during the plasma polymerization process. Chemically cleaned samples are cleaned with isopropanol while plasma cleaned samples only undergo plasma cleaning process.
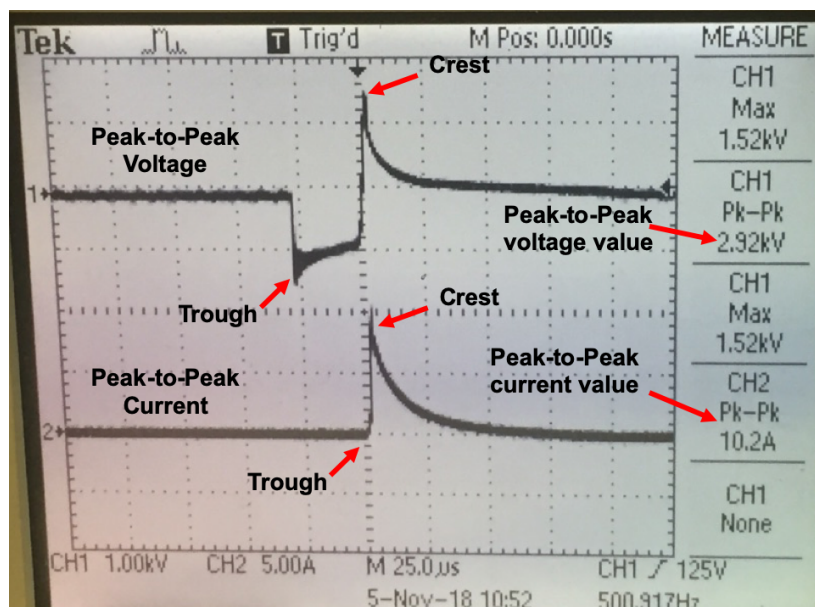
Figure 13. Oscilloscope image of peak to peak voltage and current during plasma polymerization process.
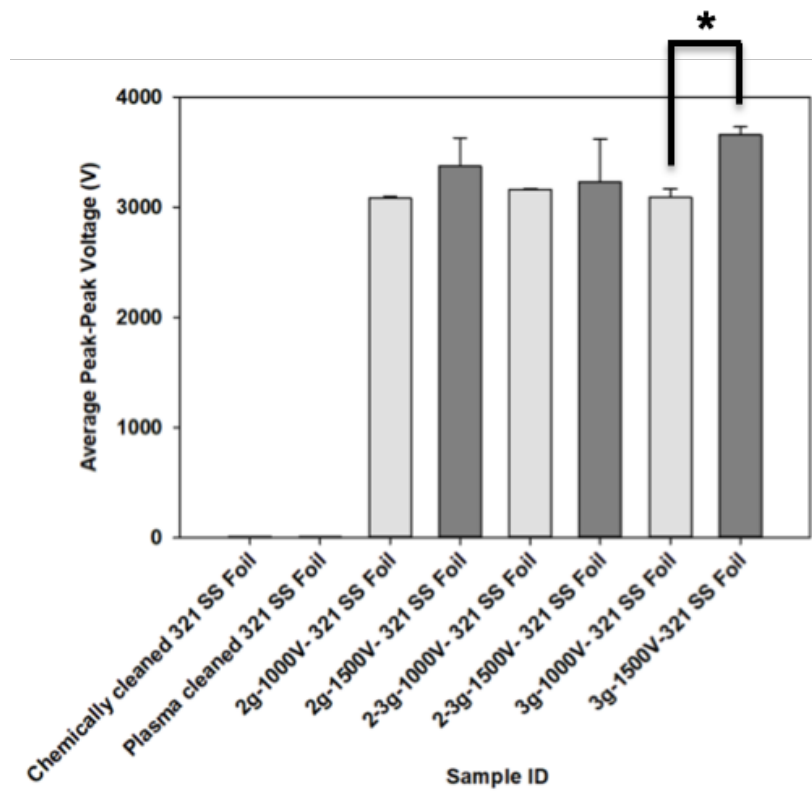
Figure 14. Average peak to peak applied voltage for HMDSO coatings (2, 2-3, and 3 g/hr) applied at 1000 V and 1500 V onto 321 SS foil. Error bars represent the standard deviation between replicates (n=3).

The peak-to-peak voltage increases by approximately 500 V when the applied voltage is raised to 1500 V on the samples coated with 3 g/hr HMDSO flow rate. At 1500 V (30 A), the current is 3X times more than at 1000 V (10 A) for all sample flow rates, as shown in **Figure 15**. This change in peak-to-peak voltage and current when the applied voltage is increased is expected. The peak-to-peak voltage observed for each applied voltage is a good indication that there is enough energy to sustain the plasma. The results of the peak-to-peak current t-test revealed a statistical difference between 1000 V vs 1500 V for all three flow rates and between the 2 and 3 g/hr for 1500 V.
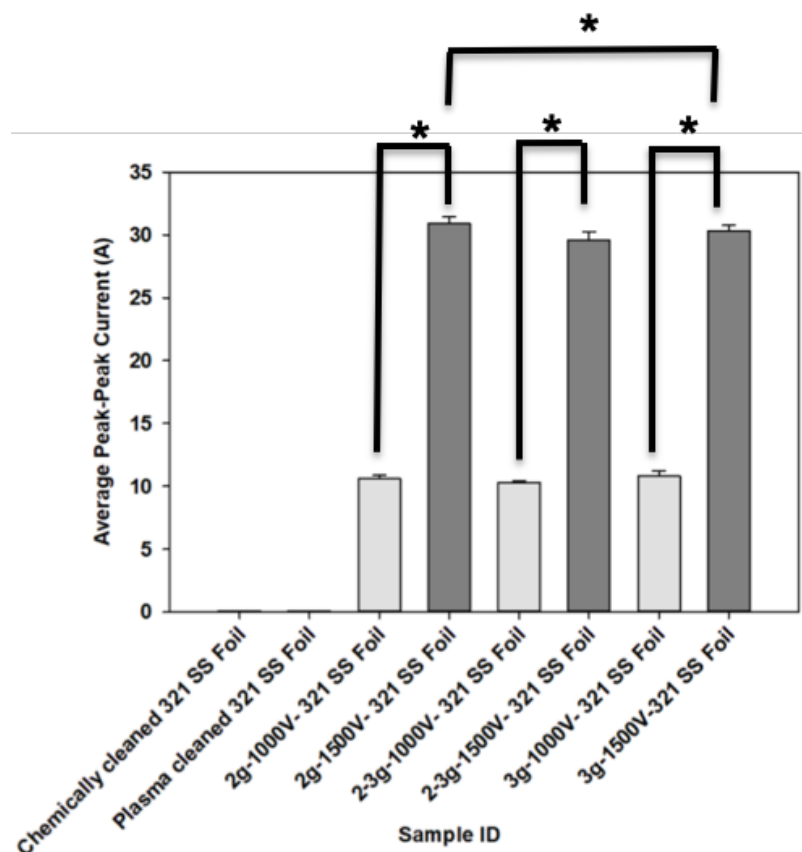
Figure 15. Average peak to peak current for HMDSO coatings (2, 2-3, and 3 g/hr) applied at 1000 V and 1500 V onto 321 SS foil. The error bars represent the standard deviation between replicates (n=3). Statistically significant difference compared with the applied voltage (*$p<0.05$) for each of the flow rates 2, 2-3 and 3 g/hr.

Figure 16 shows the thickness of the coatings as measured via profilometry. The coating thickness, wetting performance, and composition, as well as the flow rate and applied voltage utilized for generation of such coating are all interdependent. Focusing only on the flow rate, it was shown that between 2 g/hr to 2-3 g/hr, the coating thickness is increased with increasing flow rate for both 1000 V and 1500 V, respectively (**Figure 16**). In contrast, when the flow rate is increased to 3 g/hr, along with an applied voltage of 1000 V an increasing coating thickness is not observed. With 3 g/hr HMDSO flow rate, the coating thickness is ~ 25 nm lower than for coatings deposited with the lowest

HMDSO flow rate of 2 g/hr. This reduction in thickness was not expected; however, the

thickness could have been lowered as a result of some material being etched away by Ar

plasma or slightly shorter treatment time. At 1500 V, the coating thickness for samples

generated at 3 g/hr followed the expected trend in which the coating thickness increased

by ~115 nm. A similar trend was observed by Bahavana Peri, demonstrating that the

coating thickness increases with raising the flow rate.[100] The results of the t-test revealed

that the only statistically significant difference is between the 2-3 g/hr for 1000 V vs

1500 V for the coating thickness on 321 SS samples.
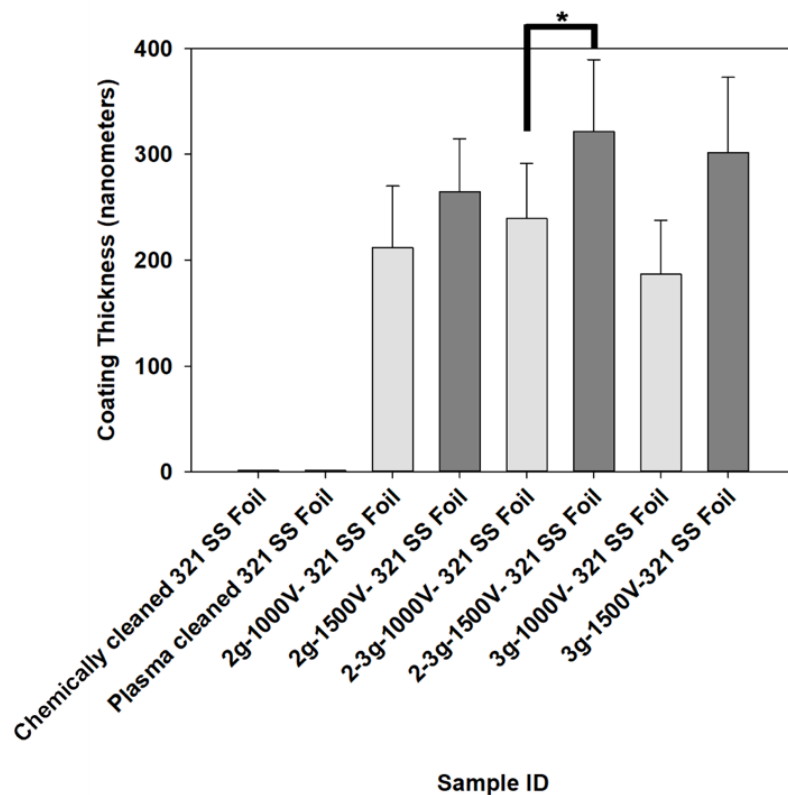
Figure 16. Average coating thickness on 321 SS foil before and after coating with
HMDSO at different flow rates and voltages. Bars represent the average coating
thickness, while the error bars represent the standard deviation between the means of
replicate measurements on independent samples (n=3). Statistically significant difference
compared with the applied voltage (*$p<0.05$) for each of the flow rates 2, 2-3 and 3 g/hr.

The wetting properties of the coatings vary based on the flow rate and applied voltage (**Figure 17**). Coatings that are deposited with an applied voltage of 1000 V exhibited a rise in the water contact angle (WCA) values with the changing flow rates of HMDSO (2, 2-3, 3 g/hr) to 78 °, 89 °, and 97 °, respectively. A recent article by Samadi, demonstrated that as the flow rate of precursor increases, changes in the chemical composition and wetting properties were observed.[99] In general, as the precursor flow rate increases, so does the WCA. At 1500 V, the lowest flow rate (2 g/hr) showed the highest WCA at 86 °. The WCA for 2-3 g/hr and 3 g/hr flow rate (1500 V) have comparable values 74 and 75 °, respectively. The parameter that generated the highest WCA (97 °) was 3 g/hr at 1000 V, while one of the lowest WCA (75 °) was generated at 3 g/hr and 1500 V. This decrease in WCA is a result of an increase in the surface energy. A high WCA is desirable for a decrease in cell adhesion properties. The results of the t-test related to the WCA shows there is only a significant difference between the coatings deposited at 3 g/hr for 1000 V and 1500 V and between the 2 and 3 g/hr at 1500 V on 321 SS samples.
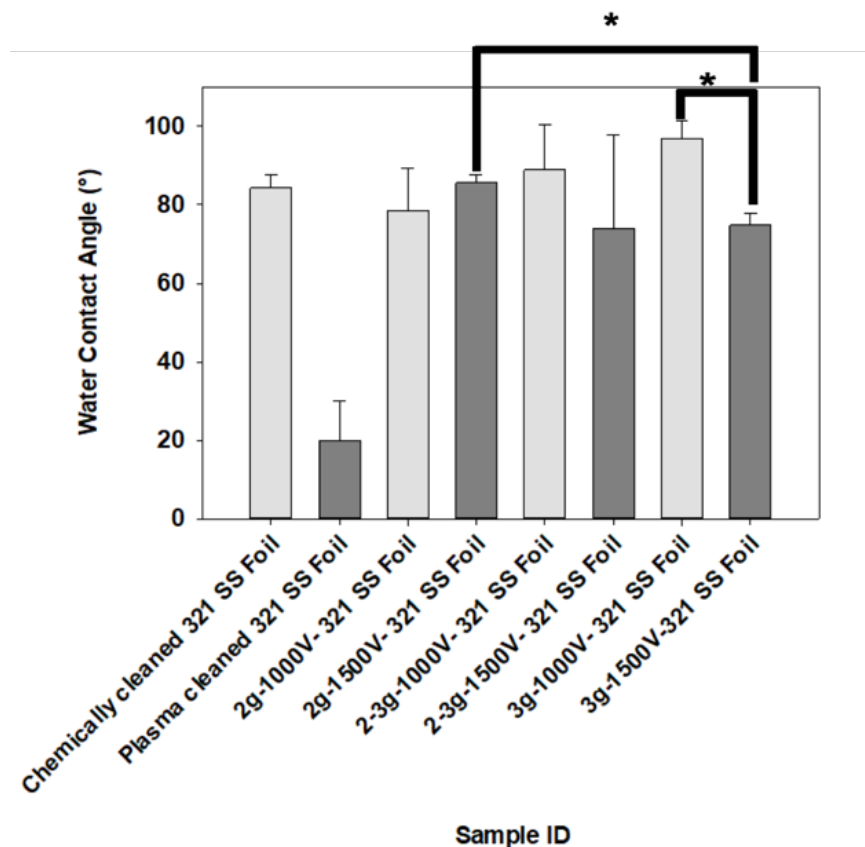
Figure 17. Water contact angle values on 321 SS foil uncoated and coated. Bars represent the average contact angle, while error bars represent the standard deviation between the means of replicate measurements on independent samples (n=3). Statistically significant difference compared with the applied voltage (*p<0.05) at 3 g/hr.

Raman spectroscopy was used to identify structural changes in the molecular composition of the deposited material at different voltages and flow rates in the spectral range of 100 - 3500 cm^{-1}. The bands were studied and assigned according to various references.[102,103] Plasma polymerized HMDSO coatings are comprised of Si-O-Si, Si-C, and Si-CH$_3$ groups. Out of these groups, the methyl group (CH$_3$) in Si-CH$_3$ presents symmetric (2900 - 2965 cm^{-1}) and asymmetric (1250 - 1400 cm^{-1}) vibration states and stretching. The Raman bands associated with HMDSO coatings produced at low voltage (1000 V) consist primarily of silicon carbide Si-C (180 - 360; 660 - 900 cm^{-1}), silicon-

oxide (Si-O, ~590 cm^{-1}), and CH$_3$ stretching and vibrations (1250 - 1400; 2900 –

2960 cm^{-1}), demonstrating the retention of the functional groups of HMDSO and the

formation of a polymer-like structure, referred to as a polymeric organosilica-like

coating. At the higher voltage, 1500 V, the plasma induces more collisions and

rearrangement of the molecules to form a coating consisting primarily of amorphous

carbon (C=C, ~1360-1610 cm^{-1}), silicon-oxide vibration (Si-O, ~590 cm^{-1}) and silicon

carbide vibrations and stretching (660 – 900 cm^{-1}) at all three HMDSO flow rates, as

shown in **Figure 18-Figure 20**. The silicon oxide and silicon carbide bands decrease

with increasing flow rate. Coatings prepared at this higher voltage are thereby referred to

as silicon oxycarbide coatings. Yasuda revealed that repeating functional groups in

plasma-polymerized coatings are reduced as the applied voltage is intensified, in

agreement with our results.[103]

As the flow rate increases (2 to 3 g/hr), the bands at 598 cm^{-1} (Si-O) increases in intensity

for the coatings generated at 1000 V. At the same time, the intensity of the peak at 2905

and 2963 cm^{-1} (CH$_3$) decreases with increasing flow rate for coatings deposited at

1000 V, as shown in **Figure 18-Figure 20**. At higher flow rate, the deposition rate

increases, leading to an increase in activated radicals that recombine at a much faster rate,

and consequently generate a coatings structure that is more disordered.[104] Focusing on

the 3 g/hr sample applied at 1500 V vs 1000 V, we see that the WCA decreases with the

increase in C=C stretching bonds and loss in CH$_3$, Si-O, and Si-C stretching and vibration

contribution. As described earlier, the WCA of coatings increased with increased

precursor flow rate from 2 g/hr to 3 g/hr at 1000 V, in agreement with our observation of

loss in CH$_3$ chemical contribution to the coating and instead increase in Si-O, Si-C and CH$_3$ stretching and vibration contribution.
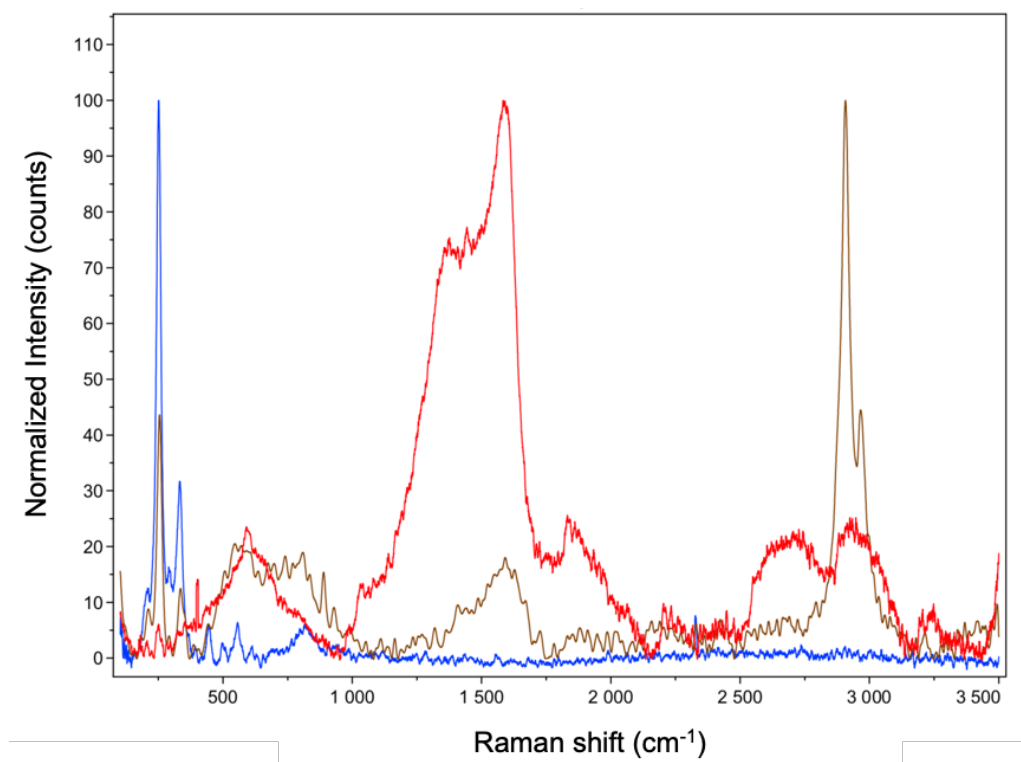
Figure 18. Raman spectroscopy of uncoated 321 SS foil (blue) and of coatings deposited on 321 SS foil at 2 g/hr HMDSO with an applied voltage of 1500 V (red, silicon oxycarbide coating), and 1000 V (brown – organosilicon polymer-like coating).
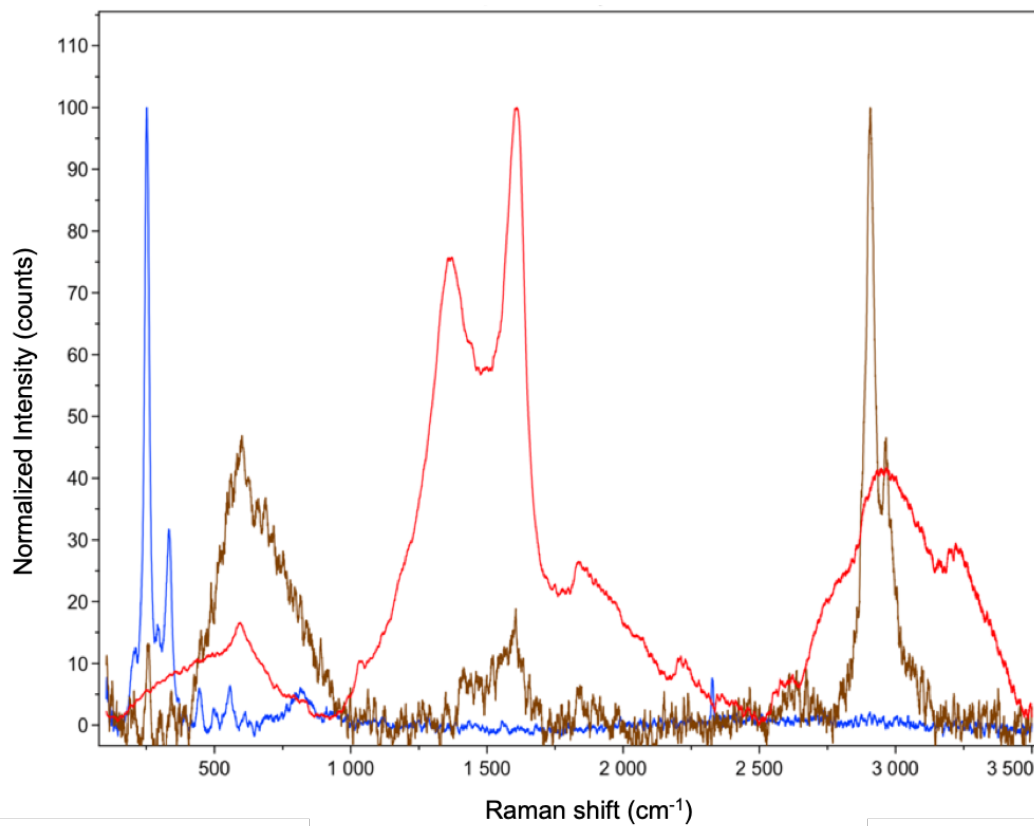
Figure 19. Raman spectroscopy of uncoated 321 SS foil (blue) and of coatings deposited on 321 SS foil at 2-3 g/hr HMDSO with an applied voltage of 1500 V (red - silicon oxycarbide coating), and 1000 V (brown – organosilicon polymer-like coating).
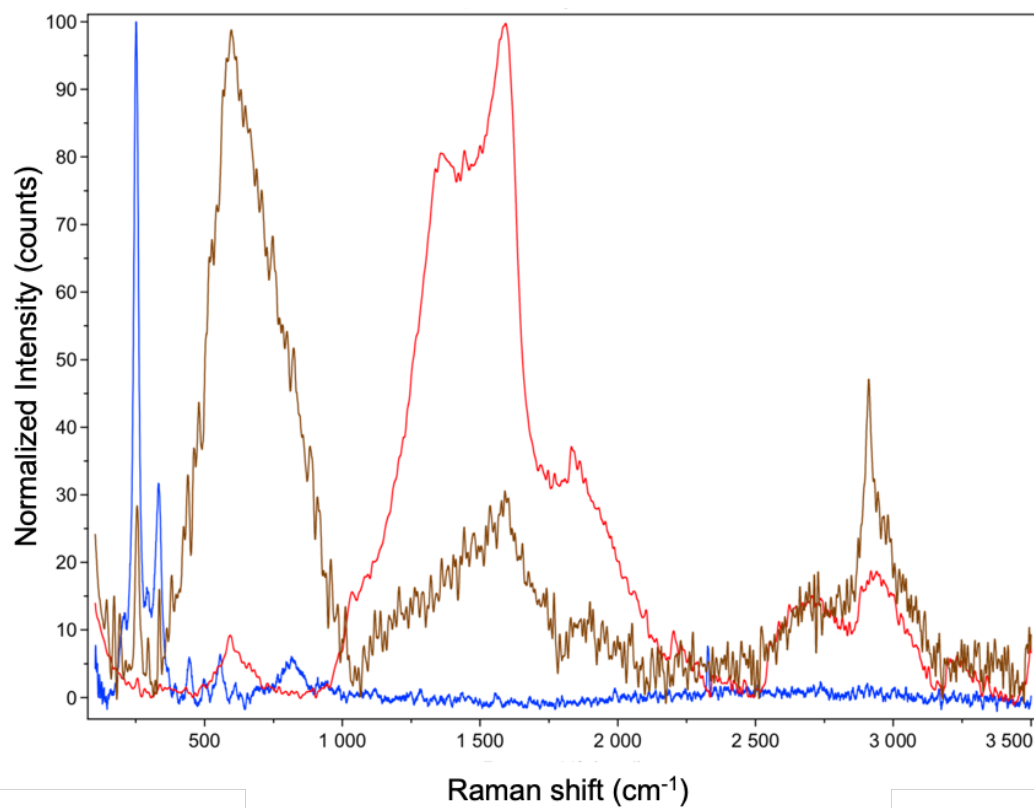
Figure 20. Raman spectroscopy of uncoated 321 SS foil (blue) and of coatings deposited on 321 SS foil at 3 g/hr HMDSO with an applied voltage of 1500 V (red - silicon oxycarbide coating), and 1000 V (brown – organosilicon polymer-like coating).

3.5.3   *Plasma Cleaning of 316 L SS Foil Samples*

The 316 L SS samples were plasma cleaned using the same parameters as the 321 SS samples. The plasma cleaning time for all the 316 L SS samples was 30 minutes. After plasma cleaning, the samples were either removed for characterization or underwent plasma polymerization using HMDSO.

3.5.4   *Plasma Deposition of HMDSO on 316 L SS Foil Samples*

The process parameters selected for coating 316 L SS samples were chosen based on the WCA and chemical composition results of HMDSO plasma polymerization on 321 SS samples. The 3g/hr HMDSO along with voltages of 1000 V and 1500 V exhibited the

desired hydrophobic (97 ° at 3g/hr, 1000 V) and hydrophilic (75 ° at 3g/hr, 1500 V) properties. Therefore, the aforementioned process parameters were employed for the 316 L SS study.

During the plasma deposition processes, the peak-to-peak voltage and current were monitored with an oscilloscope. These select parameters are checked to detect changes that may occur in the plasma process, such as arc discharge or electrical short. **Figure 21** shows the peak-to-peak voltage and current on 316 L SS foil samples. For both chemically cleaned and plasma cleaned 316 L SS samples, peak-to-peak voltage and current are zero, since these samples did not undergo the plasma polymerization process. As soon as 1000 V is applied to the 316 L SS samples the average peak-peak voltage and current become ~3070 V and 10 A, respectively during the 10-minute process. When the applied voltage is increased to 1500 V the average peak-to-peak voltage increases ~380 V to 3450 V. The average peak to peak current is tripled to 30 A, shown in **Figure 22**. Similar results were observed on the 321 SS samples. The results of the t-test revealed a significant difference between the coatings deposited at 1000 V vs 1500 V in both average peak-to-peak voltage and current.
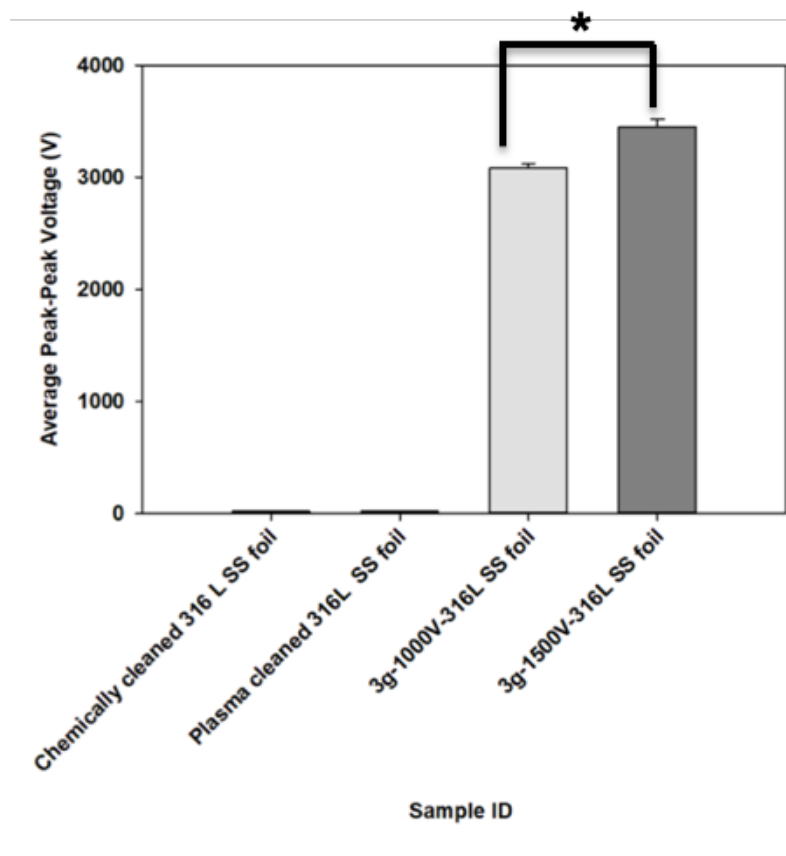
Figure 21. Average peak to peak applied voltage for HMDSO coatings (3 g/hr) applied at 1000 V and 1500 V onto 316 L SS foil. Error bars represent the standard deviation between replicates (n=3). Statistically significant difference observed between samples coated at 1000 V vs 1500V (*$p<0.05$).
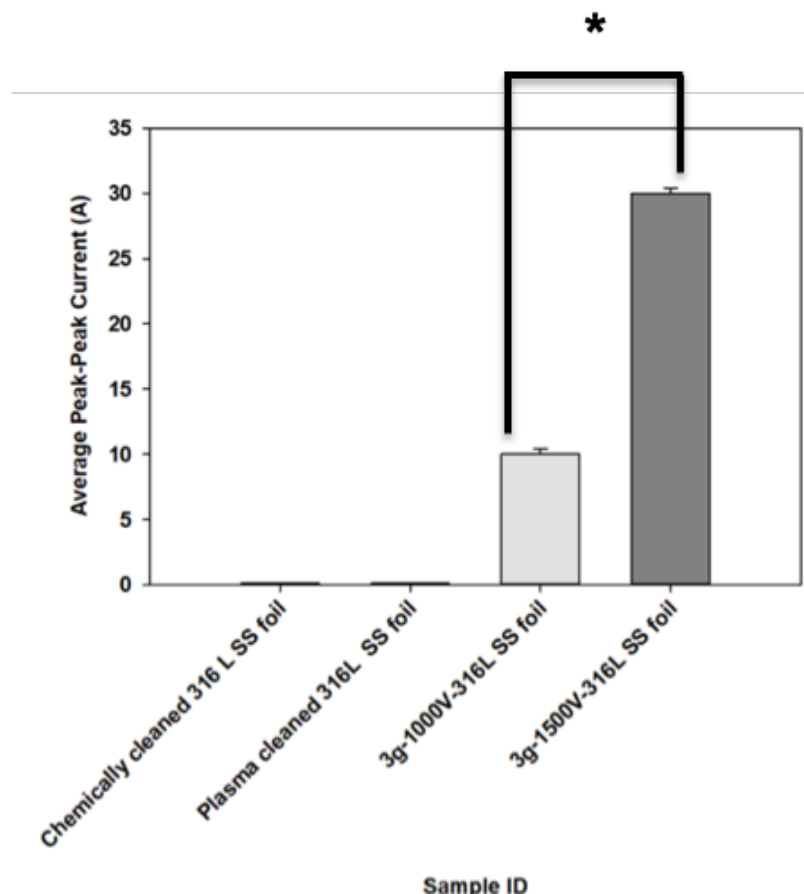
Figure 22. Average peak to peak current for HMDSO coatings (3 g/hr) applied at 1000 V and 1500 V onto 316 L SS foil. Error bars represent the standard deviation between replicates (n=3). Statistically significant difference observed between samples coated at 1000 V vs 1500 V (*p<0.05).

The target coating thickness for this study was between 100 nm to 300 nm. The thin coating should provide protection for the stainless-steel sample while at the same time maintain the shape and flexibility of the sample. The coating thickness on the silicon coupons was measured with a contact profilometer. The chemically cleaned and plasma cleaned 316 L SS foil sample revealed no coating, as expected since these samples did not undergo the plasma polymerization process. The average coating thickness for the 316 L SS foil samples that employed 1000 V was 67 nm. 316 L SS foil samples that employed 1500 V presented an average coating thickness of 108 nm, a slight increase in

thickness compared to the 1000 V samples, shown in **Figure 23**. Notably, the coating

thickness increases with increasing applied voltage when the deposition times and gas

flow rate are the same. However, the results of the t-test revealed no statistical difference

between HMDSO coating thickness on 316 L SS foil samples at 1000 V vs 1500 V.
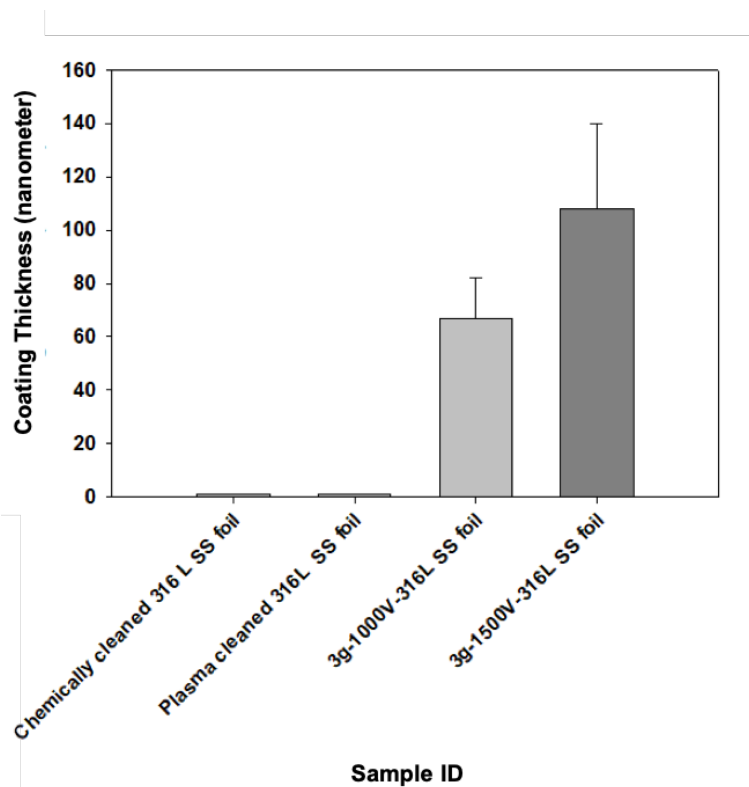
Figure 23. Coating thickness on 316 L SS foil before and after coating with HMDSO at
different flow rates and voltages. The error bars represent the standard deviation between
the replicates (n=3). There is no statistical difference in the coating thickness for samples
coated at 1000 V vs 1500 V.

Both hydrophobic (≥ 90 °) and hydrophilic (≤ 90 °) wetting properties for these coatings

were desired. The chemically cleaned and plasma cleaned 316 L SS foil samples

revealed a hydrophilic surface with the average WCA equaling 80 ° and 15 °,

respectively. The average WCA increases to 92 ° after coating the 316 L SS foil sample

surface with 3 g/hr flow of HMDSO and an applied voltage of 1000 V, shown in

Figure 24. When the applied voltage is increased to 1500 V the average WCA is

reduced to 81 °. Consequently, increasing the applied voltage reduces the average WCA.

The results of the t-test comparing change in WCA with change in voltage showed a

significant difference between the 1000 V and 1500 V coating WCA. There is a

statistical difference between plasma cleaned, and both coated samples, along with a

difference between chemically cleaned, plasma cleaned, and the coated sample applied at

1000 V.
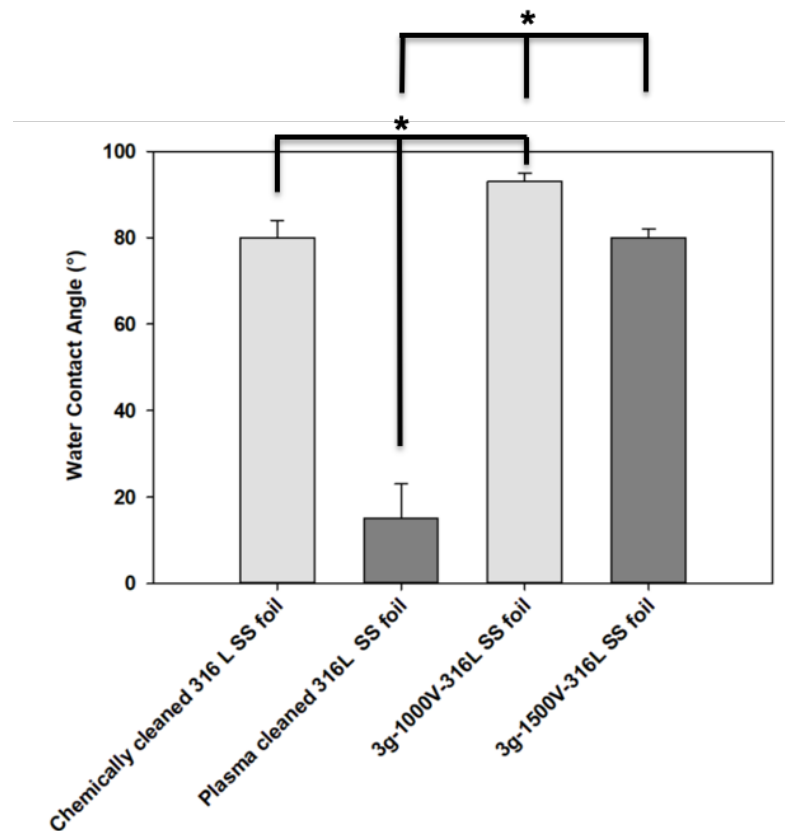
Figure 24. Water contact angle values on 316 L SS foil uncoated and coated along with results of t-test. The error bars represent the standard deviation between replicates (n=3). Statistically significant difference compared with the coated samples and cleaned samples (*p<0.05).

Chemical characterization of 316 L SS foil samples and coatings were performed using Raman spectroscopy. **Figure 25** shows the Raman spectra for the two coatings and bare 316 L SS foil. The uncoated 316 L SS foil sample revealed bands between 500 cm^{-1} and 1500 cm^{-1}. Bands 220, 287, 405, 489, 604, 674 cm^{-1} do not overlap with any of the bands observed in the coatings. Only one strong band at 2907 cm^{-1} was observed for the coating applied at 1000 V. The same coating applied on 321 SS foil yielded a similar band (C-H stretching). The coating applied at 1500 V reveal two bands at 1368 and 1602 cm^{-1} in the carbon-carbon stretching regions. This spectra is characteristic of amorphous carbon material, generally containing broad band with D peak ~1350 cm^{-1} (sp^3-hybridized) and G peak 1550-1600 cm^{-1} (sp^2-hybirdized).[105] Both the Si-O and Si-C stretching bands are missing in the spectra for the coatings on 316 L SS foil. The loss of these bands may be a result of the low signal to noise ratio. This may be a result of the low laser power.
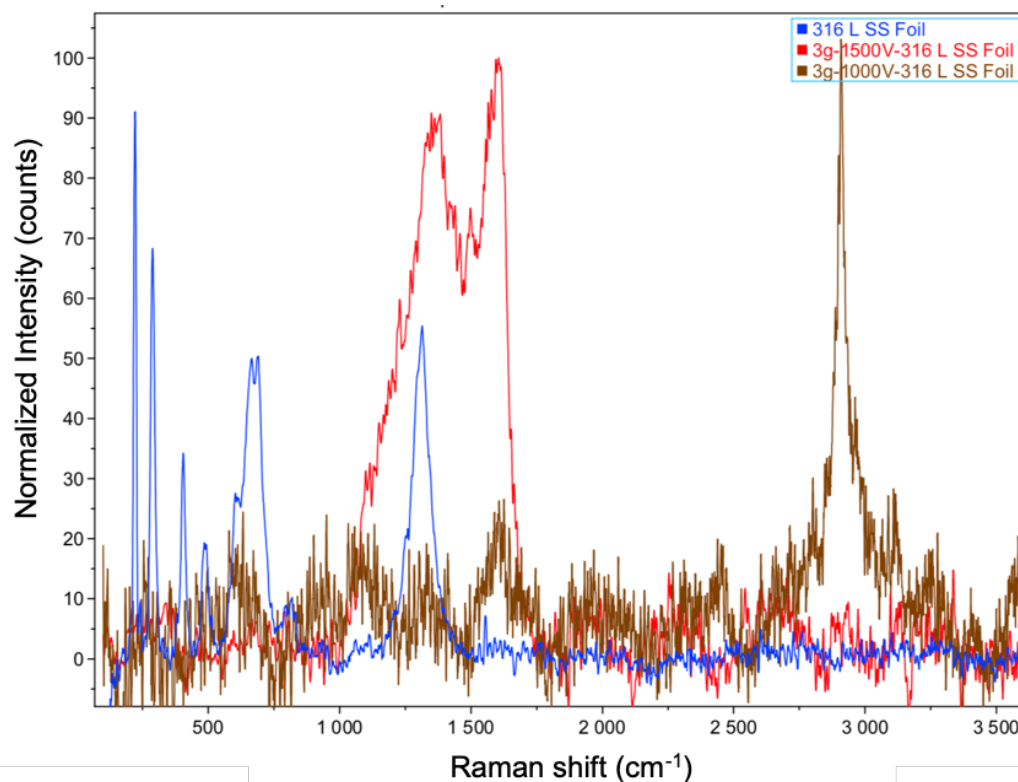
Figure 25. Raman spectroscopy of uncoated 316 L SS foil (blue) and of coatings deposited on 316 L SS foil at 3 g/hr HMDSO with an applied voltage of 1500 V (red- silicon oxycarbide coating) or1000 V (brown- organosilicon polymer-like coating).

Coating uniformity across the surface is crucial as continuous chemical functionality can lead to cell attachment or non-attachment. If the coating chemistry is different in different areas, this will lower our ability to uniformly control cell attachment across the surface. Raman spectroscopy on the organosilicon polymer-like coating on 316 L SS foil applied at 1000 V with a flow rate of 3 g/hr revealed reproducible spectra in 3 different locations along the surface, as shown in **Figure 26**.
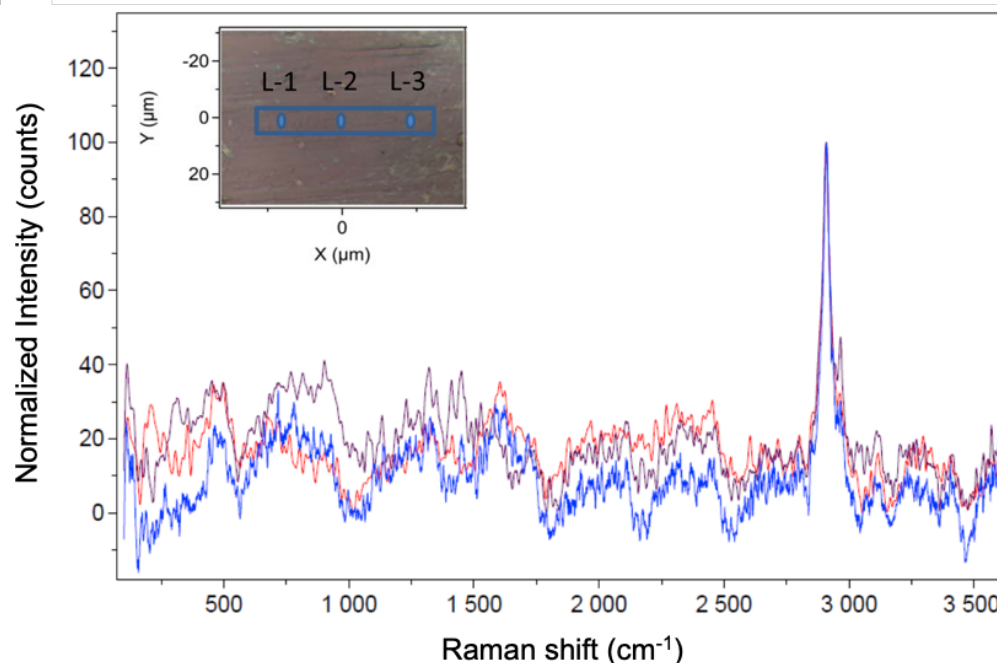
Figure 26. Raman spectroscopy of organosilicon polymer-like coatings deposited on 316 L SS foil at 3 g/hr HMDSO with an applied voltage of 1000 V. Comparison of the coating uniformity in three different locations across the surface of the coated sample. location 1- red, location 2- purple, location 3-blue.

Similar results were observed for the coatings applied at 1500 V on 316 L SS foil, with the exception of slightly different sp^2 and sp^3 contributions across the surfaces (1000 cm^{-1} – 1800 cm^{-1}), as shown in **Figure 27**. Future work will be carried out to understand the changes in sp^2 and sp^3 contributions across the surface.
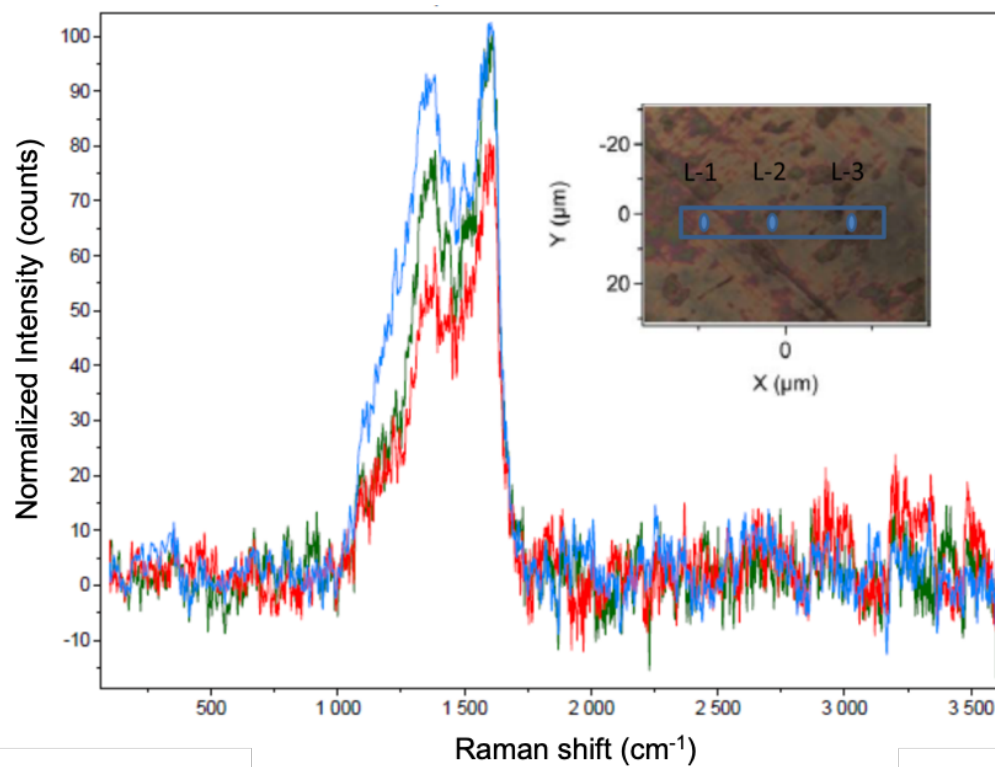
Figure 27. Raman spectroscopy of silicon oxycarbide coatings deposited on 316 L SS foil at 3 g/hr HMDSO and with an applied voltage of 1500 V. Comparison of the coating uniformity in three different locations across the surface of the coated sample. Location 1-blue, location 2- green, location 3-red.

3.6   Conclusion

Organosilicon polymer-like and silicon oxycarbide coatings were deposited onto 321 and 316 L SS foil samples by pulsed-DC-PECVD using HMDSO with different applied voltages and precursor (HMDSO) gas flow rates (with the exception of 316 L SS foil, where the flow rate was set to 3 g/hr). The average WCA measurements indicated that 97 ° and 75 ° were the maximum and minimum WCA values obtained by pulsed-DC PECVD of HMDSO with 1000 V and 1500 V at 3g/hr, respectively for 321 SS foil. The maximum and minimum WCA on 316 L SS was 92 ° and 81 ° when pulsed-DC PECVD of HMDSO with 1000 V and 1500 V at 3g/hr was employed. Coating thickness analysis shows no significant difference when the voltage is increased from 1000 V to 1500 V. The coating thickness on average is 67 nm and 108 nm thick at 3g/hr, 1000 V and 1500 V, respectively. Raman spectroscopy shows that when 1500 V are applied to HMDSO, there is a characteristic behavior of silicon oxycarbide coatings. However, when 1000 V are applied to HMDSO, methyl, silicon-methyl and silicon-oxide stretching are revealed in the coating, indicating that the composition and structure for polymerized HMDSO is retained in the coating at low voltages. While there is a significant difference of 22 ° in the WCA for both coated SS samples at 1000 V and 1500 V (3 g/hr), the difference is distinct enough for one coating to be termed hydrophobic and the other hydrophilic. At the same time the different voltages expose a distinct difference in the surface composition.

4. ENDOTHELIAL AND SMOOTH MUSCLE CELL STUDIES ON UNCOATED AND COATED 316L SS FOIL

4.1 Introduction

This chapter focuses on adhesion and proliferation of select cells on 316 L stainless steel (316 L SS) foil surfaces that were modified using pulsed-DC plasma enhanced chemical vapor deposition (PECVD) with organosilicon polymer-like or silicon oxycarbide coatings. The effect of the coating's chemistry in relation to the adhesion and proliferation of endothelial cells and smooth muscle cells will be discussed.

A blood vessel's endothelial lining, which contains a thin layer of endothelial cells, is damaged upon implantation of a stent, thereby triggering an inflammatory response, slowing endothelial cell movement, altering fibrin clotting, and stimulating smooth muscle cell migration.[6,12,106] This cascade of events leads to smooth muscle cells and platelets aggregating around the stent wall, eventually occluding the interior wall of the stent. Thus, smooth muscle and endothelial cells were selected to serve as cell models in this study. The endothelial cells used in this study were human umbilical vein endothelial cells commonly used in cell studies. The other cells assessed in this study were smooth muscles cells from human coronary arteries.

The focus of this study is on selectively reducing the accumulation of smooth muscle cells while, at the same time, allowing for adhesion of endothelial cells on the coated samples in comparison to uncoated 316 L SS foil samples.

4.2 Background

In-stent restenosis is defined as the re-obstruction of the artery or vessel after stent implantation. The reason behind in-stent restenosis is not clearly understood, but the cause is generally thought to be a result of inflammation and injury incurred from cutting and implanting the stent in the artery. Carpenter and Schoenfisch designed a schematic (**Figure 28**) of the key responses of thrombosis and restenosis in the arteries to stent implantation. The insertion of the stent results in protein and platelet adhesion, as well as recruitment and activation of macrophages and leukocytes leading to thrombosis. Cytokines and growth factors are also released. At the same time, the injury to the artery induces the activation of smooth muscle cells. Proliferation and migration of the smooth muscle cells towards the lumen of the artery[9] in a process also known as the neointima formation process is encountered. Recovery of the endothelium lining of the artery, which consist of endothelial cells, after implantation is slowed in this process.
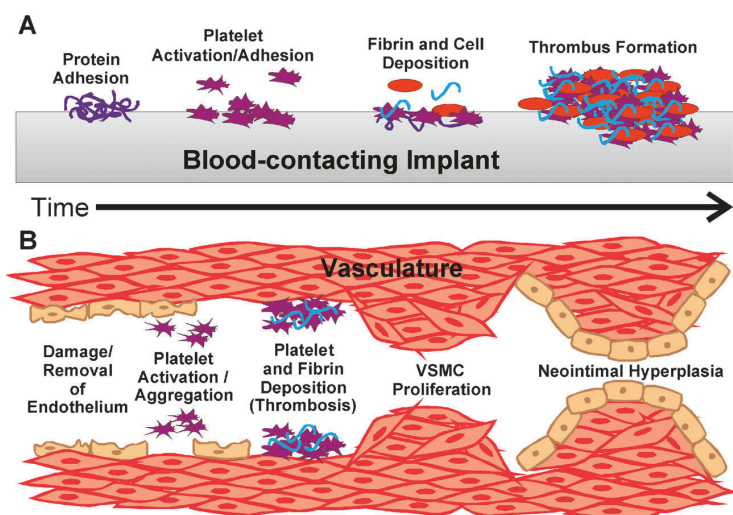
Figure 28. Schematic of artery inflammatory response to stent implantation. (A) Blood clot formation. (B) Stent implantation results in severe injury to the vessel wall leading to restenosis. Reproduced from Ref. 107 with permission from The Royal Society of Chemistry.[107]

To prevent biofouling, or the chronic aggregation of select cells on bare metal stents (BMS), surface properties such as material composition and geometry need to be carefully considered. At the same time, improving rate of proliferation and migration of endothelial cells to form the endothelium lining around the stent will help prevent or slow smooth muscle cell adhesion to the stent. Anti-biofouling surface modification techniques by way of active or passive coatings have been designed for biomedical implants. Active coatings typically elute immunosuppressant drugs (paclitaxel[12], zotoarolimus[12], and heparin[29]) to stabilize cell and protein adhesion, proliferation and migration; passive coatings (PC), on the other hand, are designed to be biologically and prevent surface adhesion. Both coating techniques have shown promise in decreasing the rate of in-stent restenosis.

Active coatings have been reported to exhibit a higher decrease of in-stent restenosis than PC, yet with only a slight increase in late stent thrombosis, and no benefit after implantation for four years.[5] PCs are considered to have a less complex design at a lower cost[1] and less long-term safety issues,[6] making them a more viable option at this time for most patients.

Most PC coatings chemistries that have been investigated incorporate silicon and carbon using radio frequency (RF) PECVD,[38–41] with only a few of these studies investigating the coatings' effect on samples other than flat coupons. The three dimensional shape, aspect ratio and complex geometry of stents creates a challenge in regard to coating uniformity, typically resulting in a thickness gradient along the inside and outside of the stent.[80] Additional regions where strain is more prevalent, i.e. sharp or rounded corners

along the stent strut, make for opportune sites for cracking and delamination of the coating.[80]

Over the years, BMS have been made from a number of metals (stainless steel, cobalt chrome, nitinol, titanium, tantalum and more) encompassing varying geometries and designs such as a corrugated ring or slotted tube.[108] The stent material and design features are understood to be crucial to the biocompatibility of these biomedical devices.[1,2,16,106,109,110] Upon implantation, proteins adsorb on the metal stent surface because of the charge transfer mechanism between the donating protein and the accepting metallic surface; for this reason, neutrally charged coating are needed.[20,111] 321 SS foils used section 3.3 were used, because of the similar elemental composition and lower cost in comparison to 316 L SS, to carry out the different plasma polymerization processes. The process that demonstrated the highest and lowest WCA (3 g/hr at 1000 V and 1500 1500 V) on 321 SS was selected to be applied to 316 L SS foil. Stainless steel (SS), 316 L alloy, has been one of the most commonly used materials for stents. However, its poor biocompatibility and moderate elasticity has resulted in the need for alternative materials and coatings. The focus of this research is on the modification of flat 316 L SS inert with HMDSO-based coatings of varying physical and chemical properties using pulsed DC PECVD.

4.3   Materials And Methods

4.3.1   Materials

Single donor cryopreserved human umbilical vein endothelial cells (HUVEC) were acquired from PromoCell (C-12200; Heidelberg, Germany) after passage II.

Cryopreserved human coronary artery smooth muscle cells (HCASMC) were purchased from PromoCell (C-12511) after passage II. PromoCell's ready-to-use endothelial growth media and supplement kit (C-22010) was used for HUVECs. PromoCell's human coronary artery smooth muscle kit II (C-22062) was used to maintain the HCASMCs. Gibco's antibiotic-antimycotic was purchased from ThermoFisher (1540062; Waltham, Massachusetts, USA).

4-(2-hydroxyethyl)1-piperazineethanesulfonic acid) (HEPES) was purchased from Hyclone (SH30237.01; Logan, Utah, USA) and Dulbecco phosphate buffered saline (DPBS) – (with magnesium and calcium) was purchased from Corning (21-031-CV; Manassas, Virginia, USA). HEPES and DPBS were mixed together and used to maintain the pH of the HUVEC cell culture after the media was removed. 0.05% Trypsin / Ethylenediaminetetraacetic acid (EDTA) was used to detach the HUVECs from the T-75 flask. PromoCell's 30 mM HEPES- buffered saline solution (BSS) (C-40010) was used to maintain the pH of the HCASMC cell culture (cell structure and function) after removing the growth medium. PromoCell's 0.04% Trypsin / EDTA (C-41010) was used to detach the HCASMCs from the T-75 flask. PromoCell's (C-41110) trypsin neutralizing solution (TNS) was used to neutralize the trypsin in the T-75 flask after the HCASMCs and HUVECs were detached.

37% formaldehyde was purchased from MilliPore Sigma (FX0410; Burlington, Massachusetts). 10 X Phosphate buffer saline was purchased from KPL (51-13-02; Gaithersburg, Maryland) and SeraCare (5460-0022; Milford, Massachusetts) to make 4% formaldehyde.

Two fluorescent stains were purchased for this study: 4,6-diamidino-2-phenylindole, dihydrochloride (DAPI) from Millipore Sigma (268298) and CytoPainter Phalloidin iFluor 594 reagent from Abcam (ab176757; Cambridge, Massachusetts). Invitrogen's Fluoromount-G mounting media (00-4958-02) was purchased from ThermoFisher Scientific.

4.3.2 Methods

4.3.2.1 Cell Culture

The anti-biofouling effectiveness of the organosilicon polymer-like coating applied at 1000 V and silicon oxycarbide coating applied at 1500 V using 3 g/hr precursor flow rate described in Chapter 3 were assessed with cells proven to adhere to both 316 L stainless steel (SS) and glass surfaces. Single donor cryopreserved HUVECs and ready-to-use endothelial cell growth medium kit which includes basal medium and supplement mix were used in this study. The supplement mix includes fetal calf serum (0.02 mL/mL), endothelial cell growth supplement (0.004 L/mL), epidermal growth factor (0.1 ng/mL), basic fibroblast growth factor (1 ng/mL), heparin (90 μg/mL), and hydrocortisone (1 μg/mL). 1 % of antibiotic-antimycotic was added to the endothelial cell growth media to prevent bacterial and fungal contamination. HUVECs were cultured in a T-75 flask with the endothelial cell growth media and incubated in a 37 ºC incubator under a 5% CO_2 atmosphere.

The HUVECs were sub-cultured after 7 days or once the T-75 flask was close to 90 % confluency, whichever came first. The cells in the T-75 flask were washed with 7.5 mL of HEPES-DPBS buffer solution (without calcium or magnesium) and then incubated at

37 ºC with trypsin for 4 minutes. The trypsinization process was then stopped by adding

7.5 mL of TNS. The cells were transferred to a centrifuge tube and centrifuged at 125 x g

for 5 min. The cells were resuspended in fresh media and counted using a

hemocytometer. Cells used for the adhesion and proliferation studies were sub-cultured

between passages V and VII.

HCASMC cells were cultured in T-75 flasks with PromoCell's ready-to-use smooth

muscle growth medium II kit which includes basal media and supplement mix.

The supplemental mix that was added to the media contained fetal calf serum

(0.05 mL/mL), epidermal growth factor (0.5 ng/mL), basic fibroblast growth factor (2

ng/mL), and insulin (recombinant human) (5 μg/mL). 1 % of antibiotic-antimycotic was

added to the smooth muscle cell growth media to prevent bacterial and fungal

contamination. HCASMCs were cultured in a T-75 flask with the smooth muscle cell

growth media and incubated in a 37 ºC incubator under a 5 % CO_2 atmosphere.

The HCASMCs were sub-cultured after 14-days or once the T-75 flask was close to 90 %

confluency, whichever came first. The cells in the T-75 flask were washed with 7.5 mL

of HEPES-BSS buffer solution and then incubated at 37 ºC with trypsin for 4 minutes.

The trypsinization process was then stopped by adding 7.5 mL of TNS. The cells were

transferred to a centrifuge tube and centrifuged at 125 x g for 5 min. The cells were

resuspended in fresh media and counted using a hemocytometer. Cells used for the

adhesion and proliferation studies were sub-cultured between passages V - VII.

4.3.2.2 Investigation of Cell Adhesion to Coated Samples

316 L SS foil samples either uncoated or coated via pulsed PECVD were used in these studies. Specifically, the performance of coatings generated with the precursor hexamethyldisiloxane (HMDSO) at a flow rate of 3 g/hr and with an input voltage of either 1000 V resulting in an organosilicon polymer-like coating, or 1500 V resulting in a silicon oxycarbide coating was studied. Prior to seeding cells, the uncoated and coated 316 L SS foil samples were cut 8.9 mm (width) by 7.8 mm (length) and ultrasonically cleaned in isopropanol, followed by autoclaving at 120 ºC for 20 minutes and then placing them inside the wells of Nunc Lab-Tek ™ II Chamber Slide System 8 well-plates were purchased from ThermoFisher Scientific (154534PK) under a laminar flow biological hood.

Earlier studies of cell proliferation protocol using HUVEC cells on stainless steel sample demonstrated proliferation of the selected cells on stainless steel samples after incubation for 1-7 days at a density of 18,000 – 20,000 cells per ml.[112] HUVEC or HCASMC cells (passages V-VII) were plated independently at a cell density of 16,000 and 10,000 cells/cm^2 in 100 µL of media, respectively, on the surface of the foils. A schematic of the well plate setup with the uncoated and coated foils is shown in **Figure 29**. The HUVEC and HCASMC then were allowed to attach to control (uncoated SS and bare glass) and coated SS foil surfaces at 37 °C under 5 % CO_2 for 2 or 7 days. For cells cultured for 7 days, the media was replaced every 2 days. The glass well was only used to verify initial cell attachment and continuous cell proliferation and health during the study.

Uncoated 316 L SS foil was used to compare adhesion and proliferation to coated 316 L SS foil samples. At the end of the time study, the cells were washed with Dulbecco's phosphate buffered saline (DPBS) once and fixed with 4% formaldehyde in PBS for 20 min. Cell growth on each sample and control was studied with at least two independent replicates.
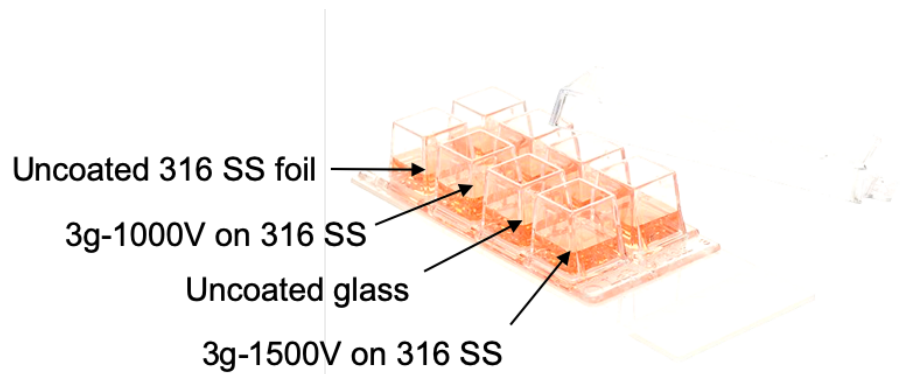
Nunc Lab-Tek II 8 well plate

Figure 29. Schematic of Nunc LabTek II well plates.

After fixing, the cells were then washed with DPBS one time. The cells were then concurrently labeled with 4,6-diamidino-2-phenylindole (DAPI) cell nuclei stain (excitation/emission wavelengths of 358/461 nm) to label nuclei with blue fluorescence and actin-binding phalloidin-iFluor 594 (excitation/emission wavelengths of 590/618 nm) to label the actin filaments of the cells with red fluorescence. Actin filament is an intercellular protein and its key roles in a cell is muscle contraction and cell movement. These stains were used because the excitation and emission bands have a small degree overlap at the tail end minimizing the degree of bleed-through, as shown in **Figure 30**.
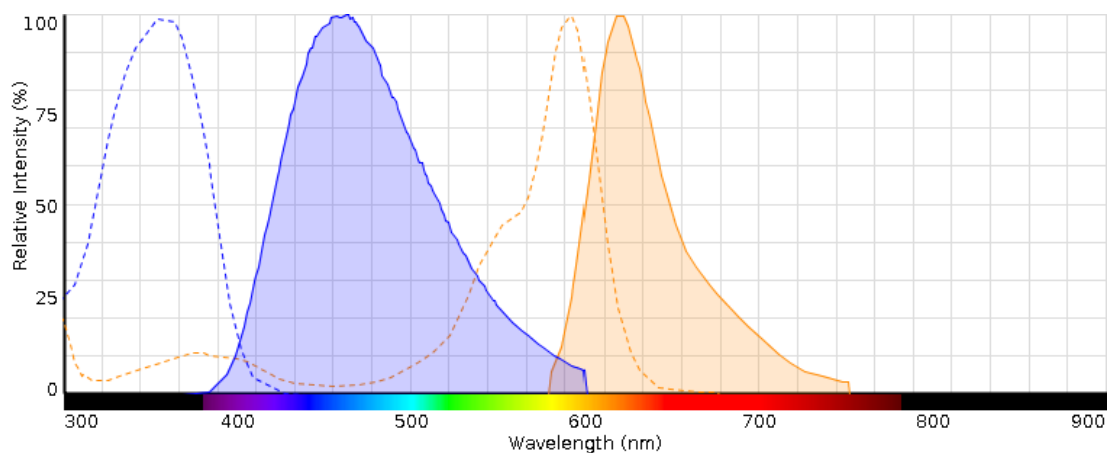
Figure 30. Excitation and emission bands for DAPI and phalloidin-iFluor 594. The blue dashed line is DAPI excitation band, blue solid line is DAPI emission band, orange dashed line is phalloidin iFluor 594 excitation band, and orange solid line is phalloidin iFluor 594 emission band.

The DAPI-phalloidin cell staining solution contained 1 µL of 1 µg/mL of DAPI along with 1 µL of 1x phalloidin and 1 mL of DPBS with 1 % bovine serum albumin. Each well was filled with 100 µL of the DAPI/phalloidin cell staining solution. The well plates were then incubated at 37 °C in an incubator for 30 - 45 mins. The DAPI-phalloidin solution was removed and the wells were washed once with DPBS. Finally, the cell layer was covered with 100 µL of DPBS. The stained cells were viewed under a fluorescent microscope at this time and then stored in a 4 °C refrigerator.

Before capturing fluorescence microscopy images of the cells, the microscope slides were detached from the well and mounted. Specifically, 25 - 40 µL of Fluoromount-G mounting media was added to the slide to reduce photobleaching. A cover slip was placed on top of the slide and sealed with clear nail polish. The mounted slides were kept in the dark for at least 2 hours before imaging the cells. Microscopic images were recorded using an EVOS FL inverted fluorescence microscope using a DAPI filter cube (λ_{EX} = 340 nm, λ_{EM} = 488 nm) for imaging of blue nuclear fluorescence and an RFP filter

cube (λ_{EX} = 590 nm, λ_{EM} = 618 nm) for imaging the red fluorescence from cytoskeleton actin filaments. Thirteen to seventeen single-frame images (0.21 mm^2) were taken across the center of the sample, using a 20 X objective lens, as shown in **Figure 31**, and stitched together to cover the surface area of 2.73 or 3.56 mm^2.
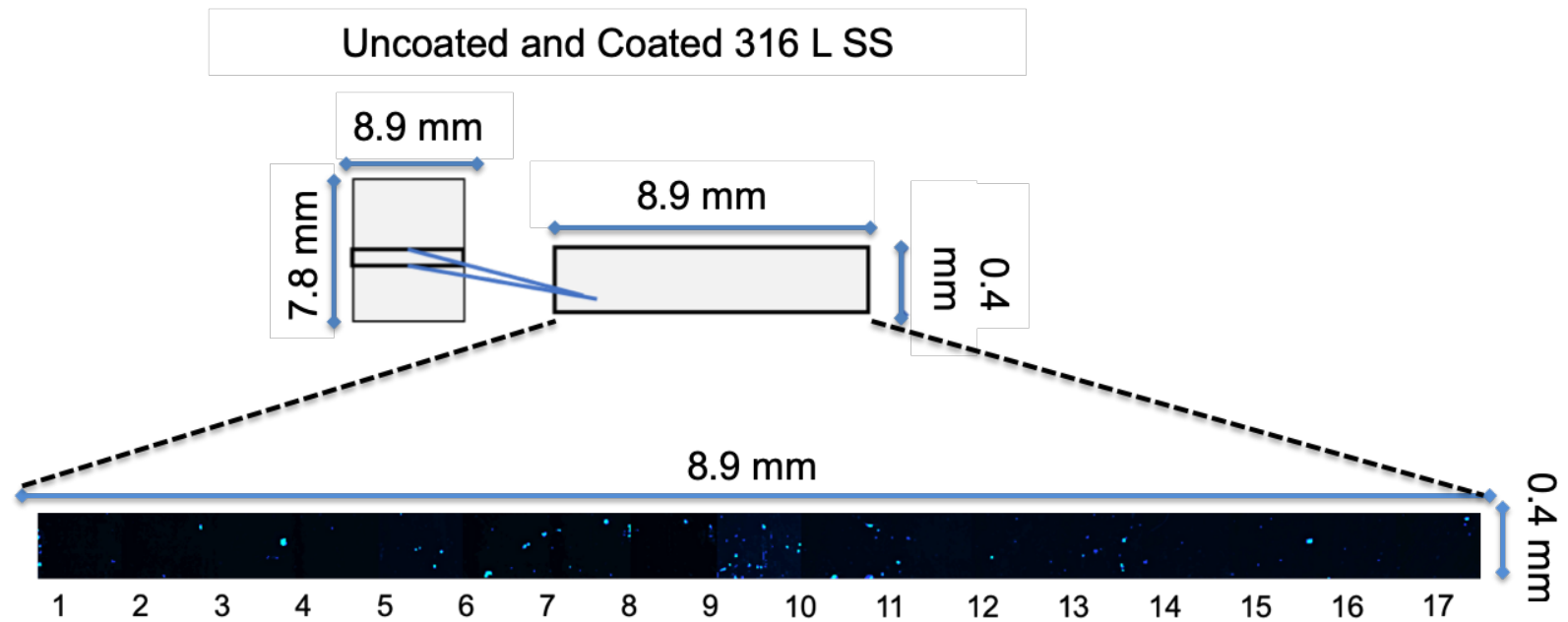
Figure 31. Uncoated and coated stainless-steel samples investigated for cell adhesion and proliferation using fluorescence microscopy. An example of the coated and uncoated stainless-steel samples and location that was interrogated using microscopy.

In an ideal scenario, high endothelial cell adhesion with uniform surface coverage on the coated samples, was desired. On the other hand, low adhesion and replication with minimal surface coverage of smooth muscle cells was desired on the coated samples. The number of cells adhered onto the samples was counted using National Institute of Health (NIH) Image J software and the automated cell counter add-on was used to count the number of cells adhered to surface of the samples. Each image was imported into Image J and then inverted and changed to an 8-bit type image. The size and circularity of the cells were defined as 225-infinity $pixel^2$ and 0.00-1.00, respectively. For each replicate sample, the average number of cells adhered to the foil in thirteen consecutive images (2.73 mm^2) across the sample was determined. The average number of cells per mm^2 was calculated for each sample from these thirteen images for each replicate. The data is then reported as the average and standard deviation in between the means of the replicates. Statistical analysis was carried out using t-test at a significance level of $p < 0.05$. The cells' affinity (2 day) to the surface when coated was compared to that of the 316 L SS foil control. The adhesion of the cells to the surface with respect to extended time (7 day) was also measured to determine if the cells proliferated across the surface.

4.4 Results And Discussions

4.4.1   Human Umbilical Vein Endothelial Cell (HUVEC) Adhesion and Proliferation

Single frame fluorescence images of the HUVECs were captured on the uncoated and coated 316 L SS foil samples. In these images, blue fluorescence indicates the location of cell nuclei while red fluorescence indicates the location of cytoskeletal actin filaments and therefore provides information about cell spreading and adhesion to the solid substrate. Cell adhesion and proliferation were observed at 2 day and 7 day, respectively. Uncoated 316 L SS foil sample revealed the greatest number of cells attached to the surface in a single frame at 2 days. While the 1000 V and 1500 V coated 316 L SS foil samples revealed an average of only one single cell attached to the surface per single frame (area of 0.21 mm^2), as shown in **Figure 32**. At day 7, both uncoated 316 L SS and 1000 V exhibit the same number of cells attached on the surface, while the 1500 V coated sample shows a similar number of cells as the 2 day samples.
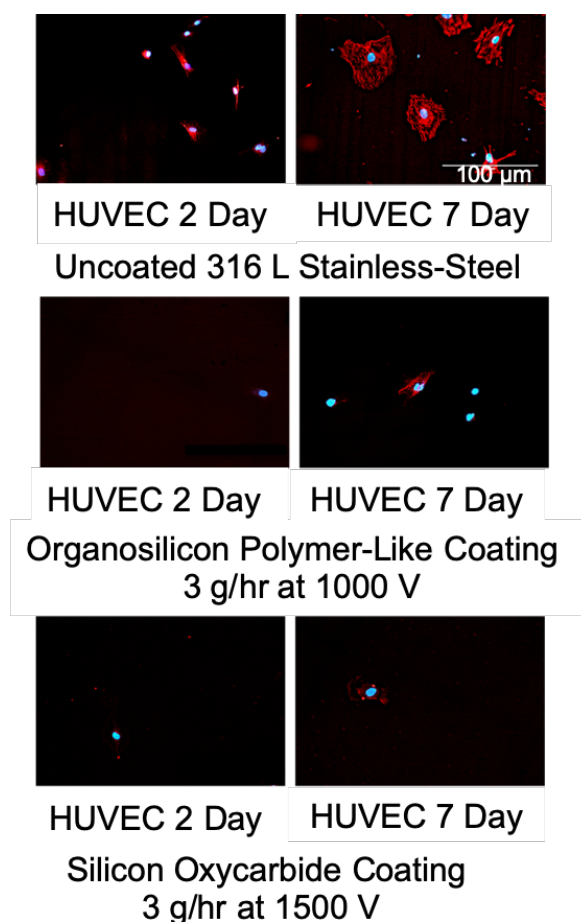
Figure 32. Single frame fluorescence images of adhesion (2 day) and proliferation (7 days) of HUVECs on uncoated and coated organosilicon polymer-like and silicon oxycarbide coatings on 316 L SS foils.

A question that came up in this study was if single frame images were representative of cell attachment across the entire sample? Our assumption was yes, based on other studies.[113],[114] To assess this hypothesis, we evaluated the middle area across the entire uncoated and coated 316 L SS foil sample, shown in **Figure 31**. A total of seventeen single frame fluorescence images were captured and stitched together to illustrate the cell adhesion and proliferation in this area on the sample.

HUVECs adhere mostly to the middle region of the uncoated 316 L SS foil for the 2-day and 7-day studies, as shown in

Figure 33. There are very few cells that adhere and proliferate on the outer edges of the uncoated 316 L SS foil samples. HUVECs arbitrarily adhere to both the coated surfaces in very low numbers. Our initial hypothesis of single frame images being representative of the entire sample was found to be invalid for HUVECs.

HUVEC 2 Day Uncoated 316 L Stainless-Steel

HUVEC 7 Day Uncoated 316 L Stainless-Steel

HUVEC 2 Day Organosilicon Polymer-Like Coating
3 g/hr 1000 V

HUVEC 7 Day Organosilicon Polymer-Like Coating
3 g/hr 1000 V

HUVEC 2 Day Silicon Oxycarbide Coating
3 g/hr 1500 V

HUVEC 7 Day Silicon Oxycarbide Coating
3 g/hr 1500 V
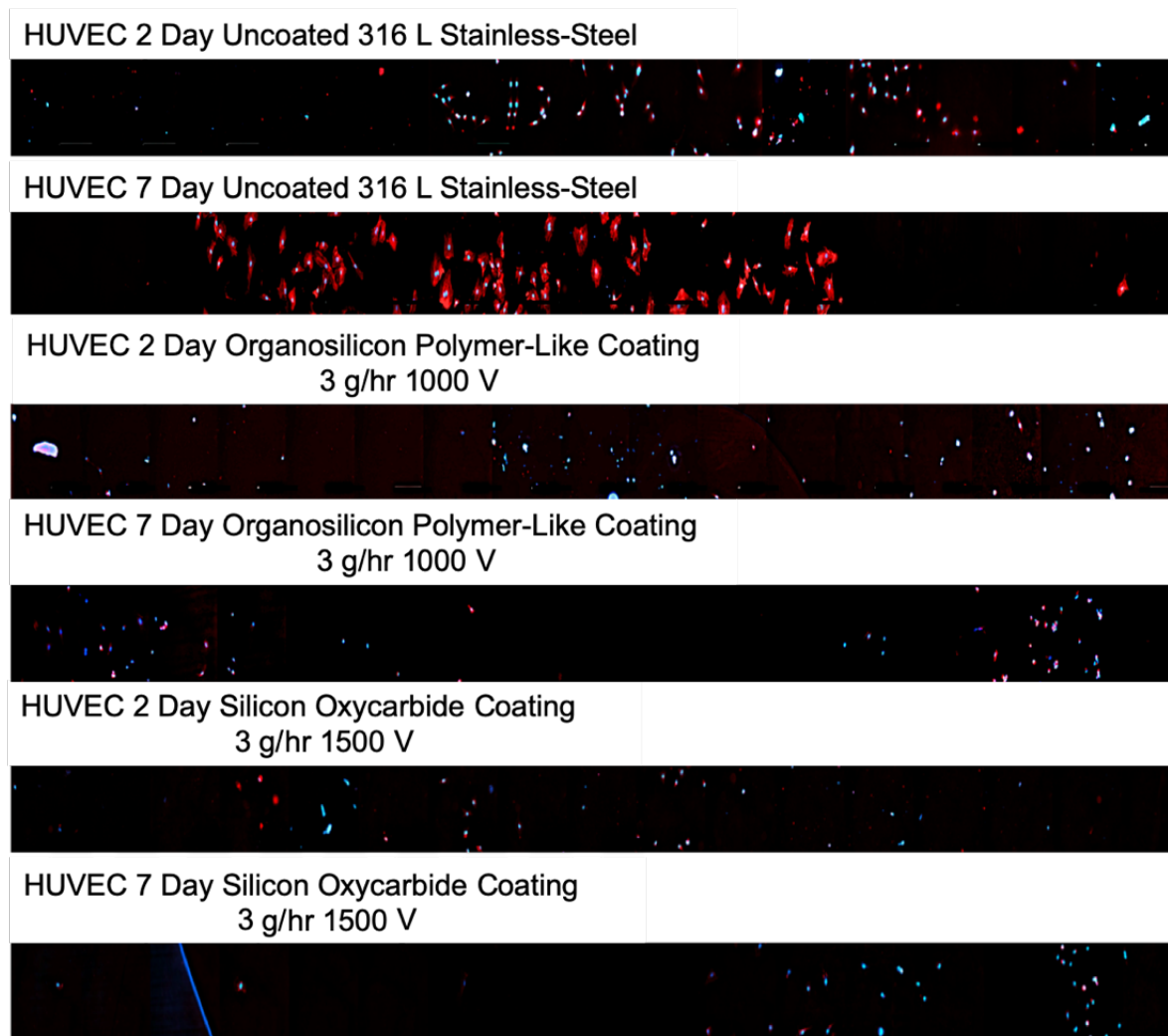
Figure 33. Stitched single frame fluorescence images of HUVECs adhered to uncoated and coated 316 L SS foil samples.

The nonuniformity of the HUVECs across the surface may be due to surface chemistry and surface roughness of the sample. To assess this assumption, we examined the adhesion of the HUVECs on glass. The cells adhere and proliferate across the entire glass substrate as shown in **Figure 34,** after 7 days with the exception of two locations. Thus, cell adhesion is selective with respect to surface chemistry. After fluorescence imaging, the cell nuclei for both HUVEC and HCASMCs were counted on the coated and uncoated 316 L SS foil samples at different incubation times with Image J. Results for HUVEC cell count at 2 and 7 days are shown in **Figure 35**. Uncoated 316 L SS foil exhibited the highest number of HUVEC cells adhered to the surface at 2 and 7 day compared to all the substrates evaluated. On day 2, there were 17 cells/mm^2 adhered to the uncoated 316 L SS foil. Five days later, the HUVEC cell number was 31 cells/mm^2. At day 2, the number of HUVECs adhered to the coated surfaces (1000 V and 1500 V) was 4 cells/mm^2 and 5 cells/mm^2, respectively. After seven days, there was no significant difference in HUVECs proliferation across the 1000 V coated samples (6 cells/mm^2) and the 1500 V coated samples (5 cells/mm^2).
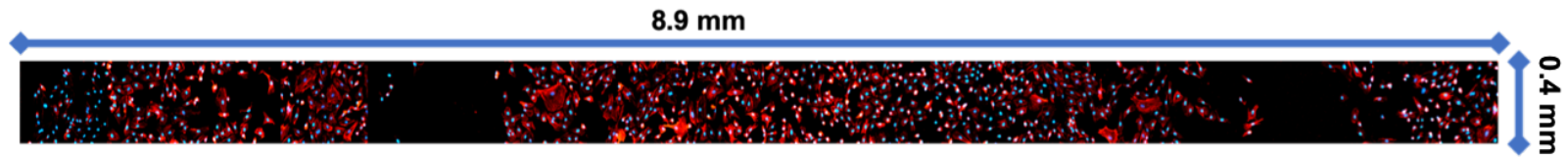
Figure 34. HUVEC cells adhesion and proliferation on glass after 7 days. Blue fluorescence represents the cell nuclei stained with DAPI and red fluorescence represents the cytoskeleton of the cells stained with phalloidin iFluor 594.
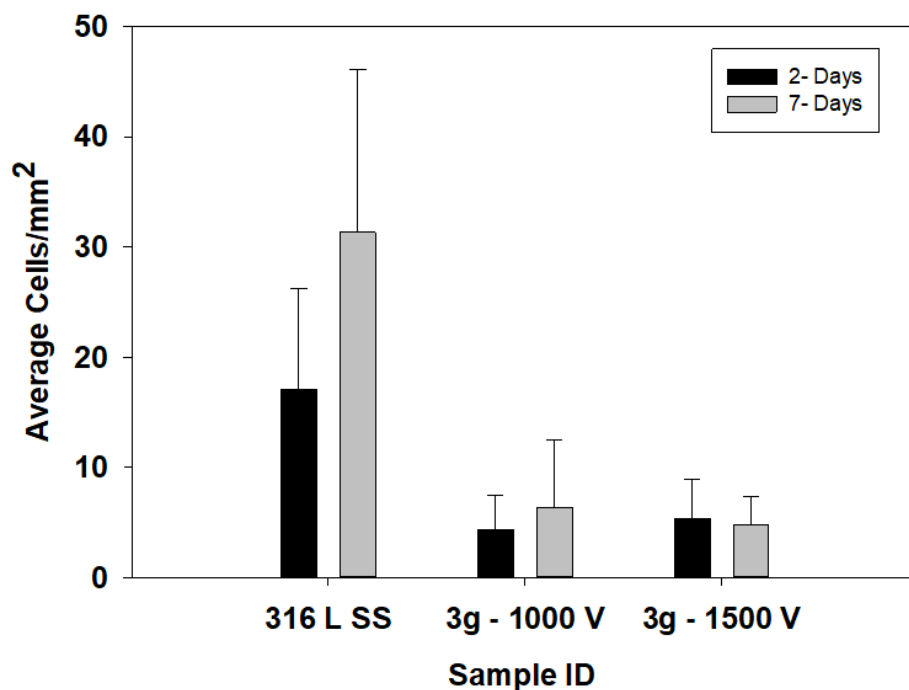
Figure 35. HUVEC cell density: cell adhesion and proliferation across uncoated and coated 316 L SS foil after 2 and 7 days. Error bars represent the standard deviation between the means of independent replicates (n=2). There was no statistically significant difference between the samples (*p<0.05).

The results of the t- test for uncoated and coated SS 316 L foil substrates revealed that there is no statistical difference in HUVEC cell adhesion in between these samples.

4.4.2 Human Coronary Artery Smooth Muscle Cells (HCASMC) Adhesion and Proliferation

A key element of new biomedical implant development is controlling cell adhesion on the material's surface. In this study, the adhesion and proliferation behavior of HCASMCs were investigated on uncoated 316 L SS foil, organosilicon polymer-like coatings, and silicon oxycarbide coatings. Fluorescence imaging and cell counting were used to distinguish the surface-dependent differences in the adhesion and proliferation HCASMCs at different time points. After culturing the cells for 2 days and 7 days, the

adhered cells were fixed and the nucleus (blue) and actin filament forming the cytoskeleton (red) were stained. Then, fluorescence imaging analysis was carried out, as shown in **Figure 36**.

Single-frame images at day 2 and 7 were captured on uncoated and coated 316 L SS foil samples (**Figure 36 A**). The density of HCASMCs adhering to both uncoated 316 L SS foil and organosilicon polymer-like coatings at day 2 in the single-frame image is similar. In addition to these findings, we observed that the HCASMC cytoskeleton does not spread on either of the aforementioned surfaces. In contrast, the silicon oxycarbide coated surface reveals a higher number of HCASMCs attached and spreading across the surface.

At day 7, HCASMCs proliferate along the uncoated and silicon oxycarbide coated 316 L SS foil samples. Alternatively, HCASMCs do not proliferate on the surface of the organosilicon polymer-like coating. Also, the cytoskeleton did not spread out along the coated surface, indicating cell-selectivity for the different uncoated and coated samples. When we evaluated a select area across the entire length of the uncoated and coated stainless steel samples (**Figure 36 B**), HCASMC's densely populate certain locations; at the same time, there are very few to no HCASMC in other locations.
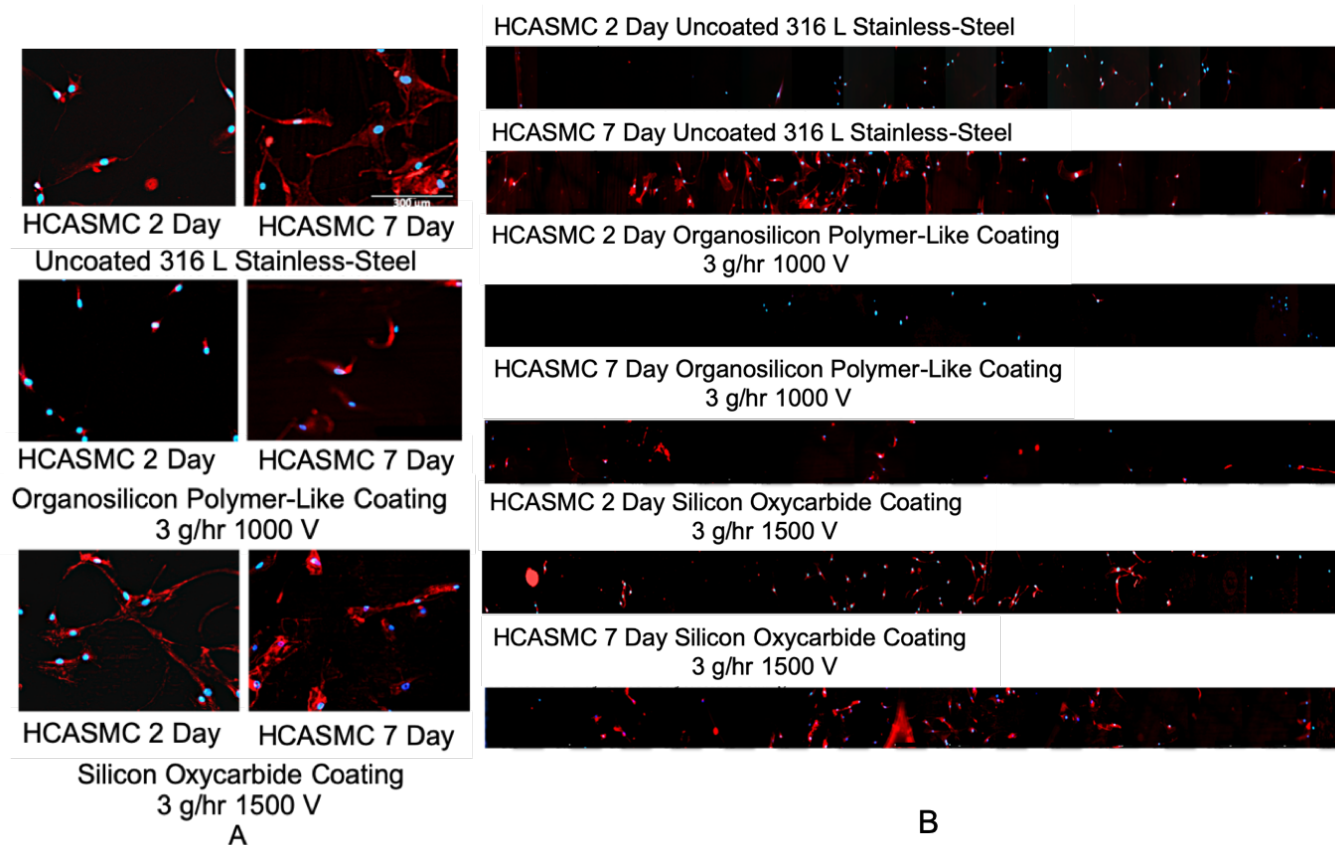
Figure 36. HCASMC 2 day and 7 day adhesion study on uncoated 316 L SS foil, organosilicon polymer-like coating and silicon oxycarbide coating on 316 L SS foil. (A) single frame image; (B) stitched single frame fluorescence images of cells adhered across the uncoated and coated sample surfaces. The nuclei of cells stained with DAPI is blue, and the cytoskeleton of cells stained with Phalloidin iFluor 594 is red.

HCASMCs exhibited higher adhesion to uncoated 316 L SS foil (10 and 18 cells/mm^2 for

2 day and 7 day) in comparison to the organosilicon polymer-like coating, as shown in

Figure 37. The organosilicon polymer-like coating, showed a significantly lower

adhesion of HCASMCs (3 and 7 cells/mm^2 for 2 day and 7 day). Therefore,

organosilicon polymer-like coating does not promote adhesion and proliferation of

HCASMCs.

The t-test revealed that there is statistical difference between the uncoated 316 L SS

samples after 2 day and 7 days of incubation, as well as between the organosilicon

polymer-like coated (3g-1000 V) samples after 2 day and 7 days. There is also a

significant difference between uncoated 316 L SS and 3 g/hr 1000 V (organosilicon

polymer-like coatings) at 2 day and 7 day for HCASMC adhesion and proliferation

(*p<0.05).
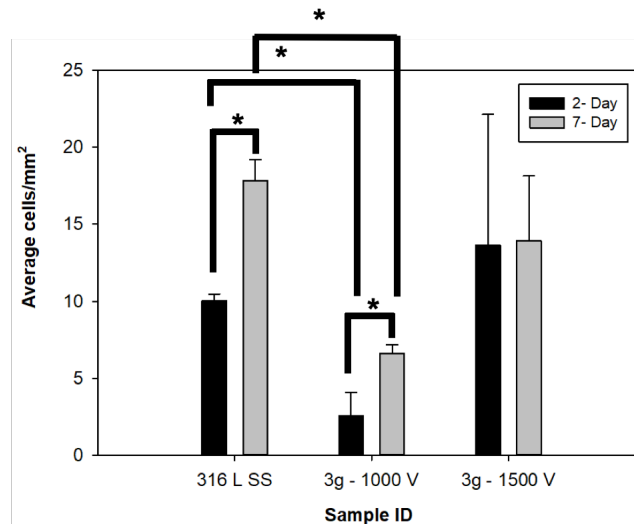
Figure 37. HCASMC cell density: cell adhesion and proliferation across uncoated and coated 316 L SS foil after 2 days and 7 days. The error bars represent the standard deviation between the means of independent replicates (n=3). Statistically significant differences were observed with respect to coating chemistry and time of incubation for HCASMC adhesion (*p<0.05).

4.5 Conclusion

In this study, we investigated the cellular response of HUVECs and HCASMCs to two different coated stent-like materials: organosilicon polymer-like and silicon oxycarbide in comparison to uncoated stent-like material 316 L SS foil. To assess the cellular behavior, we used fluorescence imaging to evaluate the adhesion and proliferation of HUVECs and HCASMCs. Qualitative and quantitative analyses of the fluorescence images showed that HUVECs adhered and proliferated more and faster on uncoated 316 L SS foil. Of the coatings, there was no statistical difference in adhesion on 2 day or 7 day samples in comparison to the uncoated 316 L SS foil. HCASMCs showed higher adhesion and proliferation on uncoated 316 L SS (10 cells/mm^2 after 2 days and 18 cells/mm^2 after 7 days) and silicon oxycarbide (14 cells/mm^2 after both 2 and 7 days). On the other hand, the organosilicon polymer-like coating demonstrated anti-biofouling properties, reducing the numbers of HCASMCs adhering to and proliferating across the surface (3 cells/mm^2 after 2 days and 7 cells/mm^2 after 7 days).

5. CONCLUSIONS & FUTURE WORK

The number one cause of death in the U.S. is coronary artery disease (CAD). Coronary stent procedures are performed to keep the artery open and allow blood flow to and from the heart. Stents have been successful at keeping the artery open for a short time; however, secondary effects have come about, such as build up plaque around the stent (in-stenosis) and blood clots. Several different types of anti-biofouling coatings including passive and drug-eluting coatings have been developed to prevent plaque build-up, blood clots, and increase the longevity of stents in the body.

In this work, two passive anti-biofouling coatings were developed and evaluated for their ability to modulate the adhesion and proliferation of human umbilical vein endothelial cells (HUVEC) and human coronary artery smooth muscle cells (HCASMC) onto stent-like material surfaces. The anti-biofouling coatings were prepared by pulsed direct current (DC) plasma-enhanced chemical vapor deposition (PECVD) using hexamethyldisiloxane (HMDSO) as the precursor. Two different parameters were changed in the process, the applied voltage (1000 V and 1500 V) and precursor gas flow rate (2, 2-3, and 3 g/hr) on 321 stainless-steel (SS) foil samples. The coating thickness ranged from 100 nm to 300 nm when 1000 V or 1500 V were applied, respectively. The wetting properties of the coatings were determined and compared to chemically cleaned, and plasma cleaned 321 SS foil surfaces. The role of the applied voltage and precursor flow rate on the wetting properties was investigated.

It was determined that at low gas flow rates, 2 g/hr, and high applied voltage, 1500 V, higher water contact angles (WCA) were observed. In contrast, at higher gas flow rates,

2-3 and 3 g/hr, and low applied voltage, 1000 V, higher WCA were obtained on 321 SS foils. Coatings applied at 3 g/hr, and 1000 V had the highest average WCA; however, when the applied voltage was increased to 1500 V, the WCA dropped to the lowest average WCA in comparison to the other coatings. In an effort to understand the differences in the wetting properties, the chemistry of the coatings was examined using Raman spectroscopy. After probing the coated and uncoated surface chemistry, it was revealed that two different surface chemistries were produced due to the different applied voltages and unrelated to the gas flow rate. The chemical composition of the coatings deposited at low applied voltage (1000 V) showed bands similar to plasma-polymerized HMDSO, preserving the CH_3, Si-C, and Si-O stretching and vibration bands; these coatings were identified as organosilicon polymer-like coatings. In contrast, with higher applied voltage, 1500 V, the coating's revealed two strong, broad bands characteristic of amorphous carbon (C=C) and weak broad bands for silicon oxide (Si-O), and alkanes (C-H); these coatings were identified as silicon oxycarbide coatings.

In the next phase of this study, coatings were generated using 3 g/hr HMDSO flow rate at 1000 V and 1500 V on medical-grade 316 L SS foil samples. The 3 g/hr at 1000 V and 1500 V process was selected for the 316 L SS, because it demonstrated the highest and lowest WCA on 321 SS. The 321 SS foils were used in this study because of the similar elemental composition and lower cost in comparison to 316 L SS, to carry out the different plasma polymerization processes. The wetting, physical, and chemical properties of the coating were assessed on the 316 L SS. Similar variances in the wetting properties were revealed between the low and high applied voltages that were observed on the 321 SS foil samples. The coating thickness was significantly lower on the 316 L

SS (108 nm) than the 321 SS foil (302 nm) for the 1500 V samples. The different coating

thickness could have been a result of coating inhomogeneity. The chemical composition

of the two coatings showed a strong alkane band (CH_3) for the coating applied at low

voltage (1000 V) labeled as an organosilicon polymer-like coating. Conversely, strong,

broad, amorphous carbon bands (C=C) were revealed for the coating applied at a high

voltage (1500 V) identified as silicon oxycarbide coatings. The absence of the weaker

bands observed on the 321 SS foil samples may have been a result of low signal to noise

ratio resulting from low laser power output.

The 316 L SS coated and uncoated surfaces discussed in the previous paragraph were

investigated further to evaluate their anti-biofouling behavior against human umbilical

vein endothelial cells (HUVEC) and human coronary artery smooth muscle cells

(HCASMC). The adhesion and proliferation of HUVECs and HCASMCs were evaluated

using fluorescence imaging. The cells were incubated on the uncoated and coated 316 L

SS foils for 2 and 7 days, then washed, fixed, and stained with DAPI and phalloidin

iFluor 594 to label the cell nuclei blue and cytoskeleton red when excited, respectively.

At day 2 and day 7, there was no statistical difference observed in HUVEC cell adhesion

and proliferation on the organosilicon polymer-like coating in comparison to the

uncoated 316 L SS foil. At the same time, a reduction in HCASMCs adhesion and

proliferation after 2 and 7 days was observed between the organosilicon polymer-like

coating and uncoated 316 L SS foil. The reduction in HCASMCs adhesion and

proliferation on the organosilicon polymer-like coating may be attributed to the alkane

(CH_3) stretching grouping in the coating. Conversely, the uncoated 316 L SS showed an

increase in adhesion and proliferation of HCASMCs after 2 and 7 days of incubation.

The silicon oxycarbide coating displayed no statistical difference in HUVEC or HCASMC adhesion and proliferation after 2 and 7 days relative to the uncoated 316 L SS foil. The high adhesion of HCASMCs to the silicon oxycarbide coating may be assigned to the silicon oxide and carbon-carbon groups in the coating. Based on these data, organosilicon polymer-like coatings were found to exhibit good anti-biofouling behavior against HCASMCs and HUVECs after 2 and 7 days of incubation. For ideal *in vitro* performance, high endothelial cell adhesion uniformly across the coated surface is desired. At the same time, low adhesion and replication with minimum surface coverage of smooth muscle cells was desired. Consequently, the organosilicon polymer-like coatings have significant potential in this field to reduce HCASMCs adhesion and proliferation, while enabling at least some adhesion of HUVECs.

In the future, process repeatability may be explored further to control coating thickness, uniformity and coating chemistry. For example, multiple depositions of the same voltage, deposition time, and flow rate should be done back to back. Metzler showed that by performing back to back depositions with the same process parameters, a very small (<7 nm) thickness variation over 18 deposition runs can be achieved.[115] Also, in-situ monitoring of the film thickness and plasma may be explored using ellipsometry, optical emission spectroscopy (OES), and quadrupole mass spectroscopy (QMS). Real-time monitoring of coating growth may allow for more consistent target thickness to be reached. OES and QMS are complementary techniques that may be used to characterize the elemental and chemical species in the plasma. The information obtained from these two techniques can then be used to correlate to the coating surface chemistry, which may

aid in understanding the deposition species that influence the coating composition and wetting properties.

In regard to cell adhesion studies, short term studies assessing the adhesion of HUVEC and HCASMCs after 2 or 4 hours would aide in understanding early cell-surface interaction. Also, measuring adhered cells via flow cytometry may be a better technique to identify the number of cells adhered to the surface. This technique may eliminate some of the losses that occur after washing the sample and prevent erroneous materials from being counted as cells. Other cells that should be explored in future studies are macrophages, which are understood to play a vital role in the pro-inflammatory response in plaque build-up.

Protein adsorption studies also should be performed, looking at fibrinogen and other relevant proteins. While we were unsuccessful at characterizing the adhesion of proteins such as bovine albumin serum to the stainless-steel foil via fluorescence spectroscopy (data not shown), other techniques may be explored such as atomic force microscope, electron microscopy, or quartz crystal microbalance.[116–118]

This study focused on flat smooth surfaces; however, the reality is that the stents are three-dimensional and have corrugated surfaces. Future studies should assess tubular shapes to determine if the plasma can evenly coat both sides and down the length of the tube. Also, an investigation into different corrugated shapes as the plasma may not be able to deposit into the small corners or may only thinly coat these areas. The effects of stress on the coating due to deployment is another area that should be studied. Stents are

tightly coiled prior to deployment in the body; however, once deployed, they are uncoiled and could experience cracking or delamination of the coating.

Finally, these anti-biofouling coatings should not be limited to just coronary artery stents. There are several other areas where stents (vascular stents, ureteral stents, prostatic stents, and esophageal stents) are applied in the body. These areas have an issue with the accumulation of plaque build-up or blood clots, which may lead to blockage in the femoral arteries, ureteral arteries, and endovascular aneurysm.

REFERENCES

(1)   Bagyura, Z.; Kiss, L.; Berta, B.; Szilágyi, Á.; Hirschberg, K.; Széplaki, G.; Lux,
       Á.; Szelid, Z.; Soós, P.; Merkely, B. High Rate of In-Stent Restenosis after
       Coronary Intervention in Carriers of the Mutant Mannose-Binding Lectin Allele.
       BMC Cardiovasc. Disord. **2017**, *17* (4), 1–5. https://doi.org/10.1186/s12872-016-
       0440-y.

(2)   Kim, J. H.; Shin, J. H.; Shin, D. H.; Moon, M. W.; Park, K.; Kim, T. H.; Shin, K.
       M.; Won, Y. H.; Han, D. K.; Lee, K. R. Comparison of Diamond-like Carbon-
       Coated Nitinol Stents with or without Polyethylene Glycol Grafting and Uncoated
       Nitinol Stents in a Canine Iliac Artery Model. *Br. J. Radiol.* **2011**, *84*, 210–215.
       https://doi.org/10.1259/bjr/21667521.

(3)   Benjamin, E. J.; Muntner, P.; Alonso, A.; Bittencourt, M. S.; Callaway, C. W.;
       Carson, A. P.; Chamberlain, A. M.; Chang, A. R.; Cheng, S.; Das, S. R.; Delling,
       F. N.; Djousse, L.; Elkind, M. S. V.; Ferguson, J. F.; Fornage, M.; Jordan, L. C.;
       Khan, S. S.; Kissela, B. M.; Knutson, K. L.; Kwan, T. W.; Lackland, D. T.; Lewis,
       T. T.; Lichtman, J. H.; Longenecker, C. T.; Loop, M. S.; Lutsey, P. L.; Martin, S.
       S.; Matsushita, K.; Moran, A. E.; Mussolino, M. E.; O'Flaherty, M.; Pandey, A.;
       Perak, A. M.; Rosamond, W. D.; Roth, G. A.; Sampson, U. K. A.; Satou, G. M.;
       Schroeder, E. B.; Shah, S. H.; Spartano, N. L.; Stokes, A.; Tirschwell, D. L.; Tsao,
       C. W.; Turakhia, M. P.; VanWagner, L. B.; Wilkins, J. T.; Wong, S. S.; Virani, S.
       S. Heart Disease and Stroke Statistics-2019 Update: A Report From the American
       Heart Association. *Circulation* **2019**, *139* (10), e56–e528.
       https://doi.org/10.1161/CIR.0000000000000659.

(4)   World Health Organization (WHO). WHO _ Cardiovascular Diseases (CVDs).
       Cardiovascular diseases (CVDs). 2015.

(5)   Cassar, A.; Holmes, D. R. J.; Rihal, C. S.; Gersh, B. J. Chronic Coronary Artery
       Disease: Diagnosis and Management. *Mayo Clin Proc* **2009**, *84* (12), 1130–1146.
       https://doi.org/10.4065/mcp.2009.0391.

(6)   Hamid, H.; Coltart, J. 'Miracle Stents'--a Future without Restenosis. *Mcgill J.
       Med.* **2007**, *10* (2), 105–111. https://doi.org/18523610.

(7)   Weir, I.; Dawkins, K. D.; Taggart, D. P. Coronary Artery Stenosis. *Ann. R. Coll.
       Surg. Engl.* **2006**, *88* (3), 265–269. https://doi.org/10.1308/003588406X106432.

(8)   Iqbal, J.; Gunn, J.; Serruys, P. W. Coronary Stents: Historical Development,
       Current Status and Future Directions. *British Medical Bulletin*. 2013.
       https://doi.org/10.1093/bmb/ldt009.

(9)   McCormick, C. Overview of Cardiovascular Stent Designs. In *Functionalised Cardiovascular Stents*; 2018; pp 3–26. https://doi.org/10.1016/b978-0-08-100496-8.00001-9.

(10)   Li, P. H.; Chu, P. K. Thin Film Deposition Technologies and Processing of Biomaterials. In *Thin Film Coatings for Biomaterials and Biomedical Applications*; 2016; pp 3–28. https://doi.org/10.1016/b978-1-78242-453-6.00001-8.

(11)   Michelmore, A. *Thin Film Growth on Biomaterial Surfaces*; Elsevier Ltd, 2016. https://doi.org/10.1016/b978-1-78242-453-6.00002-x.

(12)   Simard, T.; Hibbert, B.; Ramirez, F. D.; Froeschl, M.; Chen, Y. X.; O'Brien, E. R. The Evolution of Coronary Stents: A Brief Review. *Can. J. Cardiol.* **2014**, *30* (1), 35–45. https://doi.org/10.1016/j.cjca.2013.09.012.

(13)   Whitbeck, M. G.; Applegate, R. J. Second Generation Drug-Eluting Stents: A Review of the Everolimus-Eluting Platform. *Clin. Med. Insights Cardiol.* **2013**, *7*, 115–126. https://doi.org/10.4137/CMC.S11516.

(14)   Stefanini, G. G.; Taniwaki, M.; Windecker, S. Coronary Stents: Novel Developments. *Heart* **2014**, *100* (13), 1051–1061. https://doi.org/10.1136/heartjnl-2012-303522.

(15)   Iqbal, J.; Gunn, J.; Serruys, P. W. Coronary Stents: Historical Development, Current Status and Future Directions. *Br. Med. Bull.* **2013**, *106* (1), 193–211. https://doi.org/10.1093/bmb/ldt009.

(16)   Wieneke, H.; Sawitowski, T.; Wnendt, S.; Fischer, A.; Dirsch, O.; Karoussos, I. A.; Erbel, R. Stent Coating: A New Approach in Interventional Cardiology. *Herz* **2002**, *27*, 518–526. https://doi.org/10.1007/s00059-002-2405-4.

(17)   Hanawa, T. Materials for Metallic Stents. *J. Artif. Organs* **2009**, *12* (2), 73–79. https://doi.org/10.1007/s10047-008-0456-x.

(18)   Menown, I.; Lowe, R.; Penn, I. Passive Stent Coatings in the Drug-Eluting Era. *J. Invasive Cardiol.* **2005**, *17*, 222–228.

(19)   Garg, S.; Serruys, P. W. Coronary Stents: Looking Forward. *J. Am. Coll. Cardiol.* **2010**, *56* (10 SUPPL.), S43–S78. https://doi.org/10.1016/j.jacc.2010.06.008.

(20)   Huang, N.; Yang, P.; Leng, Y. X.; Chen, J. Y.; Sun, H.; Wang, J.; Wang, G. J.; Ding, P. D.; Xi, T. F.; Leng, Y. Hemocompatibility of Titanium Oxide Films. *Biomaterials* **2003**, *24* (13), 2177–2187. https://doi.org/10.1016/S0142-9612(03)00046-2.

(21) Song, S.-J.; Park, Y. J.; Park, J.; Cho, M. D.; Kim, J.-H.; Jeong, M. H.; Kim, Y. S.; Cho, D. L. Preparation of a Drug-Eluting Stent Using a TiO 2 Film Deposited by Plasma Enhanced Chemical Vapour Deposition as a Drug-Combining Matrix. *J. Mater. Chem.* **2010**, *20*, 4792–4801. https://doi.org/10.1039/b925409a.

(22) Mandracci, P.; Mussano, F.; Rivolo, P.; Carossa, S. Surface Treatments and Functional Coatings for Biocompatibility Improvement and Bacterial Adhesion Reduction in Dental Implantology. *Coatings* **2016**, *6* (7), 1–22. https://doi.org/10.3390/coatings6010007.

(23) Habibzadeh, S.; Li, L.; Omanovic, S.; Shum-tim, D.; Davis, E. C. Biocompatibility of Ir/Ti-Oxide Coatings: Interaction with Platelets, Endothelial and Smooth Muscle Cells. *Appl. Surf. Sci.* **2014**, *301*, 530–538. https://doi.org/10.1016/j.apsusc.2014.02.119.

(24) Murthy, R.; Shell, C. E.; Grunlan, M. A. The Influence of Poly(Ethylene Oxide) Grafting via Siloxane Tethers on Protein Adsorption. *Biomaterials* **2009**, *30* (13), 2433–2439. https://doi.org/10.1016/j.biomaterials.2009.01.051.

(25) Perrin, F.-X.; Nguyen, T. D. H.; Nguyen, D. L. Formation, Structure and Antibacterial Activities of Silazane Networks Grafted with Poly(Ethylene Glycol) Branches. *Prog. Org. Coatings* **2015**, *88*, 92–105. https://doi.org/10.1016/j.porgcoat.2015.06.022.

(26) Alcantar, N. A.; Aydil, E. S.; Israelachvili, J. N. Polyethylene Glycol-Coated Biocompatible Surfaces. *J. Biomed. Mater. Res.* **2000**, *51* (3), 343–351. https://doi.org/10.1002/1097-4636(20000905)51:3<343::AID-JBM7>3.0.CO;2-D.

(27) Pendyala, L.; Jabara, R.; Robinson, K.; Chronos, N. Passive and Active Polymer Coatings for Intracoronary Stents: Novel Devices to Promote Arterial Healing. *J. Interv. Cardiol.* **2009**, *22* (1), 37–48. https://doi.org/10.1111/j.1540-8183.2009.00423.x.

(28) Mani, G.; Feldman, M. D.; Patel, D.; Agrawal, C. M. Coronary Stents : A Materials Perspective. **2007**, *28*, 1689–1710. https://doi.org/10.1016/j.biomaterials.2006.11.042.

(29) Kong, X.; Grabitz, R. G.; Van Oeveren, W.; Klee, D.; Van Kooten, T. G.; Freudenthal, F.; Qing, M.; Von Bernuth, G.; Seghaye, M. C. Effect of Biologically Active Coating on Biocompatibility of Nitinol Devices Designed for the Closure of Intra-Atrial Communications. *Biomaterials* **2002**, *23* (8), 1775–1783. https://doi.org/10.1016/S0142-9612(01)00304-0.

(30) Seo, J.; Lee, J.; Na, K. Polymeric Materials for Drug Release System in Drug Eluting Stents. *J. Pharm. Investig.* **2016**, *46* (4), 317–324. https://doi.org/10.1007/s40005-016-0251-2.

(31) Bettini, R.; Peppas, N. A.; Colombo, P. Polymer Relaxation in Swellable Matrices Contributes to Drug Release. *Proc. Control. Release Soc.* **1998**, *25*, 36–37.

(32) P.D. Williams, M. A. Stent Selection for Percutaneous Coronary Intervention. *Contin. Cardiol. Educ.* **2017**, *1*, 64–69. https://doi.org/10.1016/B978-0-7020-2981-3.50006-4.

(33) Colombo, A.; Giannini, F.; Briguori, C. Should We Still Have Bare-Metal Stents Available in Our Catheterization Laboratory? *J. Am. Coll. Cardiol.* **2017**, *70* (5), 607–619. https://doi.org/10.1016/j.jacc.2017.05.057.

(34) Lee, D. H.; De La Torre-Hernandez, J. M. The Newest Generation of Drug-Eluting Stents and Beyond. *Eur. Cardiol. Rev.* **2018**, *13* (1), 54–59. https://doi.org/10.15420/ecr.2018:8:2.

(35) Akin, I.; Schneider, H.; Ince, H.; Kische, S.; Rehders, T. C.; Chatterjee, T.; Nienaber, C. A. Second- and Third-Generation Drug-Eluting Coronary Stents: Progress and Safety. *Herz* **2011**, *36* (3), 190–197. https://doi.org/10.1007/s00059-011-3458-z.

(36) Palmerini, T.; Biondi-Zoccai, G.; Della Riva, D.; Mariani, A.; Sabaté, M.; Smits, P. C.; Kaiser, C.; D'Ascenzo, F.; Frati, G.; Mancone, M.; Genereux, P.; Stone, G. W. Clinical Outcomes with Bioabsorbable Polymer- Versus Durable Polymer-Based Drug-Eluting and Bare-Metal Stents: Evidence from a Comprehensive Network Meta-Analysis. *J. Am. Coll. Cardiol.* **2014**, *63* (4), 299–307. https://doi.org/10.1016/j.jacc.2013.09.061.

(37) Curfman, G.D.; Morrissey, S., Jarcho, J.A.; Drazen, J. M. Drug Eluting Coronary Stents-Promise and Uncertainty. *N. Engl. J. Med.* **2007**, *356*, 1059–1060. https://doi.org/10.1056/NEJMoa1009540.6.

(38) Satyaprasad, A.; Nema, S. K.; Sinha, N. K.; Raj, B. Deposition of Thick and Adherent Teflon-like Coating on Industrial Scale Stainless Steel Shell Using Pulsed Dc and RF PECVD. *Appl. Surf. Sci.* **2010**, *256* (13), 4334–4338. https://doi.org/10.1016/j.apsusc.2010.02.027.

(39) Coyle, C. Investigation of Plasma Processes in Surface Modification with Biodiagnostic Applications, 2012.

(40) Gandhiraman, R. P.; Muniyappa, M. K.; Dudek, M.; Coyle, C.; Volcke, C.; Killard, A. J.; Burham, P.; Daniels, S.; Barron, N.; Clynes, M.; Cameron, D. C. Interaction of Plasma Deposited HMDSO-Based Coatings with Fibrinogen and Human Blood Plasma: The Correlation between Bulk Plasma, Surface Characteristics and Biomolecule Interaction. *Plasma Process. Polym.* **2010**, *7*, 411–421. https://doi.org/10.1002/ppap.200900133.

(41) Gandhiraman, R. P.; Daniels, S.; Cameron, D. C. A Comparative Study of Characteristics of SiOx CyHz, TiOx and SiO-TiO Oxide-Based Biocompatible Coatings. *Plasma Process. Polym.* **2007**, *4*, 5369–5373. https://doi.org/10.1002/ppap.200731002.

(42) Waltenberger, J.; Brachmann, J.; van der Heyden, J.; Richardt, G.; Fröbert, O.; Seige, M.; Friedrich, G.; Erglis, A.; Winkens, M.; Hegeler-Molkewehrum, C.; Neef, M.; Hoffmann, S. 5-Year Results of the BIOFLOW-III Registry. *Cardiovasc. Revascularization Med.* **2020**, *21* (1), 63–69. https://doi.org/10.1016/j.carrev.2019.03.004.

(43) Wittchow, E.; Hartwig, S. Still Room for Improvement: Preclinical and Bench Testing of a Thin-Strut Cobalt–Chromium Bare-Metal Stent with Passive Coating. *J. Biomed. Mater. Res. - Part B Appl. Biomater.* **2017**, *105* (6), 1612–1621. https://doi.org/10.1002/jbm.b.33702.

(44) Carrie, D.; Schächinger, V.; Danzi, G. B.; Macaya, C.; Zeymer, U.; Putnikovic, B.; Iniguez, A.; Moreno, R.; Mehmedbegovic, Z.; Beleslin, B. Cobalt-Chromium KAname™ CoRonary StEnt System in the Treatment of Patients with Coronary Artery Disease (Kare Study). *J. Interv. Cardiol.* **2014**, *27* (5), 491–499. https://doi.org/10.1111/joic.12144.

(45) Erbel, R.; Eggebrecht, H.; Roguin, A.; Schroeder, E.; Philipp, S.; Heitzer, T.; Schwacke, H.; Ayzenberg, O.; Serra, A.; Delarche, N.; Luchner, A.; Slagboom, T. Prospective, Multi-Center Evaluation of a Silicon Carbide Coated Cobalt Chromium Bare Metal Stent for Percutaneous Coronary Interventions: Two-Year Results of the ENERGY Registry. *Cardiovasc. Revascularization Med.* **2014**, *15* (8), 381–387. https://doi.org/10.1016/j.carrev.2014.10.002.

(46) Asano, T.; Suwannasom, P.; Katagiri, Y.; Miyazaki, Y.; Sotomi, Y.; Kraak, R. P.; Wykrzykowska, J.; Rensing, B. J.; Piek, J. J.; Gyöngyösi, M.; Serruys, P. W.; Onuma, Y. First-in-Man Trial of SiO_2 Inert-Coated Bare Metal Stent System in Native Coronary Stenosis ― The AXETIS FIM Trial ―. *Circ. J.* **2017**, *82* (2), 477–485. https://doi.org/10.1253/circj.cj-17-0337.

(47) a Johnson & Johnson Company, C. Ground-Breaking Innovation Proves Superior – The Weight of Evidence Behind the Cypher Sirolimus-Eluting Coronary Stent. *Eur. Cardiol. Rev.* **2006**, *1* (2), 1–5. https://doi.org/10.15420/ecr.2006.1.1u.

(48) Fröbert, O.; Lagerqvist, B.; Carlsson, J.; Lindbäck, J.; Stenestrand, U.; James, S. K. Differences in Restenosis Rate With Different Drug-Eluting Stents in Patients With and Without Diabetes Mellitus. A Report From the SCAAR (Swedish Angiography and Angioplasty Registry). *J. Am. Coll. Cardiol.* **2009**, *53* (18), 1660–1667. https://doi.org/10.1016/j.jacc.2009.01.054.

(49) Price, M. J.; Shlofmitz, R.; Spriggs, D.; Haldis, T.; Myers, P.; Popma-Almonacid, A.; Maehara, A.; Moe, B.; Peng, Y.; Mehran, R. Twelve Month Follow-up Data from the Onyx Core Trial: Angiograpic and Clinical Performance of next Generation Resolute Onyx Drug-Eluting Stent. *J. Am. Coll. Cardiol.* **2017**, *69* (11), 1110. https://doi.org/10.1016/s0735-1097(17)34499-6.

(50) Kufner, S.; Joner, M.; Thannheimer, A.; Hoppmann, P.; Ibrahim, T.; Mayer, K.; Cassese, S.; Laugwitz, K. L.; Schunkert, H.; Kastrati, A.; Byrne, R. A. Ten-Year Clinical Outcomes From a Trial of Three Limus-Eluting Stents With Different Polymer Coatings in Patients With Coronary Artery Disease: Results From the ISAR-TEST 4 Randomized Trial. *Circulation* **2019**, *139* (3), 325–333. https://doi.org/10.1161/CIRCULATIONAHA.118.038065.

(51) Kandzari, D. E.; Koolen, J. J.; Doros, G.; Garcia-Garcia, H. M.; Bennett, J.; Roguin, A.; Gharib, E. G.; Cutlip, D. E.; Waksman, R. Ultrathin Bioresorbable Polymer Sirolimus-Eluting Stents versus Thin Durable Polymer Everolimus-Eluting Stents for Coronary Revascularization: Three-Year Outcomes from the Randomized BIOFLOW V Trial. *JACC Cardiovasc. Interv.* **2020**, *13* (4), 4973. https://doi.org/10.1016/j.jcin.2020.02.019.

(52) Serruys, P. W. The Acute Ischaemic Stroke Team: One Great Step Forward. *EuroIntervention* **2014**, *10*, 73. https://doi.org/10.4244/EIJV10I7A133.

(53) Stone, G. W. Bioresorbable Vascular Scaffolds: Is Imaging Everything? *EuroIntervention* **2014**, *9*, 1255–1257. https://doi.org/10.4244/EIJV9I11A213.

(54) Costa, R. A.; Abizaid, A.; Mehran, R.; Schofer, J.; Schuler, G. C.; Hauptmann, K. E.; Magalhães, M. A.; Parise, H.; Grube, E. Polymer-Free Biolimus A9-Coated Stents in the Treatment of de Novo Coronary Lesions 4- and 12-Month Angiographic Follow-Up and Final 5-Year Clinical Outcomes of the Prospective, Multicenter BioFreedom FIM Clinical Trial. *JACC Cardiovasc. Interv.* **2016**, *9* (1), 51–64. https://doi.org/10.1016/j.jcin.2015.09.008.

(55) Chu, P. K.; Chen, J. Y.; Wang, L. P.; Huang, N. Plasma Surface Modification of Biomaterials. *Mater. Sci. Eng. R Reports* **2002**, *36* (5–6), 143–206. https://doi.org/10.1016/S0927-796X(02)00004-9.

(56) Gao, A.; Hang, R.; Chu, P. K. Recent Advances in Anti-Infection Surfaces Fabricated on Biomedical Implants by Plasma-Based Technology. *Surf. Coatings Technol.* **2017**, *312*, 2–6. https://doi.org/10.1016/j.surfcoat.2016.04.020.

(57) Bacakova, Lucie; Filova, Elena; Parizek, Martin; Svorcik, Valclav; Ruml, T. Modulation of Cell Adhesion, Proliferation and Differentiation on Materials Designed for Body Implants. *Biotechnol. Adv.* **2011**, *29* (6), 739–767.

(58) Chu, P. Plasma-Surface Modification of Biomaterials. *Mater. Sci. Eng. R Reports* **2002**, *36* (5–6), 143–206. https://doi.org/10.1016/S0927-796X(02)00004-9.

(59) Bandyopadhyay, A.; Sahasrabudhe, H.; Bose, S. *Laser Surface Modification of Metallic Biomaterials*; 2016. https://doi.org/10.1016/B978-0-08-100883-6.00006-X.

(60) Lu, T.; Qiao, Y.; Liu, X. Surface Modification of Biomaterials Using Plasma Immersion Ion Implantation and Deposition. *Interface Focus*. 2012, pp 325–336. https://doi.org/10.1098/rsfs.2012.0003.

(61) Trimukhe, A. M.; Pandiyaraj, K. N.; Tripathi, A.; Savio Melo, J.; and Deshmukh, R. R. Plasma Surface Modification of Biomaterials for Biomedical Applications. In *Advances in Biomaterials for Biomedical Applications*; 2017; Vol. 66, pp 95–166. https://doi.org/10.1007/978-981-10-3328-5.

(62) Paridah, M. .; Moradbak, A.; Mohamed, A. .; Owolabi, F. A. T.; Asniza, M.; Abdul Khalid, S. H. . Plasma-Enhanced Chemical Vapor Deposition: Where We Are and the Outlook for the Future. In *Chemical Vapor Deposition- Recent Advances and Applications in Optical, Solar Cells, and Solid State Devices*; 2016; pp 247–280.

(63) Kochkodan, V. M.; Sharma, V. K. Graft Polymerization and Plasma Treatment of Polymer Membranes for Fouling Reduction: A Review. *J. Environ. Sci. Heal. - Part A Toxic/Hazardous Subst. Environ. Eng.* **2012**, *47* (12), 1713–1727. https://doi.org/10.1080/10934529.2012.689183.

(64) Prasad, G. R.; Daniels, S.; Cameron, D. C.; Tully, E.; Kennedy, R. O. Biocompatible Coatings With Silicon and Titanium Oxides Deposited By Pecvd. *Power* **2006**.

(65) Chu, P. K. Surface Engineering and Modification of Biomaterials. In *Thin Solid Films*; 2013; Vol. 528, pp 93–105. https://doi.org/10.1016/j.tsf.2012.07.144.

(66) Stan, G. E.; Marcov, D. A.; Popa, A. C.; Husanu, M. A. Polymer-like and Diamond-like Carbon Coatings Prepared by RF-PECVD for Biomedical Applications. *Dig. J. Nanomater. Biostructures* **2010**, *5* (3), 705–718.

(67) Szymanowski, H.; Sobczyk, A.; Gazicki-Lipman, M.; Jakubowski, W.; Klimek, L. Plasma Enhanced CVD Deposition of Titanium Oxide for Biomedical Applications. *Surf. Coatings Technol.* **2005**, *200* (1-4 SPEC. ISS.), 1036–1040. https://doi.org/10.1016/j.surfcoat.2005.01.092.

(68)   Gandhiraman, R. P.; Karkari, S. K.; Daniels, S. M.; McCraith, B. Influence of Ion
         Bombardment on the Surface Functionalization of Plasma Deposited Coatings.
         Surf. Coatings Technol. **2009**, *203*, 3521–3526.
         https://doi.org/10.1016/j.surfcoat.2009.05.028.

(69)   Visai, L.; de Nardo, L.; Punta, C.; Melone, L.; Cigada, A.; Imbriani, M.; Arciola,
         C. R. Titanium Oxide Antibacterial Surfaces in Biomedical Devices. *Int. J. Artif.*
         Organs **2011**, *34* (9), 929–946. https://doi.org/10.5301/ijao.5000050.

(70)   Manis-levy, H.; Livneh, T.; Zukerman, I.; Mintz, M. H.; Raveh, A. Effect of
         Radio-Frequency and Low-Frequency Bias Voltage on the Formation of
         Amorphous Carbon Films Deposited by Plasma Enhanced Chemical Vapor
         Deposition. *Plasma Sci. Technol.* **2014**, *16* (10), 954–959.
         https://doi.org/10.1088/1009-0630/16/10/09.

(71)   Liu, D.; Zhou, J.; Fisher, E. R. Correlation of Gas-Phase Composition with Film
         Properties in the Plasma-Enhanced Chemical Vapor Deposition of Hydrogenated
         Amorphous Carbon Nitride Films. *J. Appl. Phys.* **2007**, *101* (2), 023304-1–10.
         https://doi.org/10.1063/1.2424402.

(72)   Corbella, C.; Rubio-Roy, M.; Bertran, E.; Andújar, J. L. Plasma Parameters of
         Pulsed-Dc Discharges in Methane Used to Deposit Diamondlike Carbon Films. *J.*
         Appl. Phys. **2009**, *106* (3), 033302-1–12. https://doi.org/10.1063/1.3183945.

(73)   Yasuda, H.; Yu, Q. Creation of Polymerizable Species in Plasma Polymerization.
         Plasma Chem. Plasma Process. **2004**, *24* (2), 325–351.
         https://doi.org/10.1023/B:PCPP.0000013204.17559.72.

(74)   Ward, A. J.; Short, R. D. A Time-of-Flight Secondary Ion Mass Spectrometry and
         X-Ray Photoelectron Spectroscopy Investigation of the Structure of Plasma
         Polymers Prepared from the Methacrylate Series of Monomers. *Polymer (Guildf).*
         1993, *34* (20), 4179–4185. https://doi.org/10.1016/0032-3861(93)90174-9.

(75)   Lewis, H. G. P.; Edell, D. J.; Gleason, K. K. Pulsed-PECVD Films from
         Hexamethylcyclotrisiloxane for Use as Insulating Biomaterials. *Chem. Mater.*
         2000, *12* (11), 3488–3494. https://doi.org/10.1021/cm0003370.

(76)   von Keudell, A.; Jacob, W. Properties of Amorphous Carbon; SRP Silva, Ed.;
         INSPEC, The Institution of Electrical Engineers: London, 2003; pp 285–289.

(77)   Huang, C.; Lin, J. H.; Li, C. H.; Yu, I. C.; Chen, T. L. Atmospheric-Pressure-
         Plasma-Enhanced Fabrication of Nonfouling Nanocoatings for 316 Stainless Steel
         Biomaterial Interfaces. In *Japanese Journal of Applied Physics*; 2018; pp 03EK05-
         1–7. https://doi.org/10.7567/JJAP.57.03EK05.

(78) Kuhn, S.; Kroth, J.; Ritz, U.; Hofmann, A.; Brendel, C.; Müller, L. P.; Förch, R.; Rommens, P. M. Reduced Fibroblast Adhesion and Proliferation on Plasma-Modified Titanium Surfaces. *J. Mater. Sci. Mater. Med.* **2014**, *25* (11), 2549–2560. https://doi.org/10.1007/s10856-014-5278-1.

(79) Wei, J.; Yoshinari, M.; Takemoto, S.; Hattori, M.; Kawada, E.; Liu, B.; Oda, Y. Adhesion of Mouse Fibroblasts on Hexamethyldisiloxane Surfaces with Wide Range of Wettability. *J. Biomed. Mater. Res. - Part B Appl. Biomater.* **2007**, *81* (1), 66–75. https://doi.org/10.1002/jbm.b.30638.

(80) Santos, M.; Bilek, M.; Wise, S. G. Plasma-Synthesised Carbon-Based Coatings for Cardiovascular Applications. *Biosurface and Biotribology* **2015**, *1*, 146–160. https://doi.org/10.1016/j.bsbt.2015.08.001.

(81) Waterhouse, A.; Wise, S. G.; Yin, Y.; Wu, B.; James, B.; Zreiqat, H.; McKenzie, D. R.; Bao, S.; Weiss, A. S.; Ng, M. K. C.; Bilek, M. M. M. In Vivo Biocompatibility of a Plasma-Activated, Coronary Stent Coating. *Biomaterials* **2012**, *33* (32), 7984–7992. https://doi.org/10.1016/j.biomaterials.2012.07.059.

(82) Malmsten, M.; Muller, D.; Lassen, B. Sequential Adsorption of Human Serum Albumin (HSA), Immunoglobulin G (IgG), and Fibrinogen (Fgn) at HMDSO Plasma Polymer Surfaces. *J. Colloid Interface Sci.* **1997**, *193* (1), 88–95. https://doi.org/10.1006/jcis.1997.5039.

(83) Malmsten, Martin, Lassen, B. Competitve Protein Adsorption at Plasma Polymer Surfaces. *J. Colloid Interface Sci.* **1997**, *186* (1), 9–16. https://doi.org/10.1006/jcis.1995.1231.

(84) Zuri, L., Silverstein, M.S., Narkis, M. Organic-Inorganic Character of Plasma Polymerized Hexamethyldisiloxane. *J. Appl. Polym. Sci.* **1996**, *62*, 2147–2154.

(85) Inagaki, N.; Kondo, S.; Murakami, T. Preparation of Siloxane-like Films by Glow Discharge Polymerization. *J. Appl. Polym. Sci.* **1984**, *29* (11), 3595–3605. https://doi.org/10.1002/app.1984.070291133.

(86) Ong, S. E.; Zhang, S.; Du, H.; Too, H. C.; Aung, K. N. Influence of Silicon Concentration on the Haemocompatibility of Amorphous Carbon. *Biomaterials* **2007**, *28* (28), 4033–4038. https://doi.org/10.1016/j.biomaterials.2007.05.031.

(87) Okpalugo, T. I. T.; Ogwu, A. A.; Maguire, P. D.; McLaughlin, J. A. D. Platelet Adhesion on Silicon Modified Hydrogenated Amorphous Carbon Films. *Biomaterials* **2004**, *25* (2), 239–245. https://doi.org/10.1016/S0142-9612(03)00494-0.

(88) Rzany, A.; Schaldach, M. Smart Material Silicon Carbide: Reduced Activation of Cells and Proteins on a SiC:H-Coated Stainless Steel. *Prog Biomed Res* **2001**, *4*, 182–194.

(89) Liang, W.; Wu, C.; Cai, Z.; Sun, Y.; Zhang, H.; Wu, P.; Cai, C. Tuning the Electron Transport Band Gap of Bovine Serum Albumin by Doping with Vb12. *Chem. Commun.* **2019**, *55* (19), 2853–2856. https://doi.org/10.1039/c9cc00688e.

(90) PRNewswire. Medical Coatings Market by Type (Hydrophilic and Hydrophobic coatings), Application (Medical Devices, Implants, Medical Equipment & Tools and Others) and Geography - Regional Trends & Forecast to 2019 http://www.prnewswire.com/news-releases/medical-coatings-market-by-type-hydrophilic-and-hydrophobic-coatings-application-medical-devices-implants-medical-equipment--tools-and-others-and-geography---regional-trends--forecast-to-2019-300041596.html.

(91) McPherson, T.; Kidane, A.; Szleifer, I.; Park, K. Prevention of Protein Adsorption by Tethered Poly(Ethylene Oxide) Layers: Experiments and Single-Chain Mean-Field Analysis. *Langmuir* **1998**, *14* (1), 176–186. https://doi.org/10.1021/la9706781.

(92) Wei, R. Development of New Technologies and Practical Applications of Plasma Immersion Ion Deposition (PIID). *Surf. Coatings Technol.* **2010**, *204* (18–19), 2869–2874. https://doi.org/10.1016/j.surfcoat.2010.01.046.

(93) Tabata, Y. Biomaterial Technology for Tissue Engineering Applications. *J. R. Soc. Interface* **2009**, *6 Suppl 3* (March), S311–S324. https://doi.org/10.1098/rsif.2008.0448.focus.

(94) Zou, M.; Beckford, S.; Wei, R.; Ellis, C.; Hatton, G.; Miller, M. A. Effects of Surface Roughness and Energy on Ice Adhesion Strength. *Appl. Surf. Sci.* **2011**, *257* (8), 3786–3792. https://doi.org/10.1016/j.apsusc.2010.11.149.

(95) Zlatanović, M.; Popović, I. Gas Discharge Static Characteristics in Pulse Regime. *Contemp. Mater.* **2011**, *1* (2), 138–143. https://doi.org/10.5767/anurs.cmat.100102.en.138z.

(96) Chen, F. F. *Introduction to Plasma Physics and Controlled Fusion*; 2016. https://doi.org/10.1007/978-3-319-22309-4.

(97) Walton, S. G.; Greene, J. E. Plasmas in Deposition Processes. In *Handbook of Deposition Technologies for Films and Coatings*; 2010; pp 32–92. https://doi.org/10.1016/B978-0-8155-2031-3.00002-8.

(98) Goujon, M.; Belmonte, T.; Henrion, G. OES and FTIR Diagnostics of HMDSO/O2 SiOx Deposition Assisted by RF Plasma. *Surf. Coatings Technol.* **2004**, *188–189* (1-3 SPEC.ISS.), 756–761. https://doi.org/10.1016/j.surfcoat.2004.07.048.

(99) Samadi, M.; Eshaghi, A.; Bakhshi, S. R.; Aghaei, A. A. The Influence of Gas Flow Rate on the Structural, Mechanical, Optical and Wettability of Diamond-like Carbon Thin Films. *Opt. Quantum Electron.* **2018**, *50* (4), 1–15. https://doi.org/10.1007/s11082-018-1456-6.

(100) Peri, B.; Borah, B.; Dash, R. K. Effect of RF Power and Gas Flow Ratio on the Growth and Morphology of the PECVD SiC Thin Films for MEMS Applications. *Bull. Mater. Sci.* **2015**, *38* (4), 1105–1112. https://doi.org/10.1007/s12034-015-0881-4.

(101) Carteret, C.; Labrosse, A. Vibrational Properties of Polysiloxanes: From Dimer to Oligomers and Polymers. 1. Structural and Vibrational Properties of Hexamethyldisiloxane (CH3)3SiOSi(CH3)3. *J. Raman Spectrosc.* **2010**, *41* (9), 996–1004. https://doi.org/10.1002/jrs.2537.

(102) Hamada, K.; Morishita, H. Raman, Infrared and H1-NMR Spectra of Hexamethyldisiloxane and Hexamethyldisilazane. *Spectrosc. Lett.* **1983**, *16* (10), 717–729. https://doi.org/10.1080/00387018308062384.

(103) Yasuda, H.; Yasuda, T. Competitive Ablation and Polymerization (CAP) Principle and the Plasma Sensitivity of Elements in Plasma Polymerization and Treatment. *J. Polym. Sci. Part A Polym. Chem.* **2000**, *38*, 943–953. https://doi.org/10.1002/(SICI)1099-0518(20000315)38:6<943::AID-POLA3>3.0.CO;2-3.

(104) Biederman, H; Osada, Y. *Plasma Polymerization Processes*; Elsevier: Amsterdam, 1992.

(105) Rojas, E.; Maass, F. Characterization of Diamond Like Carbon Thin Coating on Stainless Steel 316 L Through Pulsed DC. *Mater. Res. Soc. Symp. Proc. Vol.* **2010**, *1275*, 191–196.

(106) Mitra, A. K.; Agrawal, D. K. In Stent Restenosis: Bane of the Stent Era. *J. Clin. Pathol.* **2006**, *59* (3), 232–239. https://doi.org/10.1136/jcp.2005.025742.

(107) Carpenter, A. W.; Schoenfisch, M. H. Nitric Oxide Release: Part II. Therapeutic Applications. *Chem. Soc. Rev.* **2012**, *41* (10), 3742–3752. https://doi.org/10.1039/c2cs15273h.

(108) Thierry, B.; Merhi, Y.; Bilodeau, L.; Trépanier, C.; Tabrizian, M. Nitinol versus Stainless Steel Stents: Acute Thrombogenicity Study in an Ex Vivo Porcine Model. *Biomaterials* **2002**, *23*, 2997–3005. https://doi.org/10.1016/S0142-9612(02)00030-3.

(109) Chen, Q.; Thouas, G. A. Metallic Implant Biomaterials. *Materials Science and Engineering R: Reports*. 2015, pp 1–57. https://doi.org/10.1016/j.mser.2014.10.001.

(110) Nouri, A.; Wen, C. Introduction to Surface Coating and Modification for Metallic Biomaterials. *Surface Coating and Modification of Metallic Biomaterials*. 2015, pp 3–60. https://doi.org/10.1016/B978-1-78242-303-4.00001-6.

(111) Windecker, S.; Mayer, I.; De Pasquale, G.; Maier, W.; Dirsch, O.; De Groot, P.; Wu, Y. P.; Noll, G.; Leskosek, B.; Meier, B.; Hess, O. M.; Working Group on Novel Surface Coating of Biomedical Devices (SCOL), in collaboration with the W. G. on N. S. C. of B. D. Stent Coating with Titanium-Nitride-Oxide for Reduction of Neointimal Hyperplasia. *Circulation* **2001**, *104* (8), 928–933. https://doi.org/10.1161/hc3401.093146.

(112) Li, L.; Pan, S.; Zhou, X.; Meng, X.; Han, X.; Ren, Y.; Yang, K.; Guan, Y. Reduction of In-Stent Restenosis Risk on Nickel-Free Stainless Steel by Regulating Cell Apoptosis and Cell Cycle. *PLoS One* **2013**, *8* (4), 1–11. https://doi.org/10.1371/journal.pone.0062193.

(113) Yin, Y.; Wise, S. G.; Nosworthy, N. J.; Waterhouse, A.; Bax, D. V.; Youssef, H.; Byrom, M. J.; Bilek, M. M. M.; McKenzie, D. R.; Weiss, A. S.; Ng, M. K. C. Covalent Immobilisation of Tropoelastin on a Plasma Deposited Interface for Enhancement of Endothelialisation on Metal Surfaces. *Biomaterials* **2009**, *30* (9), 1675–1681. https://doi.org/10.1016/j.biomaterials.2008.11.009.

(114) Xiao, Y.; Zhao, L.; Shi, Y.; Liu, N.; Liu, Y.; Liu, B.; Xu, Q.; He, C.; Chen, X. Surface Modification of 316L Stainless Steel by Grafting Methoxy Poly(Ethylene Glycol) to Improve the Biocompatibility. *Chem. Res. Chinese Univ.* **2015**, *31* (4), 651–657. https://doi.org/10.1007/s40242-015-5027-0.

(115) Metzler, M.; Patel, R. ScholarlyCommons Plasma Enhanced Chemical Vapor Deposition (PECVD) of Silicon Dioxide (SiO2) Using Oxford Instruments System 100 PECVD Plasma Enhanced Chemical Vapor Deposition (PECVD) of Silicon Dioxide (SiO2) Using Oxford Instruments System 100 PECVD Pl. **2017**.

(116) Szotts, L.M., Horbett, T. A. Protein Interaction with Surfaces: Cellular Response, Complement Activation and, Newer Methods. *Curr. Opin. Chem. Biol.* **2011**, No. 15, 677–682.

(117) Rabe, M.; Verdes, D.; Seeger, S. Understanding Protein Adsorption Phenomena at Solid Surfaces. *Adv. Colliod Interface Sci.* **2011**, *162*, 87–106.

(118) Boujday, S.; Methivier, C.; Beccard,B.; Pradier, C. M. Innovative Surface Characterization Techniques Applied to Immunosensor Elaboration and Test: Comparing the Efficiency of Fourier Transform-Surface Plasmon Resonance, Quartz Crystal Microbalance with Dissipation Measurements and Polarization Modulation-Ref. *Anal. Biochem.* **2009**, *287*, 194–201.